SHRP-C-629

Cement Paste Aggregate Interface Microstructure

D. M. Roy
M.W. Grutzeck
D. Shi
G. Lui

Materials Research Laboratory
The Pennsylvania State University
University Park, PA 16802

Strategic Highway Research Program
National Research Council
Washington, DC 1993

SHRP–C–629
Contract C-201

Program Manager: *Don M. Harriott*
Project Manager: *Inam Jawed*
Production Editor: *Marsha Barrett*
Program Area Secretary: *Ann Saccomano*

May 1993

key words:
cement
concrete
interface
microscopy
microstructure
model
packing
permeability
porosimetry
scanning electron microscopy
simulation

Strategic Highway Research Program
National Academy of Sciences
2101 Constitution Avenue N.W.
Washington, DC 20418

(202) 334-3774

350/NAP/593

Acknowledgments

The research described herein was supported by the Strategic Highway Research Program (SHRP). SHRP is a unit of the National Research Council that was authorized by section 128 of the Surface Transportation and Uniform Relocation Assistance Act of 1987.

Contents

Abstract ---------- 1
Executive Summary ---------- 3
Introduction ---------- 5
References ---------- 7
I. Interface Simulation Model ---------- 10
    Introduction ---------- 10
    Simulation Algorithm ---------- 11
    Simulation Results ---------- 14
    Discussions and Implications ---------- 27
    Summary ---------- 30
    References ---------- 31
II. Microstructure of Concrete Interfaces ---------- 33
III. Microstructure of Engineered Interface Samples ---------- 37
IV. Microstructure of Paste/Sand Interfaces in Mortars ---------- 44
    SEM ---------- 47
    Polished Sections—Reflected Light ---------- 56
    Hg Porosimetry ---------- 63
    Air Permeability ---------- 73
Summary and Conclusions ---------- 76

Abstract

This report describes research into the nature of the interfacial region in concrete. The characteristics of the paste-aggregate interfaces found in concrete may, more than any other single factor, influence the long-term performance of the material. The interfacial region considered more porous than the paste itself, could act both as a localized "weakness" where fractures are initiated, and as an avenue of attack for aggressive chemical agents.

Computer simulations of particle packing against an aggregate surface demonstrate that it is the efficiency by which particles pack against the aggregate during mixing which influences the nature and strength of the interfacial region which develops over time. Furthermore, simulation results suggest that the degree of flocculation and the intensity of mixing are not entirely independent variables.

Scanning electron microscopy (SEM), thin section, and mercury-porosimetry evaluations of a series of pastes and mortars made with half the volume of the paste replaced with silica sand confirmed the belief that mortars contain zones of enhanced interfacial porosity. Mixes made with Class C fly ash were the only exceptions where interfacial porosity was nearly non-existent. Data also suggests that air permeability may be directly related to the presence of larger pores -200 nm (200 Å) rather than the smaller paste pores -20 nm (200 Å). Finally, it was observed that differences in interfacial and paste porosities became less significant at longer curing times.

EXECUTIVE SUMMARY

The interfacial region which develops around both fine and coarse aggregate in concrete has been the object of extensive research. To date, it has been demonstrated that the interfacial region has a finite thickness and enhanced porosity. As such, it is often referred to as the weakest part of concrete, where fractures are initiated, and as an avenue of attack for corrosive chemical agents.

The present report details the results of SHRP-funded research into the nature of the interfacial region in concrete. The study was divided into three parts: a literature review, computer simulation of particle packing at an interface, and experiments designed to explore the effect of interfacial porosity on microstructure and permeability.

Computer simulation of packing at an aggregate surface was undertaken to show the effect of four variable parameters on interfacial porosity profiles: original particle density (which we are equating with w/c), travel distance of particles to the surface of the aggregate, sticking probability (tendency of particles to flocculate), and amplitude of particle motion (assumed to be related to energy of mixing).

In all cases, simulations demonstrated that interface porosity decreased from nearly 100% directly at the interface to that of the bulk paste at 2 to 3 particle diameters. It is evident that, more than any other factor, the initial packing of the cement particles against the aggregate which occurs during mixing dictates the character of the interfacial zone which develops over the life of the concrete.

Flocculation was found to be the single most significant variable. Highly flocculated systems produced very porous interfaces. If flocculation was reduced, packing became more efficient and lower interfacial porosities were achieved. It was also found that amplitude of motion, which we equate with energy of mixing, was not an entirely independent variable. For example, if the tendency to flocculate was high, gentle mixing was found to lead to better packing and a less porous interface. If, on the other hand, flocculation was low (in a real system this could be the result of using a superplasticizer), then vigorous mixing was observed to produce better packing. Thickness of the water film surrounding the aggregate (travel distance) was found to have little effect. And finally, the original density of particles used in the simulation (w/c) was found to have no effect.

The experimental program was divided into a number of parts. The first dealt with the most efficient way of examining interfaces. After initial attempts at characterizing actual concrete samples failed, so called "engineered" samples were prepared. In this case, a rectangular block of limestone or quartzite was actually mixed with a large batch of concrete and then placed in a mold and filled with sand-containing paste screened from the concrete. After curing in lime water, these samples were cut and examined with the SEM and

petrographic microscope. Complex interfacial zones were obvious with both aggregate types. When silica fume and Class C fly ash were added to the concrete, these zones were much reduced in size. Although this method was an improvement over examining actual concrete specimens, the engineered samples tended to be very susceptible to drying shrinkage—cracks were seen to develop along the interface.

As a result, it was decided to study interfaces in a more indirect fashion. It was hypothesized that if 1/2 of the volume of paste was replaced by quartz sand (having zero porosity), any interface porosity associated with the sand surfaces would show up as a measured positive deviation (microstructure, Hg-porosimetry, air permeability) to the baseline paste values.

Four paste and mortar samples were prepared. One was an OPC, while others contained fly ash (F, C) or condensed silica fume. Volumes of components were calculated using measured densities. Characteristics of each pair of samples on a given day were determined using the SEM, fluorescent microscopy, Hg-porosimetry, and air permeability. These studies resulted in the following general observations.

In all cases, with the possible exception of the Class C and silica fume-containing samples, interfacial porosity was significantly higher than surrounding bulk paste porosities. As the original interfacial porosity filled with hydration products, the porosity of the sample decreased. In a mortar or concrete, the concentration of the hydration products are presumably lower in the interfacial region, because more space must be filled. Additionally, due to the nature of the hydration reaction which produces excess lime, the interfacial region may also provide both space and nucleation sites for $Ca(OH)_2$ crystals to grow.

As a result, this zone may be more sensitive to effects of carbonation and drying. For example, our studies have shown that sand-paste interfaces are often cracked, contain carbonate and eroded due to polishing. Hg-porosimetry and air permeability results confirmed higher than expected values in early age mortar samples when compared to pure paste samples. In addition, air permeability data suggested that permeability in the mortar samples was directly related to the number of ~200 nm (2000 Å) interfacial pores present in the mortar. The pastes tended to contain relatively few such pores. The pastes normally contained 20 nm (200Å) pores. The mortars, on the other hand, were dominated by 200 nm or larger pores associated with interfaces. Finally, it was demonstrated that differences in interfacial and paste porosities became less significant at longer curing times.

The most significant result of the report is the finding that mixing may be an important variable in determining interface characteristics. Unfortunately, this aspect of the work was not examined experimentally. It is, however, an area where future work could take place if funding became available.

INTRODUCTION

The nature of the contact between cement paste and aggregate (large and small) which occurs in mortar and concrete has been and still remains somewhat of an enigma. Various groups and individuals have studied the interfacial regions and observed a number of interesting phenomena. For example, the transition in physical properties one observes as one crosses an aggregate-paste boundary is not a sharp discontinuity, but a gradual one. The so-called "Auréole de transition" (transition zone) has both a real extent and thickness, and as such it can be considered as a separate entity having discrete intrinsic properties, properties which impact on the performance of mortars and concrete.

Farran (1) was among the first to note that the interface formed between aggregate and "bulk" cement paste was not sharp, and that the cement paste in contact with the aggregate differed from the "bulk" cement paste. Barnes et al. (2,3) and more recently Yuan and Odler (4) and Yuan and Guo (5) found evidence of a duplex-film consisting of 2-3 μm of massive orientated $Ca(OH)_2$ plus a thin layer of "hair-brush" C-S-H occurring at the interface. Langton and Roy (6) found a similar duplex film for non-reactive aggregates, and as many as four interfacial layers for reactive aggregates. However, Struble and Mindess (7) and Struble (8), suggested that a duplex film did not exist in all cases, although a layer of well oriented $Ca(OH)_2$ did. Recently, Zhang et al. (9), Maso (10), and Javelas et al. (11), demonstrated that a small layer of C-S-H was present between the aggregate and the massive $Ca(OH)_2$ layer directly adjacent to the aggregate. As more attention was focused upon the interfacial region, Perrin et al. (12), Maso (10), Monteiro et al. (13), Pinchin and Tabor (14), Ollivier and Grandet (15) and Carles-Gibergues and Grandet (16), demonstrated that the interfacial region was on the order of 40-50 μm wide and contained porosity and $Ca(OH)_2$ concentration gradients. Grandet and Ollivier (17) further demonstrated that the width of the transition zone increased with increasing w/c ratio (20 μm at 0.25 and 50 μm at 0.33).

Perhaps the most common thread in all of these models is the ubiquitous occurrence of oriented $Ca(OH)_2$ at interfaces (2-4,7,8,16,18-23). In addition, the $Ca(OH)_2$ is also observed to gradually decrease in concentration and orientation with distance from the aggregate surface into the cement paste. It has been suggested by Zimbelmann (24,25) and Chatterji and Jeffery (26) that this variation in $Ca(OH)_2$ content and orientation may be a function of the void space that is available at the interface for precipitation of $Ca(OH)_2$. Zimbelmann suggests that the size of the water film present around the hydrating cement particles plays a major role in preventing efficient packing at the interface. This phenomenon results in a greater percentage of void space directly adjacent to the aggregate surface which is then filled by precipitating $Ca(OH)_2$. The idea of reducing the size of the film and thus increasing

bond strength by reducing initial porosity has been tested by Maso (10) and Wu et al. (27) resulting in improved bonding as the film size was reduced. The ability to pack against an interface has been modeled by Maksimov (28). He has shown that a larger percentage of the porosity occurs at the interface as a result of inefficient packing. Papers by Berger et al. (18), and by Stucke and Majumdar (19) suggest that very dense $Ca(OH)_2$ may actually enhance bonding since fracture is not confined to the interface itself, but occurs in the transition zone (20,29). This is seemingly in agreement with measurements made across the interface which show that the cement paste microhardness near the aggregate is larger than that of the bulk cement paste itself (30). Various researchers have observed that, with the possible exception of aggregates composed primarily of $CaCO_3$, bond strength is not generally affected by the nature of the aggregate (26,31). In the case of $CaCO_3$-based aggregates, strength is usually unexplainably high. Yuan and Guo (5) suggest that increased bond strength may be due to the conversion of calcite to $Ca(OH)_2$ at the interface as the calcite dissolves in alkaline solutions, or as a consequence of the reaction of calcite with calcium aluminate hydrate to form a carboaluminate hydrate ($3CaO{\cdot}Al_2O_3{\cdot}CaCO_3{\cdot}11H_2O$) (4,5,21,32). Farran (1) suggests epitaxial growth of $Ca(OH)_2$ on the calcite aggregate. This phenomenon suggests that reactivity of the aggregate might in some cases play a role in bonding. Results for silicate aggregates are less definitive, but reactivity has been observed when the concrete was formulated with a quartzite aggregate (33).

Studies of surface roughness versus bond strength suggest a direct correlation of strength to surface roughness (5,34,35). Perry and Gillott used marbles whose surfaces were roughened in a ball mill to test this hypothesis and found that compressive strength of concrete made with the marble aggregate exhibited a similar relationship (36). Alexander and Wardlaw (37) have shown a direct relationship of bond strength to the log of the aggregate surface area available for bonding. Results by Monteiro et al. (38), and Grandet and Ollivier (32), have also demonstrated similar relationships.

Effects of additives on the transition zone are mixed (39). High surface area (use of condensed silica fume) removes water from the matrix, generally reducing film size and as a result the size of the transition zone. Pozzolans tend to reduce the percentage and orientation of $Ca(OH)_2$ in the transition zone and also its width (16,26). Slag, on the other hand, increased the size of the transition zone (39). In addition to $Ca(OH)_2$, ettringite was also observed in the transition zone (40-42).

Even with all of this information, the mechanisms by which the interface forms and the actual contribution of the interfacial zone to the physical and mechanical properties of mortars and concrete are still not clearly resolved. The present study of the interface in mortars and concrete was initiated in order to address these shortfalls in our

understanding of the interfacial region. Details of the four-part study of the transition zone are given below.

REFERENCES

1. J. Farran, "Mineralogical Contribution to the Study of Adhesion Between the Hydrated Constituents of Cement and the Embedded Material," Revue des Materiauxde Construction, 155-172, 191-209 (1956).
2. B.D. Barnes, S. Diamond, and W.L. Dolch, "The Contact Zone Between Portland Cement Paste and Glass 'Aggregate' Surfaces," Cem. Concr. Res. 8, 233-244 (1978).
3. B.D. Barnes, D. Diamond, and W.L. Dolch, "Micromorphology of the Interfacial Zone Around Aggregates in Portland Cement Mortars," J. Amer. Ceram. Soc. 62, 21-24 (1979).
4. C.Z. Yuan and I. Odler, "The Interfacial Zone Between Marble and Tricalcium Silicate Paste," Cem. Concr. Res. 17, 784-792 (1987).
5. C.Z. Yuan and W.J. Guo, "Bond Between Marble and Cement Paste," Cem. Concr. Res. 17, 544-552 (1987).
6. C.A. Langton and D.M. Roy, "Morphology and Microstructure of Cement Paste/Rock Interfacial Regions," 7th ICCC, Paris, III, VII-127 - 132 (1980).
7. L. Struble and S. Mindess, "Morphology of the Cement-Aggregate Bond," Int. J. Cement Composites and Lightweight Concrete 5, 79-86 (1983).
8. L. Struble, "Microstructure and Fracture at the Cement Paste-Aggregate Interface," Mat. Res. Soc., Boston, 1987 (in press).
9. X. Zhang, G.W. Groves, and S.A.Rodger, "The Microstructure of Cement Aggregate Interfaces," Mat. Res. Soc., Boston, 1987 (in press).
10. J.C. Maso, "The Bond Between Aggregates and Hydrated Cement Paste," 7th ICCC, Paris, I, VII-1/4 - 1/5 (1980).
11. R. Javelas, J.C. Maso, J.P. Ollivier, and B. Thenoz, "Observation directe au Microscope Electronique par Transmission de la Liaison pate de Ciment-Granulats dans des Mortiers de Calcite et de Quartz," Cem. Concr. Res. 5, 285-293 (1975).
12. B. Perrin, J.C. Maso, J. Farran, and R. Javelas, "Existence d'une auréole de transition entre les granulats d'un Mortier ou d'un béton et la masse de la pâte de ciment hydraté. Conséquences sur les propriétés mécaniques," C.R. Ac. Sc. Paris 275, 1467-1468 (1972).
13. P.J.M. Monteiro, J.C. Maso, and J.P. Ollivier, "The Aggregate-Mortar Interface," Cem. Concr. Res. 15, 953-958 (1985).
14. D.J. Pinchin and D. Tabor, "Interfacial Phenomena in Steel Fibre Reinforced Cement, I: Structure and Strength of Interface Region," Cem. Concr. Res. 8, 15-24 (1978).

15. J.P. Ollivier and J. Grandet, "Sequence of Formation of the Aureole of Transition," Coll. Int. Liaisons Pâtes de Ciment Matériaux Associés (Toulouse) A.14 - A.22 (1982).
16. A. Carles-Gibergues, J. Grandet, and J.P. Ollivier, "Contact Zone Between Cement Paste and Aggregate," in Bond in Concrete, P. Bartos, Ed., Applied Science Publ, London (1982).
17. J. Grandet and J.P. Ollivier, "Orientation of Hydration Products Near Aggregate Surfaces," 7th ICCC, Paris, III, VII-63 - 68 (1980).
18. R.L. Berger, D.S. Chan, and J.D. McGregor, "Calcium Hydroxide as a Binder in Portland Cement Paste," J. Amer. Ceram. Soc. 53, 57-58 (1970).
19. M.S. Stucke and A. Majumdar, "Microstructure of Glass Fibre-Reinforced Cement Composites," J. Mat. Sci. 11, 1019-1030 (1976).
20. M.N. Al Khalaf, "Steel/Mortar Interfaces: Microstructural Features and Mode of Failure," Cem. Concr. Res. 9, 197-208 (1979).
21. J.P. Ollivier and J. Grandet, "Disorientation of Portlandite Crystals in the 'Aureole of Transition'," Coll. Int. Liaisons Pâtes de Ciment Matériaux Associés (Toulouse), A23 - A27 (1982).
22. J. Grandet and J.P. Ollivier, "New Method for the Study of Cement-Aggregate Interfaces," 7th ICCC, Paris, III, VII 85-89 (1980).
23. Zhong-Wei Wu, L. Bao-Yuan, and X. Song-Shan, "Interfacial Zones in Cement-Based Composite Materials," Coll. Int. Liaisons Pâtes de Ciment Matériaux Associés (Toulouse), A28 - A32 (1982).
24. R. Zimbelmann, "A Contribution to the Problem of Cement-Aggregate Bond," Cem. Concr. Res. 15, 801-808 (1985).
25. R. Zimbelmann, "A Method for Strengthening the Bond Between Cement Stone and Aggregates," Cem. Concr. Res. 17, 651-660 (1987).
26. S. Chatterji and J.W. Jeffery, "The Nature of the Bond Between Different Types of Aggregates and Portland Cement," Indian Concrete J., 346-349 (1971).
27. Xuequan Wu, L. Dongxu, B. Qinghan, G. Liqun, and Mingshu Tang, "Preliminary Study of a Composite Process in Concrete Manufacture," Cem. Concr. Res. 17, 709-714 (1987).
28. Yu. V. Maksimov, "Packing Density of Highly Dispersed Particles on the Surface of Coarsely Dispersed Inclusions, Kollidnyi Zhurnal 48, 813-814 (1986).
29. F. Massazza and M. Pezzuoli, "Cement Paste-Quartz Bond in Autoclaved Concretes," 7th ICCC, Paris, VII-16 (1980).
30. M. Saito and M. Kawamura, "Resistance of the Cement-Aggregate Interfacial Zone to the Propagation of Cracks," Cem. Concr. Res. 16, 653-661 (1986).

31. T. Yu Lyubimova and E.R. Pinus, "Crystallization Structure in the Contact Zone Between Aggregate and Cement in Concrete," Colloid J. USSR 24 (5), 491-498 (1962).
32. J. Grandet and J.P. Ollivier, "Etude de la Formation du Monocarboaluminate de Calcium Hydrate au Contact d'un Granulat Calcaire dans une Pate de Ciment Portland," Cem. Concr. Res. 10, 759-770 (1980).
33. C.F. Scholer, "The Role of Mortar-Aggregate Bond in the Strength of Concrete," Highw. Res. Rec. 210, 108-117 (1967).
34. H. Hornain, B. Mortureux, and M. Regourd, "Physico-Chemical and Mechancial Aspects of the Cement Paste-Aggregate Bond," Coll. Int. Liaisons Pâtes de Ciment Matériaux Associés (Toulouse), C56 - C65 (1982).
35. M. McN. Alford and A.B. Poole, "The Effect of Shape and Surface Texture on the Fracture Toughness of Mortars," Cem. Concr. Res. 9, 583-589 (1979).
36. C. Perry and J.E. Gillott, "The Influence of Mortar-Aggregate Bond Strength on the Behavior of Concrete in Unaxial Compresson," Cem. Concr. Res. 7, 553-564 (1977).
37. K.M. Alexander and J. Wardlaw, "Dependence of Cement-Aggregate Bond-Strength on Size of Aggregate," Nature 187, 230-231 (1960).
38. P.J.M. Monteiro, J.C. Maso, and J.P. Ollivier, "The Aggregate-Mortar Interface," Cem. Concr. Res. 15, 953-958 (1985).
39. A. Carles-Gibergues, J. Grandet, and J.P. Ollivier, "Evolution of the 'Aureole de Transition' with Ageing in Blended Cement Pastes," Coll. Int. Liaisons Pâtes de Ciment Matériaux Associés (Toulouse), B11 - B16 (1982).
40. P.J.M. Monteiro and P.K. Mehta, "The Transition Zone Between Aggregate and TypeK Expansive Cement," Cem. Concr. Res. 16, 111-114 (1986).
41. J.P. Ollivier and J.C. Maso, "Control of Hydration of C_3A by the Sulfates in the Contact Zone of Cement Paste and Aggregate," in Proc. Int. Sem. Calcium Aluminates,Turin, Italy, 1982, 210-218, Polytechnico de Turino, Italy (1983).
42. P.J.M. Monteiro and P.K. Mehta, "Ettringite Formation on the Aggregate-Cement Paste Interface," Cem. Concr. Res. 15, 378-380 (1985).

I. INTERFACE SIMULATION MODEL

INTRODUCTION

The origins of the interfacial zone which develops between cement paste and aggregate in concrete can be visualized as a two-step process. During the mixing of concrete, micrometer-sized cement particles are brought into contact with the surfaces of both fine and coarse aggregate. Transport can occur either through air or a thin film of water. Once initial packing has taken place, subsequent chemical reactions occur between the cement particles and the surrounding water which ultimately fill the interparticle voids with hydration products.

To date most of the experimental work reported in the literature has been descriptive, concentrating on exploring changes in bulk chemistry and porosity across the interfacial zone. Although this work is important, we feel that the observations are merely a reflection of the efficiency of the initial packing of cement particles against aggregate surfaces. Thus a knowledge of how particles pack against surfaces could be quite valuable to the cement chemist both in terms of explaining already documented material as well as a design aid to produce a better concrete.

Traditionally, an experimental approach has been used to examine the geometrical aspects of random packing (1-6). For example, using mathematical modeling and experiments, it has recently been shown that denser packing of cements, sand and aggregate led to improved workability, and a stronger, less permeable concrete (7,8). As powerful as the method is, comprehensive investigations were often not practical because the experiments were tedious and time-consuming. However, in the last two decades, computer simulation has become more and more of an attractive alternative (9-21). The entire range of packing problems, including the packing of particles against surfaces have been studied using such simulations.

It has been a long-held belief that, in composite materials such as concrete, porosity near the interface between different phases, e.g, cement paste and aggregate, is higher than that in the bulk material. Therefore, the higher porosity in the interfacial region is often viewed as detrimental. The high porosity near an interface between cement paste and aggregate has been quantified by using advanced image analysis techniques (22). However, using experimental means alone, one is not able to identify the cause of the higher porosity near the interface. It can only be postulated that the local packing of cement particles near the surface of the aggregate is poor (23).

As we report below, by using computer simulations, one can run numerous experiments in a relatively short time and in this way easily display the build-up of high

porosities near a surface, porosities which can be attributed to the so-called wall effect (11). Recently, Garboczi and Bentz used such an approach to investigate the cement paste-aggregate interfacial zone in concrete (24).

The problem associated with using a computer simulation is how accurately it simulates a real process. All of the existing simulation methods invariably involve sequential addition of particles to an existing accumulation of particles. Normally, there is no interaction between particles. Programs of this type neglect phenomena such as flocculation, agglomeration, and clustering. For example, cement paste is always flocculated unless it is batched with an effective dispersant (23), and even in this instance, flocculation is not entirely eliminated. Our simulation is slightly different in that it was designed to emulate simultaneous packing of a large number of particles. Therefore particle interactions could be build into the program. The degree of agglomeration is controlled by a user-definable parameter, referred to as sticking probability. It is worth noting that out computer program is more appropriate to model physical mechanisms (packing of hard spheres) rather than chemical mechanisms dealing with hydration and the development of pore structures. At early stages, after water and solid are mixed, other than surface protonation ($Ca^{++} = 2H^{+}$), no significant chemical reaction occurs (25,26). Therefore, the initial packing of cement particles against the surface of aggregates can be considered to be mainly a physical process resulting from the mixing of dry ingredients with water.

For the purpose of this report, we are assuming that the aggregate is moist and that cement particle transport occurs through a thin film of water adhering to the aggregate surface. Depending on surface charges, the cement particles will experience different degrees of flocculation as they move toward the aggregate surface.

The following sections contain a description of the simulation algorithm and a series of simulated interfacial pore structures illustrating the effect of four variables, initial particle density, sticking probability, amplitude of motion and distance to aggregate surface, on interfacial porosity.

Discussions will focus on the physical interpretations of the generated interface porosity profiles and other phenomena observed in the simulations. For example, one set of simulations suggests that a concrete which exhibits a large degree of flocculation would benefit from very gentle rather than vigorous mixing. In this instance, gentle mixing apparently leads to better packing and lower porosity at the interface.

SIMULATION ALGORITHM

The program is written in C language and will run on an IBM or compatible with an EGA graphics adaptor. The buildup of particles at the interface can be followed by watching

the monitor screen (see Figure 1). The bottom line in this figure represents the aggregate surface, and cement particles are represented by spheres of equal of unequal sizes. The diameter and, if any, the distribution of sphere size, are user-definable. In this instance, they are all 12 pixels* in diameter. Particles generated by the computer are placed at random in a rectangular area at a user-definable distance above the bottom line (aggregate). The size of the rectangular area and the original packing density are also user-definable. In this instance, the size of the rectangular area has been fixed at 640 × 150 pixels and packing density was varied, 0.4 and 0.2, respectively. Particles can be generated set by set or all at once. The next set of particles will be generated when the previous set of particles have settled at the interface. The total number of sets of particles is user-definable. In this instance we have used a single set of particles. The initial packing density can be viewed as a volume-defined water/cement (w/c) ratio. The 0.4 simulation contains 40 volume% spheres and 60 volume% void (water filled). The distance to the interface can be viewed as the thickness of the water film surrounding the aggregate. We are assuming that surface active agents such as superplasticizers reduce surface tension and the thickness of the water film. In order to emulate this difference, the distance to the interface was alternately set at 50 and 200 pixels.

Particles move towards the bottom line at random. Particles are not allowed to move upward. This limitation can be considered to simulate compaction associated with any form of particle packing. It can be referred to as directed randomness (27). Alternatively we could have chosen another method used in some random aggregation simulations (28): if a randomly moving particle moves too far away from the surface, it is replaced by a re-generated particle. We chose the directed randomness method because it seemed more realistic. Suspended cement particles come in contact with aggregate surfaces during mixing. The aggregate is usually wet before the addition of the cement powder. As a result there exists a discrete water film through which the cement particles must move. Most mixers use circular motion of some sort to aid in the mixing process. The large aggregate tends to pack together, held in place by centrifugal motion and gravity, the paste tends to flow around the large aggregate. We have assumed that mixing, predominantly shearing, imparts enough energy to the cement particles so that they are directed towards the aggregate surface, penetrate the water film, and eventually pack against the aggregate. Therefore, the randomness of movement simulated by the computer does not represent any specific mechanism associated with Brownian movement. Another reason for choosing

* A pixel is the smallest spot a computer is able to define. Our monitor screen is 640 pixels wide and 350 pixels high.

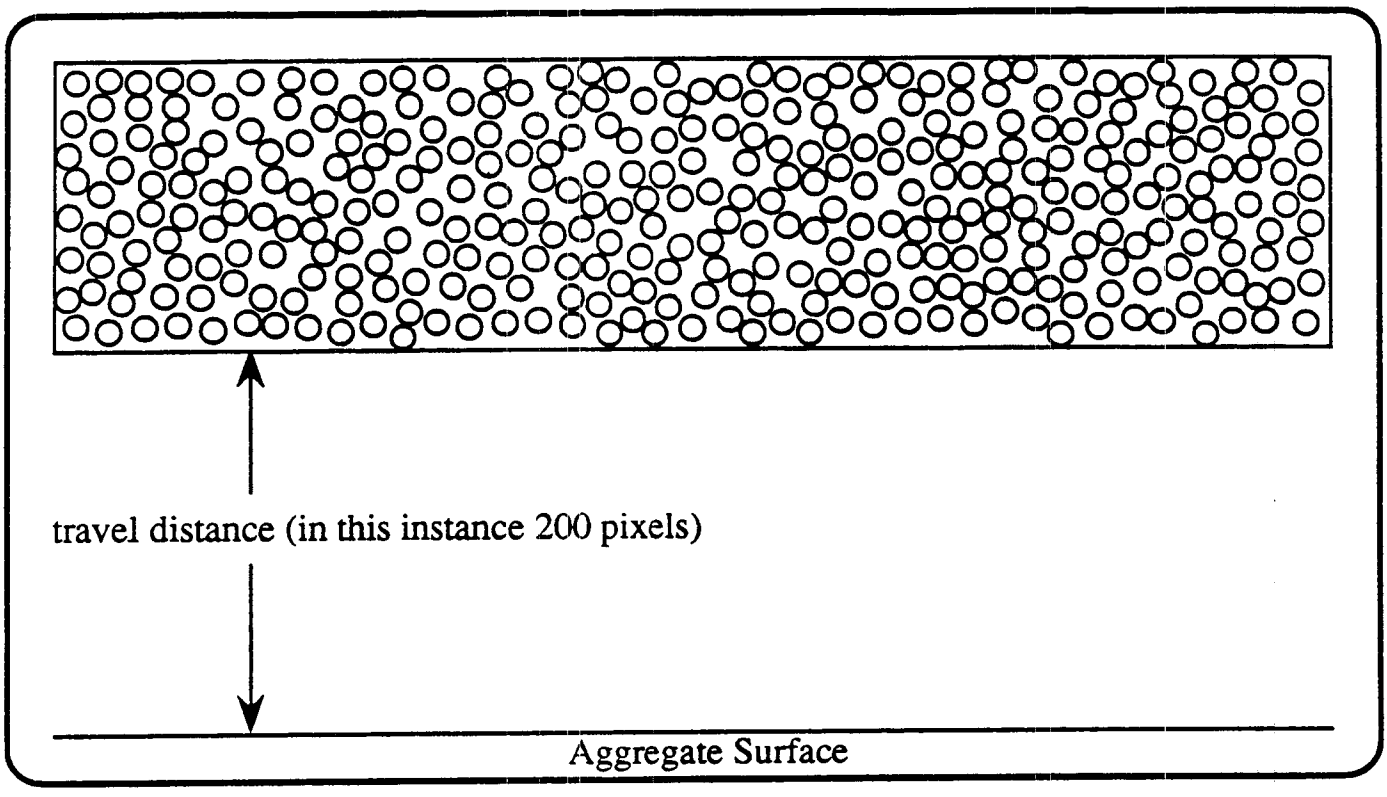

Figure 1. Computer monitor screen showing various components of the simulation. Rectangular area at top is where particles are generated at random (640 × 150 pixels). Travel distance represents the water film surrounding moist aggregate particles, and the bottom line represents the aggregate surface. Monitor screen is 640 pixels wide and 350 pixels high.

directed random movement is that agglomeration of particles during ballistic movement cannot take place even if particles are given a discrete sticking probability. Another way to form agglomerates is to randomly select a pair of neighboring particles or clusters and define them as a new cluster (29). Once again we chose the directed random movement method because it seemed more realistic; clustering seems more appropriate for modeling nucleation and growth. It is worth noting that if no random movement is involved, simultaneous packing and sequential packing should not produce any significant differences. Our microcomputer contains only one CPU, therefore real simultaneous movement of particles is impossible. Real simultaneous movement of particles can be approached only by reducing the sequential movement of each particle to an infinitely small step.

The magnitude of particle movement is randomly selected according to a user-defined parameter called amplitude of motion. The smaller the amplitude, the more nearly simultaneously the particles move. We are correlating amplitude of motion with the energy imparted to the system by mixing. We are assuming that particles will move further relative to each other and the interfaces if mixing is vigorous. When two particles or clusters of particles strike one another, the computer will determine if they will stick together, according to a user-defined parameter called sticking probability. A single or two different probabilities may be used for head-on and side by side collisions. In the present paper, a single value was used. Sticking probability is clearly related to the degree of flocculation which occurs in a given cement paste. We are assuming that a surface active agent such as a superplasticizer reduces interparticle attractions and thus reduces the degree of flocculation the cement particles experience. For purposes of the report, the action of such agents was emulated by the varying sticking probability from 1% (superplasticized) to 10% (non-superplasticized). When a particle cluster reaches the interface, it will become permanently attached and be referred to as an 'interface particle/ cluster.' In addition, any particle/cluster will become an 'interface particle/cluster' if it hits and sticks to an existing 'interface particle/cluster.'

The output of the program consists of a visual display of packed particles and a graph of interparticle porosity as a function of distance from the aggregate surface. The user can select boundaries within which the computer will calculate the porosity profile. By doing so, the user can avoid simulation boundary effects.

SIMULATION RESULTS

Table 1 represents the starting parameters used to generate the particle packings given in Figures 2 to 19. To generate figures for the report, the diameter of the particle was

Table 1. Parameters used to generate particle packings.

Figure number	Run number	Initial packing density	Sticking probability	Amplitude	Distance between aggregate surface and initial rectangular area
2, 3, 4	1	0.4	0.1	10	200
5	2	0.4	0.1	10	50
6	3	0.4	0.1	1	200
7	4	0.4	0.1	1	50
8	5	0.4	0.01	10	200
9	6	0.4	0.01	10	50
10	7	0.4	0.01	1	200
11	8	0.4	0.01	1	50
12	9	0.2	0.1	10	200
13	10	0.2	0.1	10	50
14	11	0.2	0.1	1	200
15	12	0.2	0.1	1	50
16	13	0.2	0.01	10	200
17	14	0.2	0.01	10	50
18	15	0.2	0.01	1	200
19	16	0.2	0.01	1	50

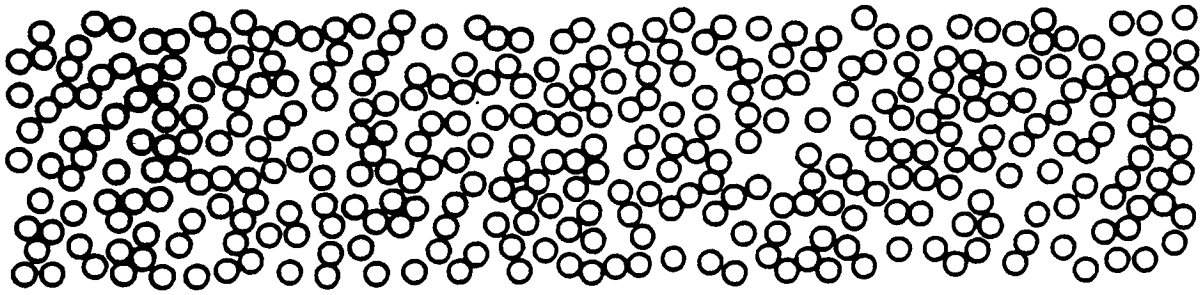

Figure 2. Initial stage of simulation. Particles have been generated and are just beginning to move towards the aggregate surface.

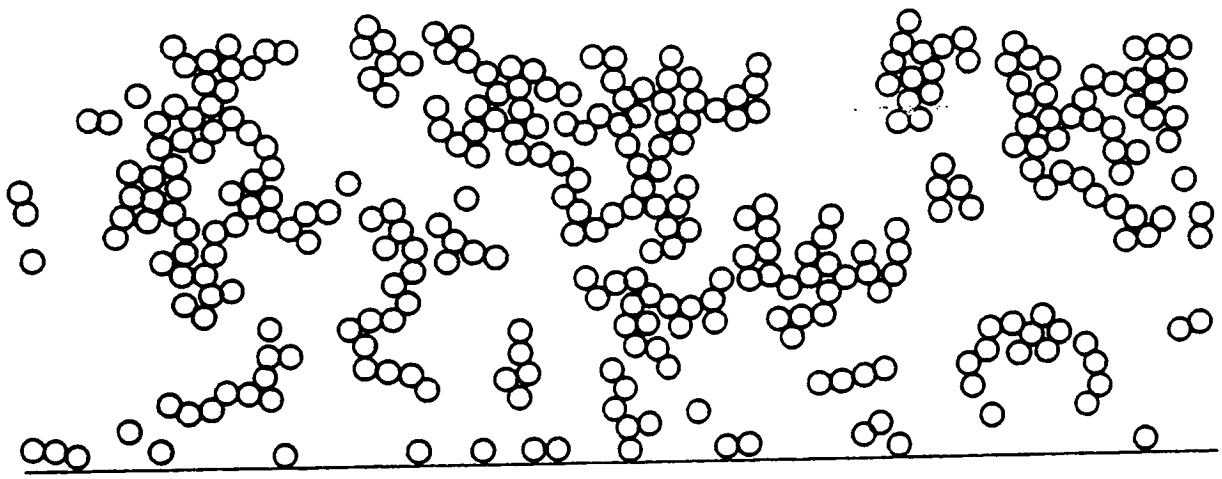

Figure 3. Intermediate stage of simulation. Some particles have settled on the aggregate surface while others are still agglomerating and moving towards it.

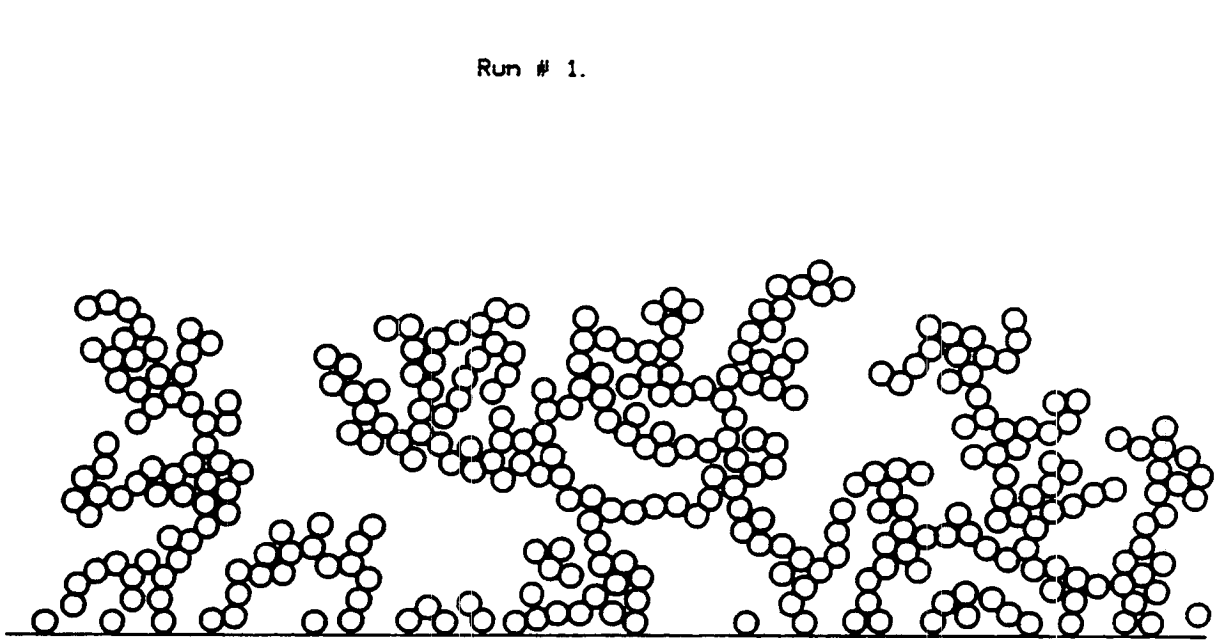

Figure 4. Final stage of simulation. All particles are fixed on the aggregate surface. Open spaces represent initial porosity, for the most part filled with water. Simulation conditions: 0.4 packing density, 0.1 sticking probability, 10 pixelsamplitude and 200 pixels to aggregate.

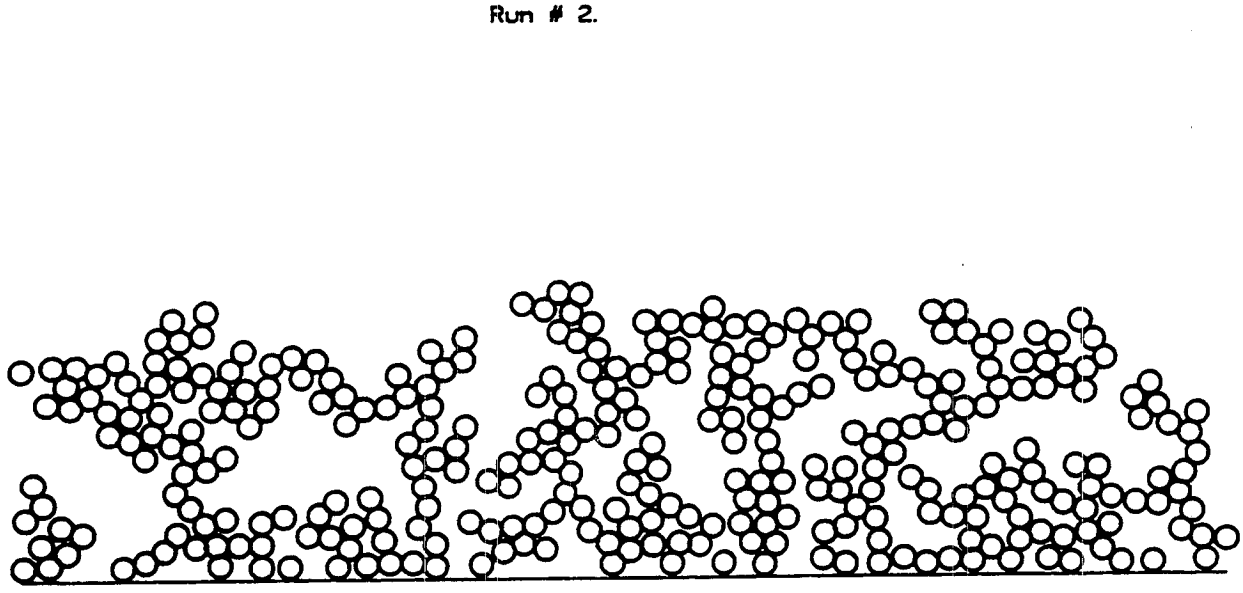

Figure 5. Final stage of simulation. Simulation conditions: 0.4 packing density, 0.1 sticking probability, 10 pixelsamplitude and 50 pixels to aggregate.

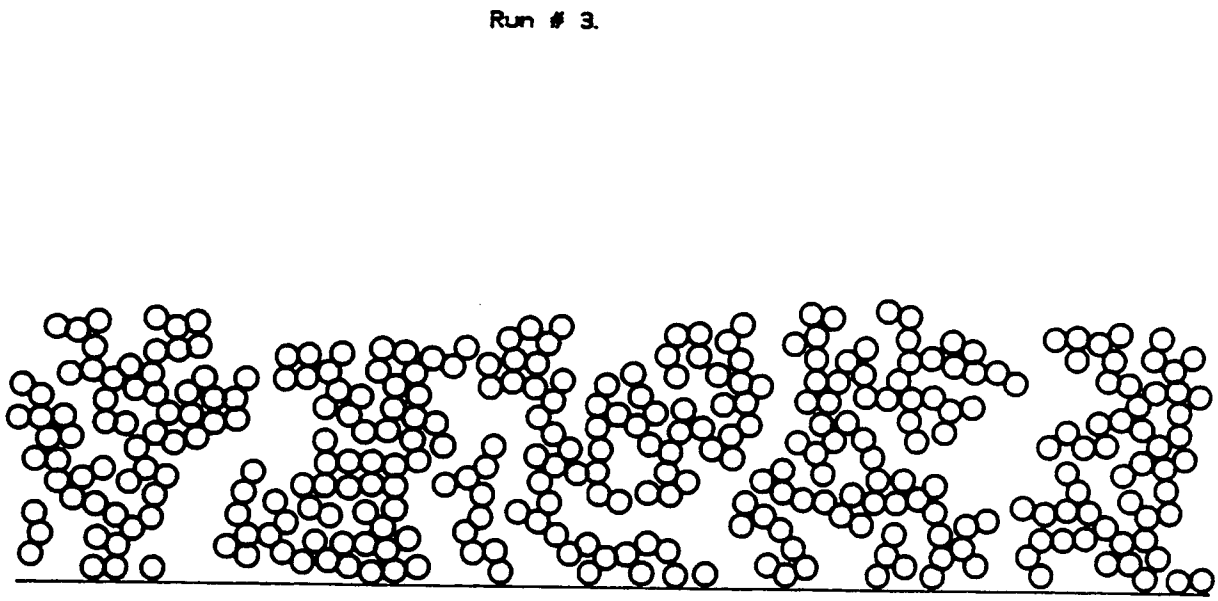

Figure 6. Final stage of simulation. Simulation conditions: 0.4 packing density, 0.1 sticking probability, 1 pixel amplitude and 200 pixels to aggregate.

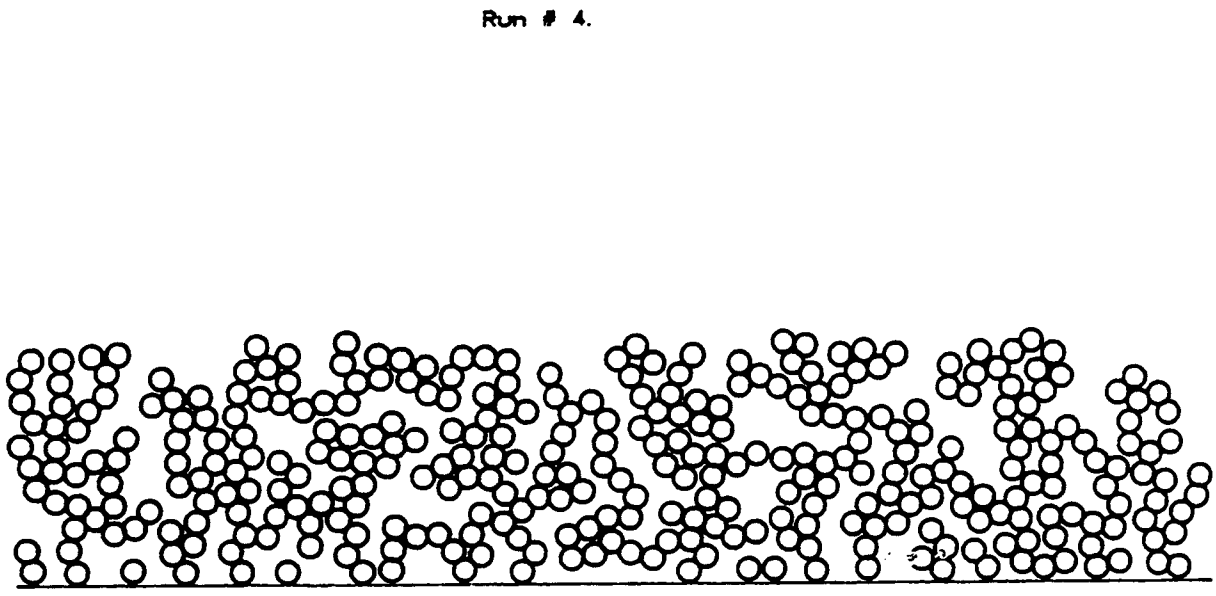

Figure 7. Final stage of simulation. Simulation conditions: 0.4 packing density, 0.1 sticking probability, 1 pixel amplitude and 50 pixels to aggregate.

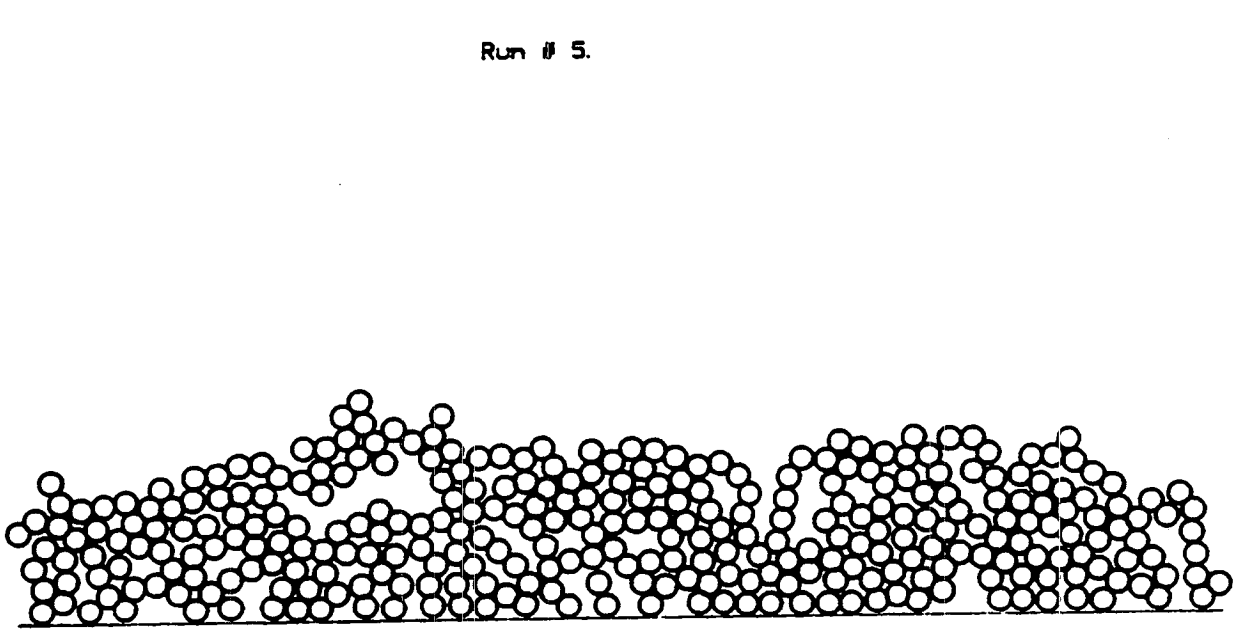

Figure 8. Final stage of simulation. Simulation conditions: 0.4 packing density, 0.01 sticking probability, 10 pixels amplitude and 200 pixels to aggregate.

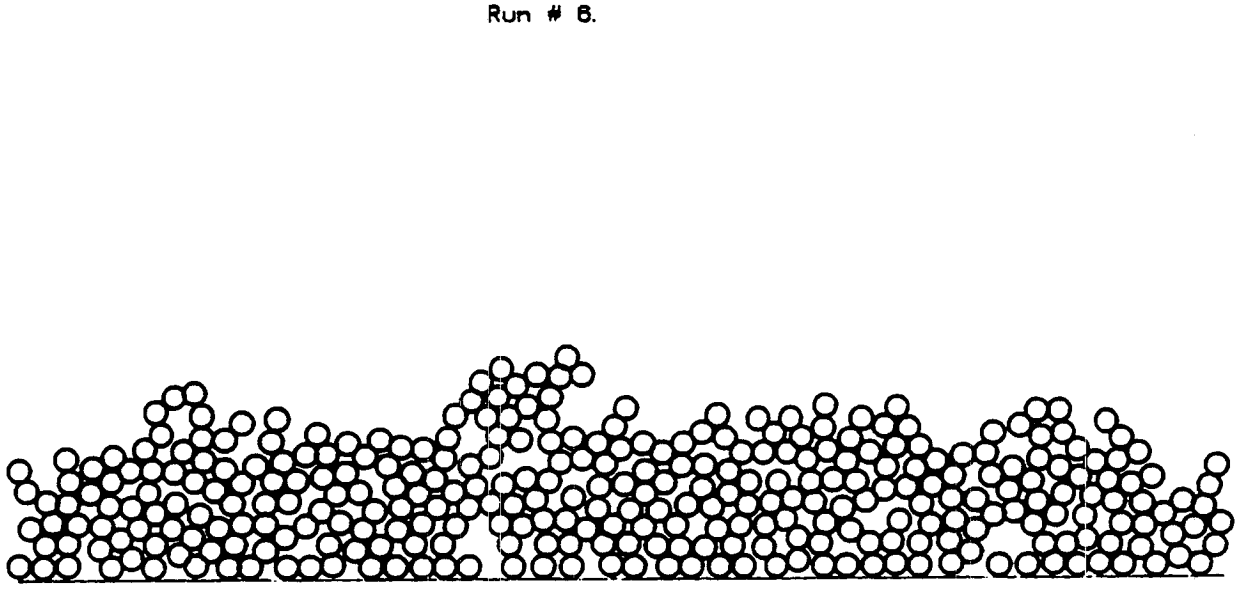

Figure 9. Final stage of simulation. Simulation conditions: 0.4 packing density, 0.01 sticking probability, 10 pixels amplitude and 50 pixels to aggregate.

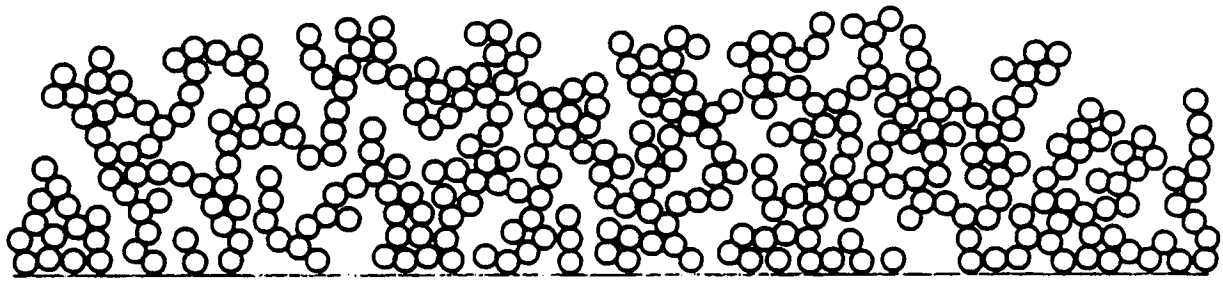

Figure 10. Final stage of simulation. Simulation conditions: 0.4 packing density, 0.01 sticking probability, 1 pixel amplitude and 200 pixels to aggregate.

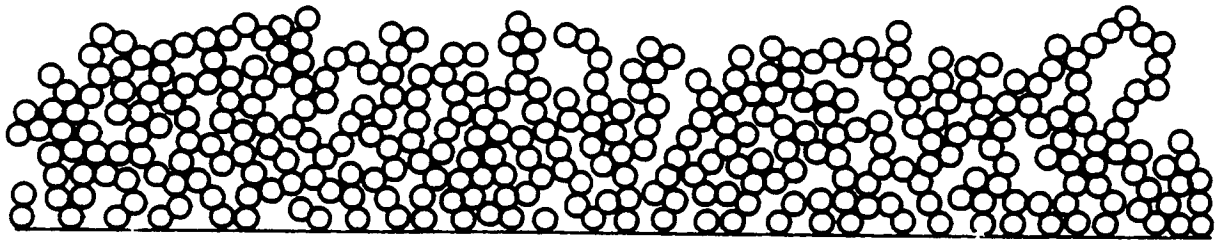

Figure 11. Final stage of simulation. Simulation conditions: 0.4 packing density, 0.01 sticking probability, 1 pixel amplitude and 50 pixels to aggregate.

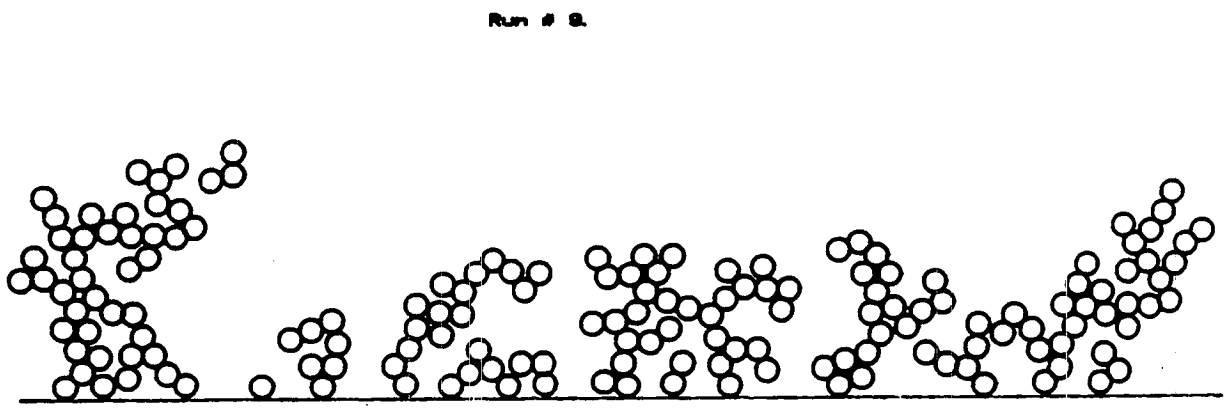

Figure 12. Final stage of simulation. Simulation conditions: 0.2 packing density, 0.1 sticking probability, 10 pixel amplitude and 200 pixels to aggregate.

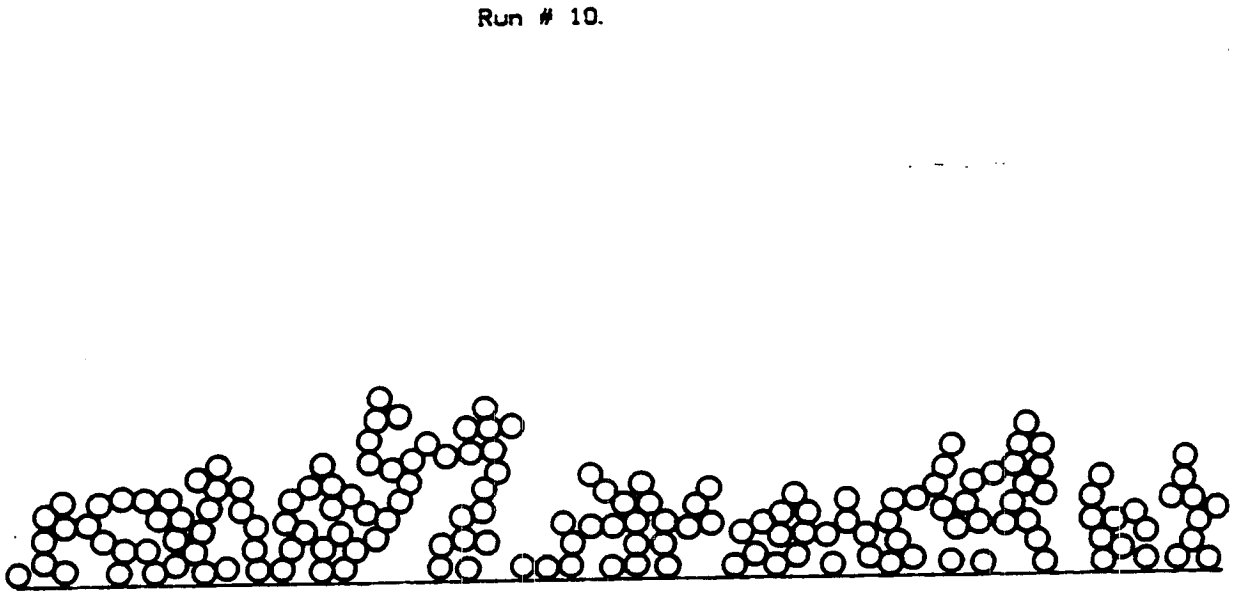

Figure 13. Final stage of simulation. Simulation conditions: 0.2 packing density, 0.1 sticking probability, 10 pixel amplitude and 50 pixels to aggregate.

Run # 11.

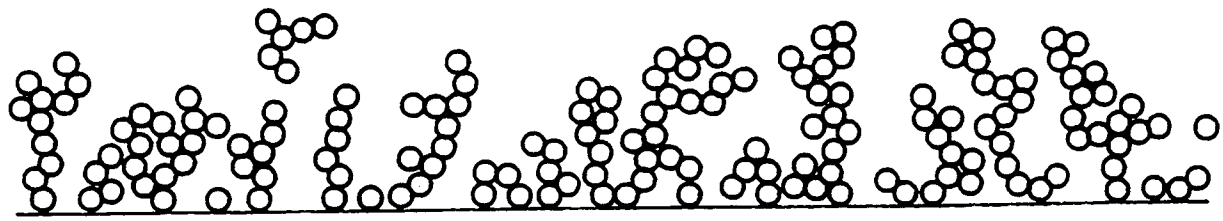

Figure 14. Final stage of simulation. Simulation conditions: 0.2 packing density, 0.1 sticking probability, 1 pixel amplitude and 200 pixels to aggregate.

Run # 12.

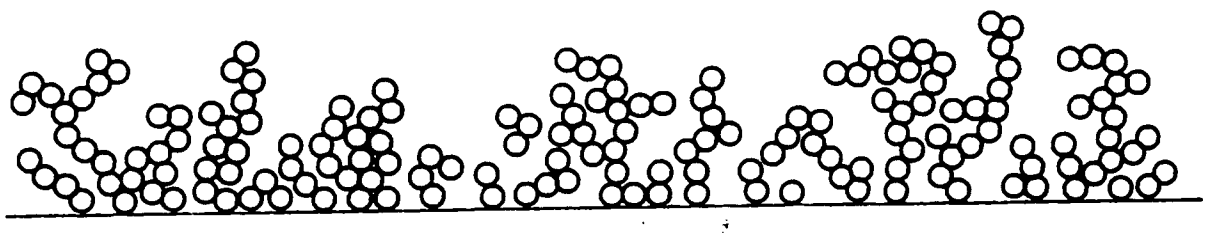

Figure 15. Final stage of simulation. Simulation conditions: 0.2 packing density, 0.1 sticking probability, 10 pixels amplitude and 50 pixels to aggregate.

Run # 13.

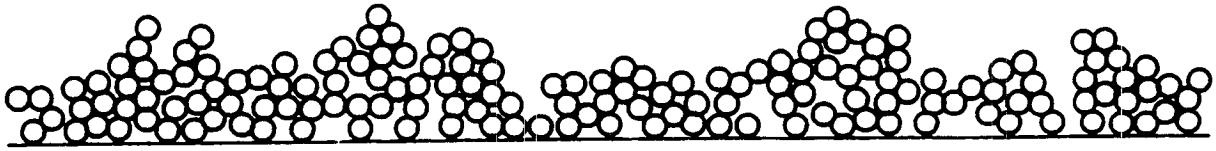

Figure 16. Final stage of simulation. Simulation conditions: 0.2 packing density, 0.01 sticking probability, 10 pixelsamplitude and 200 pixels to aggregate.

Run # 14.

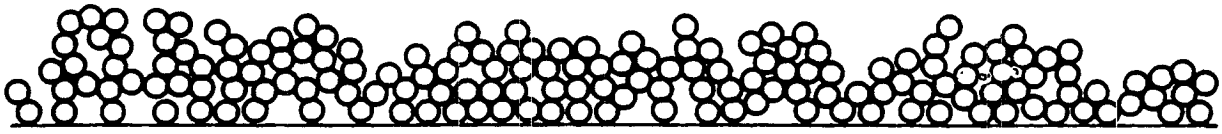

Figure 17. Final stage of simulation. Simulation conditions: 0.2 packing density, 0.01 sticking probability, 10 pixelsamplitude and 50 pixels to aggregate.

Run # 15.

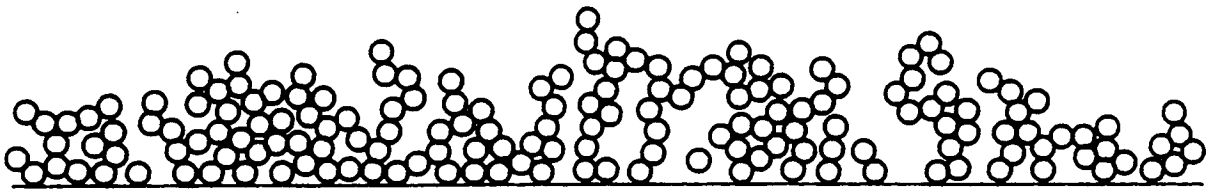

Figure 18. Final stage of simulation. Simulation conditions: 0.2 packing density, 0.01 sticking probability, 1 pixel amplitude and 200 pixels to aggregate.

Run # 16.

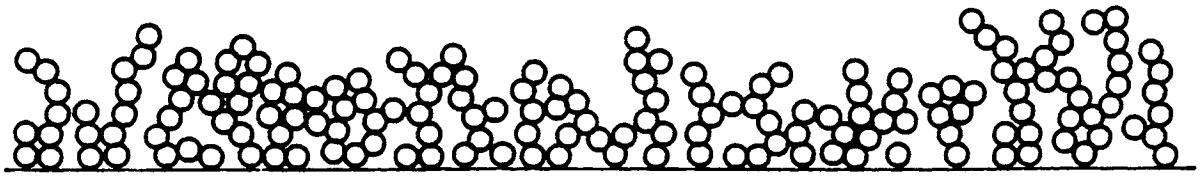

Figure 19. Final stage of simulation. Simulation conditions: 0.2 packing density, 0.01 sticking probability, 1 pixel amplitude and 50 pixels to aggregate.

fixed at 12 pixels and the original number of particles limited to a rectangular area 640 × 150 pixels in size. A 12 pixel particle was used to aid in graphical representation. It is obvious that using smaller sized particles and a larger rectangle will lead to better statistics.

Figures 2 to 4 represent different steps in the simulation process. Figure 2 shows the bottom line as a flat aggregate surface (or part of a surface) and the particles generated at random in the rectangular area (no longer shown) at a very early stage of the simulation. In this instance, the rectangular area had a height of 150 pixels. The initial packing density (% solids in the rectangular area) was 0.4. The distance between the bottom line and the rectangular area is 200 pixels. Figure 3 shows the intermediate stage during packing. In this instance, the sticking probability is 0.1. Some agglomeration is evident. Figure 4 shows the final packing. Because of the agglomeration of particles, pore structures in both bulk phase and interfacial zone are, as expected, highly porous.

Comparing Figures 4 and 8, Figures 5 and 9, Figures 6 and 10, Figures 7 and 11, Figures 12 and 16, Figures 13 and 17, Figures 14 and 18, and Figures 15 and 19 shows that a change in sticking probability from 0.1 to 0.01 will definitely affect the pore structure in both the bulk and the interfacial zone. For these runs, the sticking probability of head-on or side-by-side collisions were the same. As one might expect, if particles do not agglomerate, resulting packing will be more efficient. A plot of porosity as a function of distance from the interface (measured in pixels) for Figure 5 (0.4, 0.1, 10, 50) and Figure 9 (0.4, 0.01, 10, 50) is given in Figure 20. The plot is representative of the group as a whole. Simulations with lower sticking probability always result in lower porosity and better packing in the interfacial zone. Very low sticking probabilities may simulate the effects of a water-reducer or any cement dispersant which reduces the degree of flocculation of the cement paste particles.

Comparing Figures 4 and 5, Figures 6 and 7, Figures 8 and 9, Figures 10 and 11, Figures 12 and 13, Figures 14 and 15, Figures 16 and 17, and Figures 18 and 19, it can be seen that the distance between the aggregate surface and the rectangular area does not affect the final particle packing to any great extent. The plots given in Figure 21 for distributions given in Figure 6 (0.4, 0.1, 1, 200) and Figure 7 (0.4, 0.1, 1, 50) are once again fairly typical of the group as a whole. There is a suggestion that a smaller water film results in a less porous interface. In light of this, it would appear that the major action of a superplasticizer is the reduction of interparticle attractions, rather than the reduction of water film thickness.

Comparing Figures 4 and 6, Figures 5 and 7, Figures 8 and 10, Figures 9 and 11, Figures 12 and 14, Figures 13 and 15, Figures 16 and 18, and Figures 17 and 19, one can see the effect of the amplitude on the particle packing. Amplitude of movement can be considered as a factor of the simulation which affects the degree of simultaneous movement of the particles (i.e. energy of mixing). A smaller amplitude leads to a smaller incremental step which

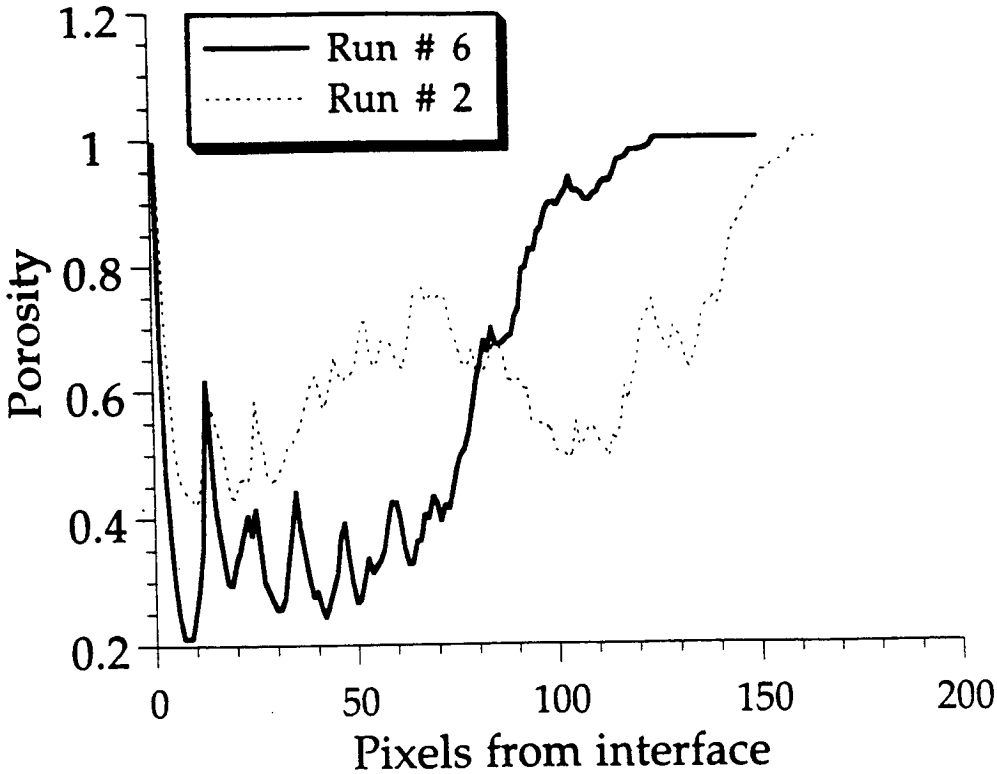

Figure 20. Effect of sticking probability (1, 10) on porosity profiles. Run #6 = 1%. Run #2 = 10%. Other variables were fixed (0.4, 10, 50).

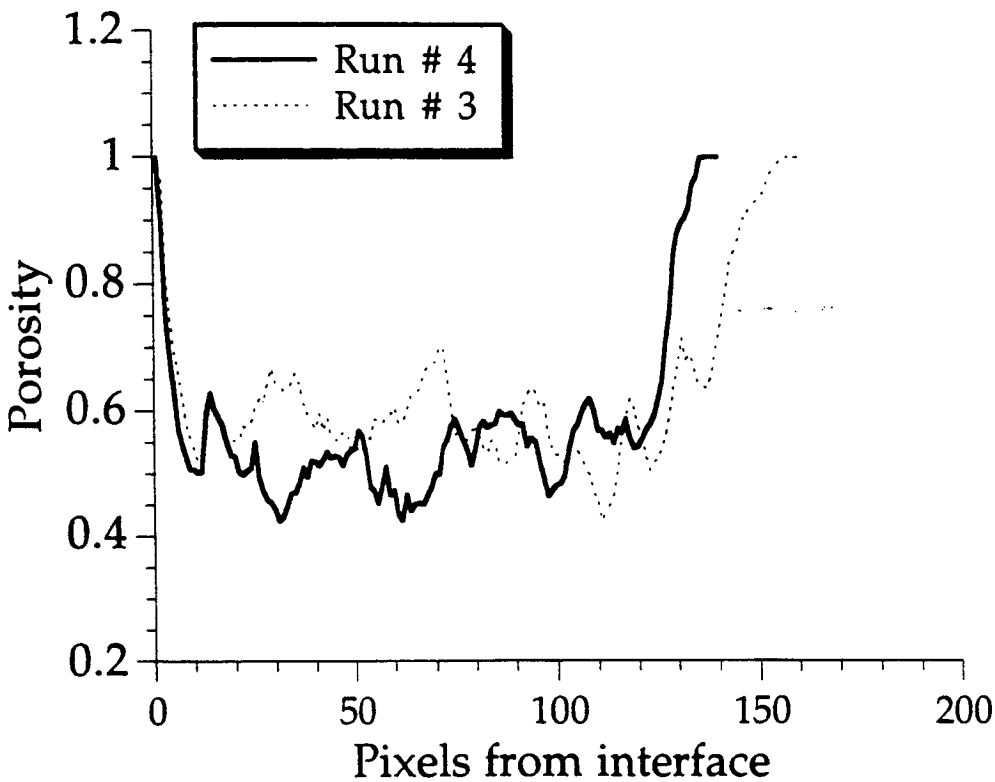

Figure 21. Effect of distance to aggregate surface (50, 200) on porosity profiles. Run #4 = 50. Run #3 = 200. Other variables were fixed (0.4, 0.1, 1).

simulates near-simultaneous movement of particles. The effect of amplitude of motion is not an entirely independent variable. It was found that sticking probability influenced the outcome of the simulations. In those runs made with a 10% sticking probability (see Figure 22A) the simulations having a small amplitude of motion (1 pixel) exhibited better packing than their 10 pixel counterpart. In the present case, the porosity profiles of the individual simulations are very "noisy" and comparisons are hard to make. Thus, each simulation was run an additional four times and the average of five simulations were plotted against each other. This reduced the noise, eliminated overlap beyond the first particle, and confirmed the observation that run #3 is definitely less porous than run #1. Conversely, if the sticking probability was reduced to 1%, then the greater amplitude of motion simulation (10 pixels) exhibited better packing than its counterpart (see Figure 22B). This is an interesting and unexpected result. A priori, it was assumed that more vigorous movement (mixing) would lead to better packing at the interface. These results suggest that the agglomeration of particles during mixing is an important phenomenon which can have a significant impact on both interface and bulk porosity. By varying the sticking probability along with the amplitude movement of the particles one can control the degree of porosity in the packed particles.

Finally, comparing Figures 4 and 12, Figures 5 and 13, Figures 6 and 14, Figures 7 and 15, Figures 8 and 16, Figures 9 and 17, Figures 10 and 18, and Figures 11 and 19 one can see that the initial packing density has little or no effect on the final packing. This is quite obviously the case when porosity profiles of particle accumulations in Figure 4 (0.4, 0.1, 10, 200) and Figure 12 (0.2, 0.1, 10, 200) are compared (see Figure 23).

DISCUSSIONS AND IMPLICATIONS

Many investigators have shown that porosity decreases as one moves away from the surface of aggregates (30). Therefore, at least in a qualitative sense, our simulations confirm these observations. Porosity is seen to drop from nearly 100% directly at the interface to anywhere from 20 to 60% as one moves multiples of the particle diameter (12 pixels) from the interface. Not surprisingly, the sticking probability was found to have the single most significant effect in determining both interface and bulk porosity. Distance to the interface (thickness of water film around aggregate) was shown to have a lesser effect, while original particle density (w/c) had little or no effect.

What was surprising was the discovery that the amplitude of motion, which we are equating with energy of mixing, was not an independent variable. The outcome of simulations in which amplitude of mixing was varied from 1 to 10 pixels were dependent upon sticking probability. The results presented earlier seem to imply that in a highly

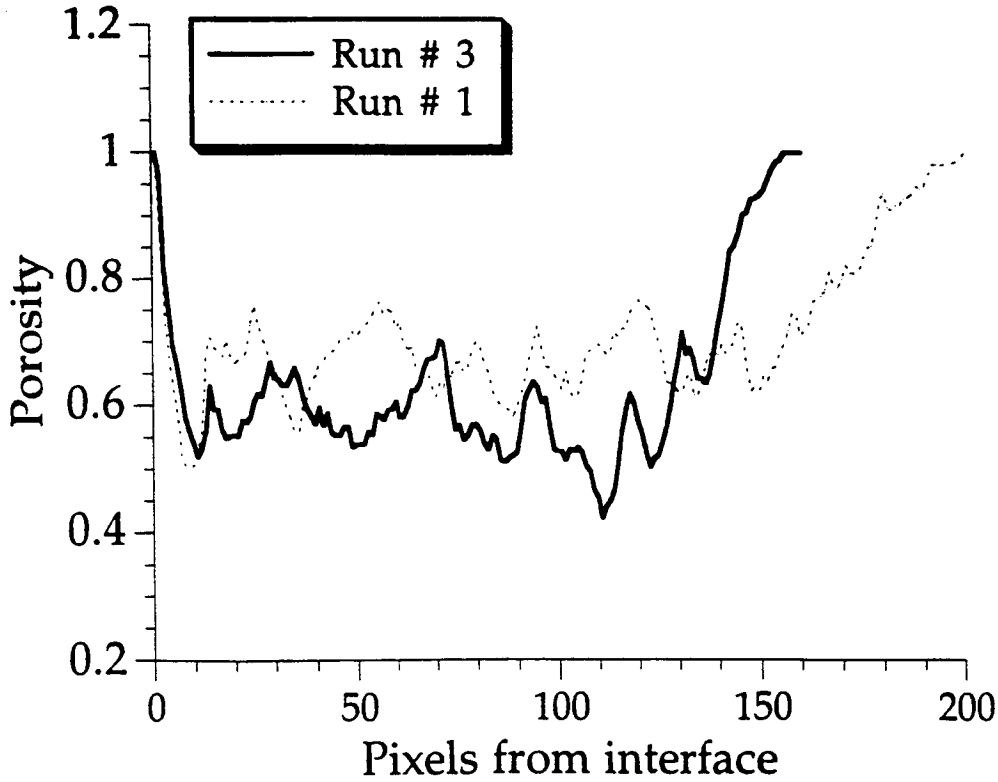

Figure 22A. Effect of amplitude of motion (1, 10) and 10% sticking probability on porosity profiles. Run #3 = 1. Run #1 = 10. Other variables were fixed (0.4, 200).

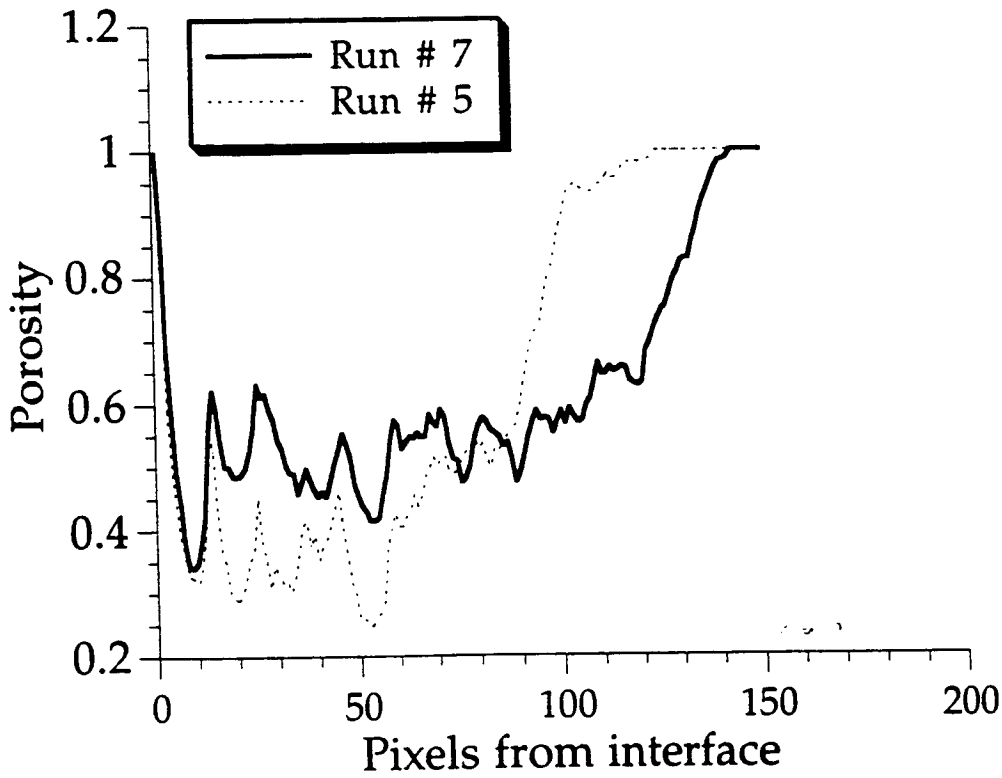

Figure 22B. Effect of amplitude of motion (1, 10) and 1% sticking probability on porosity profiles. Run #7 = 1. Run #5 = 10. Other variables were fixed (0.4, 200).

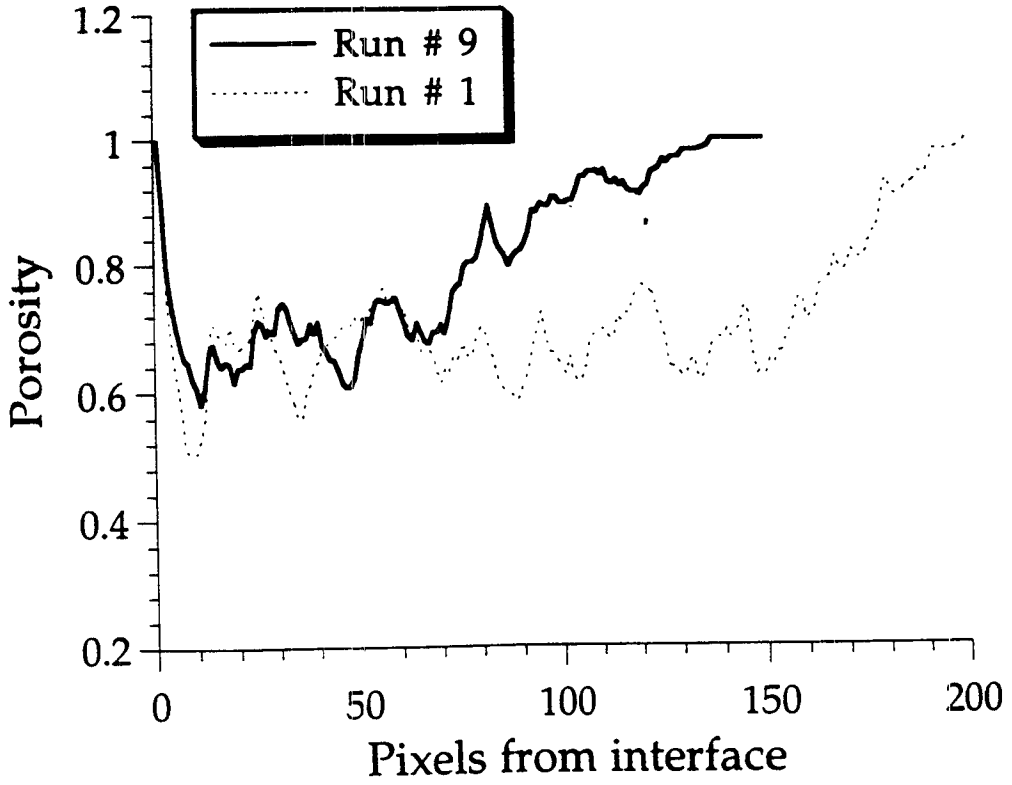

Figure 23. Effect of original particle density (0.4, 0.2) on porosity profiles. Run #9 = 0.2. Run #1 = 0.4. Other variables were fixed (0.1, 10, 200).

flocculated system, gentle mixing (small amplitude of motion) would lead to a significant porosity reduction, whereas in a non-flocculated system, a more vigorous mixing would achieve similar results. If this is correct, this suggests that a non-superplasticized concrete is best mixed gently, thereby reducing interface porosity and improving mechanical performance. At the other extreme, a superplasticized concrete should apparently be mixed as vigorously as possible to reduce interface porosity. Experiments are underway to verify these predictions.

A final observation concerns the periodicity of the porosity profiles. For example, see Figure 20. The variation in porosity is due to the formation of rudimentary layers of particles. Therefore, porosities are at a minimum at approximately 1/2 the particle diameter and reach a maximum at 12 pixels. If packing is less efficient, the periodicity is not as regular, and peaks and valleys are less intense. Nevertheless, this phenomena may explain why cracks sometimes propagate a small distance away from the exact interface between paste and aggregate. Although the voids are soon filled with hydration products, the presence of such periodicity in 2- or 3-dimensions suggests that, next to the interface itself, these planes of high porosity could act as zones of weakness between the paste and aggregate.

SUMMARY

Computer modeling has allowed us to carry out packing experiments under carefully controlled conditions, conditions which are impossible to examine experimentally. By using the described model, we were able to study the effect of four variables on the porosity distribution which developed across interfacial zones. In all cases, the experimentally documented decrease in porosity with distance from the surface of the aggregate was confirmed using this approach. Although the relevance of the results may be questionable, they do in fact point the way to new areas of research. For example, simulation results suggest that a reduction in the degree of flocculation and an increase in the energy of mixing seem to offer the best combination of variables leading to the lowest overall porosity profiles across the interfacial zone. In addition, two high porosity planes have been identified, the interface itself and a series of planes which are approximately one particle diameter apart. Results are encouraging and suggesting that further investigation, using both experimental research and computer simulation may yield even deeper insight into the nature of the interfacial pore structures which develop during mixing.

REFERENCES

1. R.K. McGeary, "Mechanical Packing of Spherical Particles," J. Am. Ceram. Soc. 44, 513-522 (1961).
2. K. Ridgway and K.J. Tarbuck, "The Random Packing of Spheres," Brit. Chem. Eng. 12, 384-388 (1967).
3. D.J. Cumberland and R.J. Crawford, "The Packing of Particles," in Handbook of Powder Technology, Eds. J.C. Williams and T. Allen, Vol. 6, Elsevier, NY (1987).
4. Do Ik Lee, "Packing of Spheres and Its Effect on the Viscosity of Suspensions," J. Paint Tech. 42, 579-587 (1970).
5. J.D. Bernal and J. Mason, "Co-ordination of Randomly Packed Spheres," Nature 188, 910-911 (1960).
6. G. David Scott, "Packing of Equal Spheres," Nature 188, 908-909 (1960).
7. SHRP–87–C201: Concrete Microstructure, First Quarterly Report—Year 2, April 1989.
8. Patrick J. Creegan, "Properly Coping with the Low Water-Cement Ratios Required by ACI 350R-83," Conc. Int., 33-36 (April 1990).
9. Einar L. Hinrichsen, Jen Feder and Torstein Jøssang, "Random Packing of Disks in Two Dimensions," Phys. Rev. A 41, 4199-4209 (1990).
10. I. Lee Davis and Roger G. Carter, "Random Particle Packing by Reduced Dimension Algorithms," J. Appl. Phys. 67, 1022-1029 (1990).
11. S.K. Chan and K.M. Ng, "Geometrical Characteristics of a Computer-Generated Three-Dimensional Packed Column of Equal and Unequal Sized Spheres with Special Reference to Wall Effects," Chem. Eng. Commun. 48, 215-236 (1986).
12. J. Rodríguez, "A Computer Method for Random Packing of Spheres of Unequal Size," Powder Tech. 47, 25-33 (1986).
13. Karl Heinz Schüßler and Lutz Walter, "Computer Simulation of Randomly Packed Spheres—A Tool for Investigating Polydispersed Materials," Part. Charact. 3, 129-139 (1986).
14. H.W. Lotwick, "Simulation of Some Spatial Hard Core Models and the Complete Packing Problem," Stat. Comp. Simul. 15, 315-331 (1982).
15. M.J. Powell, "Computer-Simulated Random Packing of Spheres," Powder Tech. 25, 45-52 (1980).
16. J.L. Finney, "Fine Structure in Randomly Packed, Dense Cluster of Hard Spheres," Matl. Sci. Eng. 23, 199-205 (1976).
17. William M. Visscher and M. Bolsterli, "Random Packing of Equal and Unequal Spheres in Two and Three Dimensions," Nature 239, ???-??? (1972).

18. A.J. Matheson, "Computation of a Random Packing of Hard Spheres," J. Phys. C 7, 2569-2576 (1974).
19. Charles H. Bennett, "Serially Deposited Amorphous Aggregates of Hard Spheres," J. Appl. Phys. 43, 2727-2734 (1972).
20. E.M. Tory, B.H. Church, M.K. Tam and M. Ratner, "Simulated Random Packing of Equal Spheres," Can. J. Chem. Eng. 51, 484-493 (1973).
21. D.J. Adams and A.J. Matheson, "Computation of Dense Random Packing of Hard Spheres," J. Chem. Phys. 56, 1989-1994 (1972).
22. Karen Scrivener, "The Microstructure of Concrete," in Materials Science of Concrete I, Eds. J. Skalny, ACers (1989).
23. Sidney Diamond, "Cement Paste Microstructure in Concrete," in Microstructural Development During Hydration of Cement, Eds. L. Struble and P. Brown, MRS (1986).
24. Edward J. Garboczi and Dale P. Bentz, "Digital Simulation of the Aggregate-Cement Paste Interfacial Zone in Concrete," J. Mat. Res. (submitted).
25. G.W. Groves, "TEM Studies of Cement Hydration," in Microstructural Development During Hydration of Cement, Eds. L. Struble and P. Brown, MRS (1986).
26. E.M. Gartner and J.M. Gaidis, "Hydration Mechanism I," in Materials Science of Concrete I, Eds. J. Skalny, ACerS (1989).
27. R. Jullien, M. Kolb and R. Botet, "Diffusion Limied Aggregation with Directed and Anisotropic Diffusion," J. Physique 45, 395-399 (1984).
28. Paul Meakin, "Diffusion-Controlled Deposition of Fibres and Surfaces," Phys. Rev. A 27, 2616-2623 (1983).
29. W.D. Brown and R.C. Ball, "Computer Simulation of Chemically Limited Aggregation," J. Phys. A 18, L517-L521 (1985).
30. S. Mindess, "Interface in Concrete," in Materials Science of Concrete, Ed. J. Skalny, ACerS (1989).

II. MICROSTRUCTURE OF CONCRETE INTERFACES

Initial work on interfaces focused on using the SEM to evaluate the nature of interfaces in actual SHRP concrete. SHRP concrete samples S89-1 to S89-7 were formulated with various cement contents and sand/aggregate ratios (see Figure 24). After curing for various lengths of time, the samples were cut with a diamond saw and solvent exchanged with ethyl alcohol. The samples were then coated with gold and the as-cut paste-aggregate interfaces examined using a variety of analytical techniques.

Interfaces between limestone aggregate and the paste were generally tight and in some instances difficult to observe in secondary electron imaging (SEI). For example, see Figure 25 (top) for a SEI photomicrograph of S89-1 and Figure 26 for a photomicrograph of S89-7. Si x-ray maps given as accompanying lower photos show the locations of interfaces. The paste contains Si as calcium silicates (anhydrous and hydrated) and silica sand, whereas the limestone does not. Occasional Si spots in the limestone are associated with noise and impurities in the limestone.

Because of the difficulty in locating interfaces with the SEM, a second approach was initiated. In this instance, small rectangular blocks were cut from either quartzite or limestone and mixed with mortar screened from actual SHRP concretes. Efforts in this area are described in the next section.

Thin section data on concretes have been presented in an accompanying supplemental report (SHRP Supplemental Report No. 3). The thin section method was very good for locating and examining actual concrete interfaces. However, the data were often mixed, i.e., in some instances interfaces were tight while in other instances they were cracked. In all cases, it was difficult to understand the underlying reasons for the observed behavior and whether or not the cracks were artifacts of sample preparation.

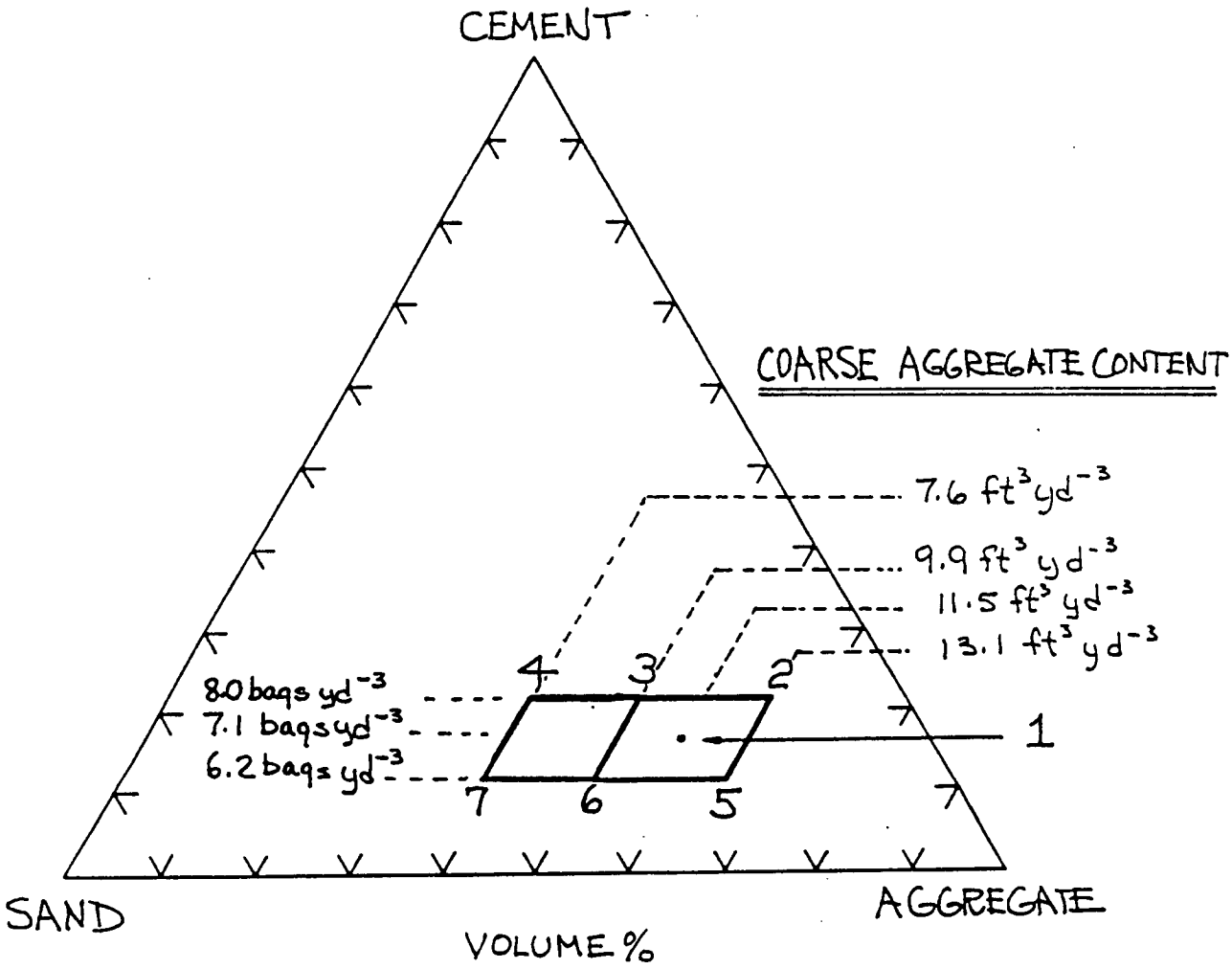

Figure 24. Figure showing relative formulations of studied concretes. The composition and w/c ratios of these concretes are described in an accompanying supplemental report (Supplemental Report No. 3).

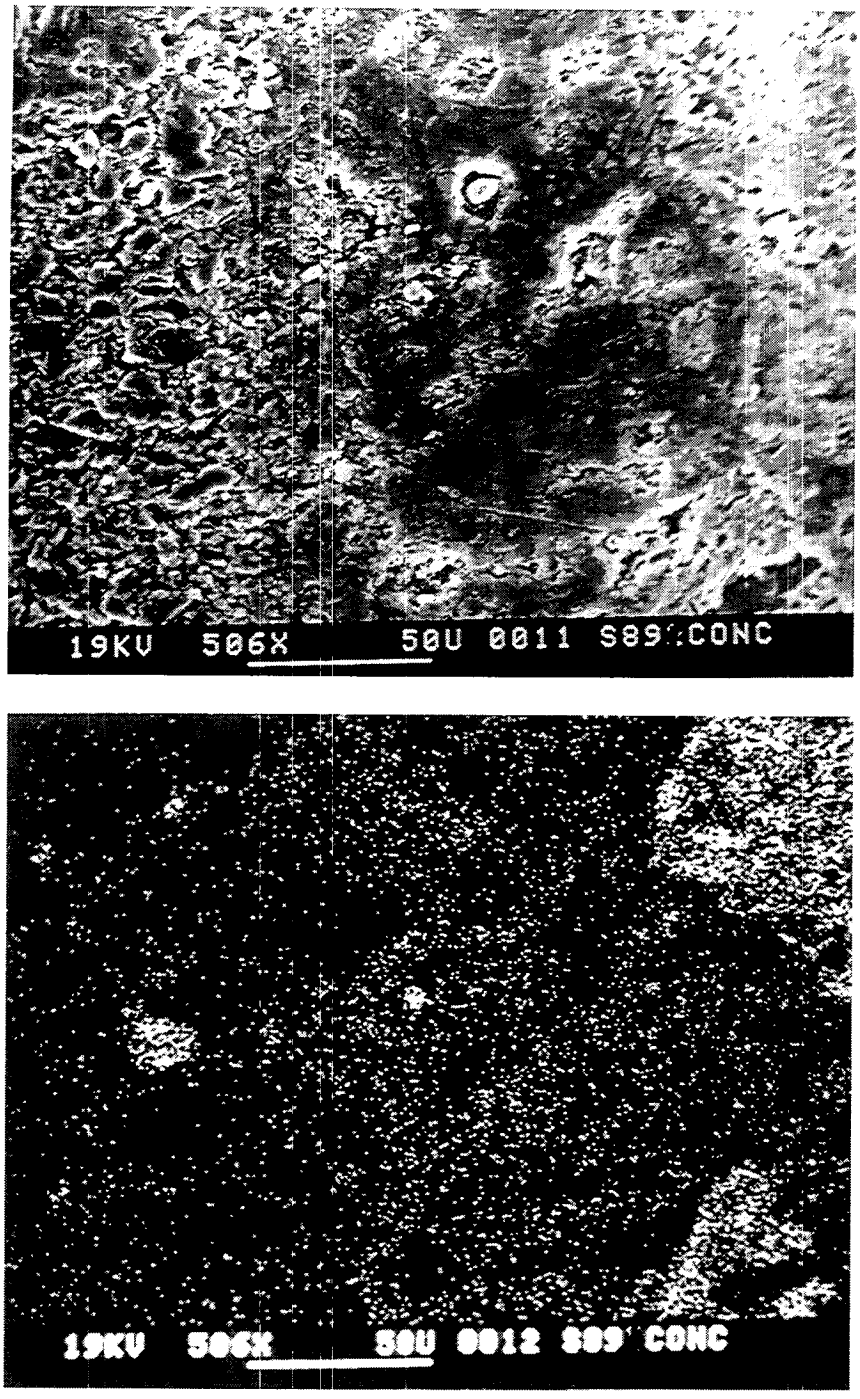

Figure 25. SEM images of S89-1 concrete. Upper photo is a secondary electron image (SEI) of paste/mortar (right) in contact with limestone (left). The Si x-ray map (bottom photo) confirms the location of the interface. Si is present in the cement paste on the right, but not in the limestone aggregate on the left.

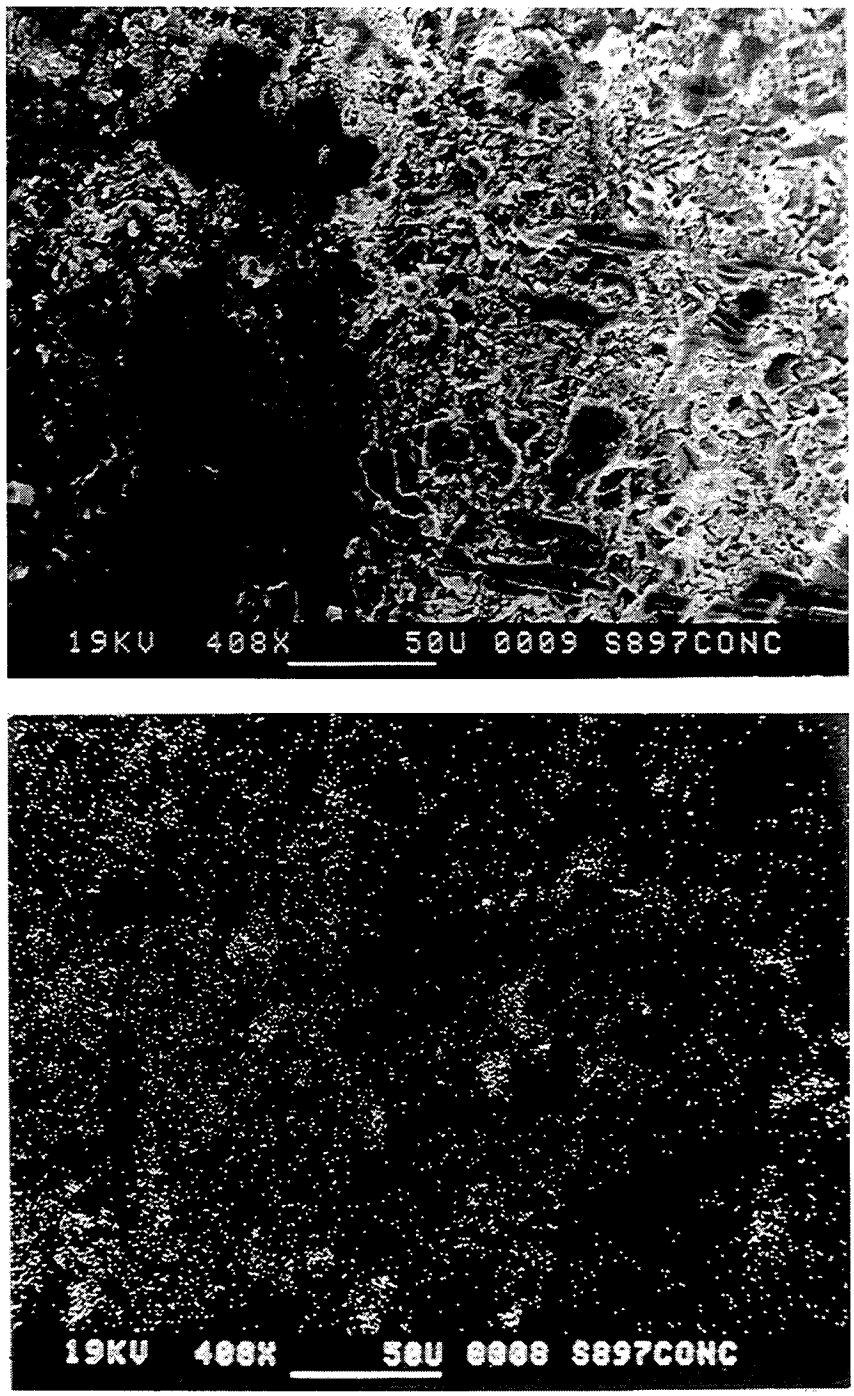

Figure 26. SEM images of S89-7 concrete. Upper photo is a secondary electron image (SEI) of paste/mortar (left) in contact with limestone (right). The Si x-ray map (bottom photo) confirms the location of the interface. Si is present in the cement paste on the left, but not in the limestone aggregate on the right.

III. MICROSTRUCTURE OF ENGINEERED INTERFACE SAMPLES

Engineered interface samples were produced for SHRP S89-3 to S89-13 samples. At first, the screened mortar was placed against the rock slab whereas in later samples the rock slab was actually mixed with the concrete, removed from the mixer with traces of mortar on its surface, and molded with screened mortar. Four-inch ID samples were cured in saturated $Ca(OH)_2$ solution, and at appropriate times cored, cut and examined with the SEM.

Interfaces of limestone-paste samples were generally stronger than their quartzite counterparts. The former were easily cut and prepared (dried), while the quartzite pair tended to separate on drying. S89-3 and S89-5 in contact with limestone slabs have been presented in earlier quarterly reports (for example, Third Quarterly Report—Year 2, October 17, 1989). Figure 27 represents an engineered interface between a quartzite slab and S89-7 screened mortar. This is one of the few quartzite samples which we were able to examine. For additional details, see Quarterly Report mentioned above.

In addition to the SEM, thin sections of some of the engineered samples were also examined with the optical microscope. Engineered interface samples for S89-11, 12 and 13 containing Class F fly ash, Class C fly ash, and silica fume cast against both limestone and quartzite slabs. Additional data are also presented in a supplementary report on Concrete Microscopy (SHRP Supplemental Report No. 3). The examples given below are of regular thin sections observed in plain and polarized light.

Figure 28 is a view of S89-11 engineered interface sample, showing the paste some distance away from the interface. The upper photo is representative of a limestone sample, the lower photo representative of a quartzite sample. What is striking in these photos and in Figure 29, which is presented next (S89-12 engineered interface sample), is the ubiquitous presence of highly birefringent overgrowths around both limestone and quartzite aggregate particles. These are probably related to higher interfacial porosity and subsequent precipitation of $Ca(OH)_2/CaCO_3$. Figure 29 represents a sample of S89-12 screened mortar cast against limestone (upper photo) and quartzite (lower photo) blocks. Once again a great deal of birefringent material is associated with the interfaces. Both of these samples (Figs. 28 and 29) contain fly ash (Class F and C, respectively). However, if we substitute silica fume (S89-13) the results are very different (see Figure 30). In this case, the birefringence associated with interfaces no longer exists. Interface porosity is of the same order as the paste. In this instance, the pozzolanic reaction may have filled interfacial porosity with calcium silicate hydrate rather than $Ca(OH)_2$. Packing of fine particles (<0.01 μm) between larger cement and fly ash particles in open pores near the interface seems also to be playing a role here. In addition, unlike S89-11 and 12, S89-13 was formulated with a

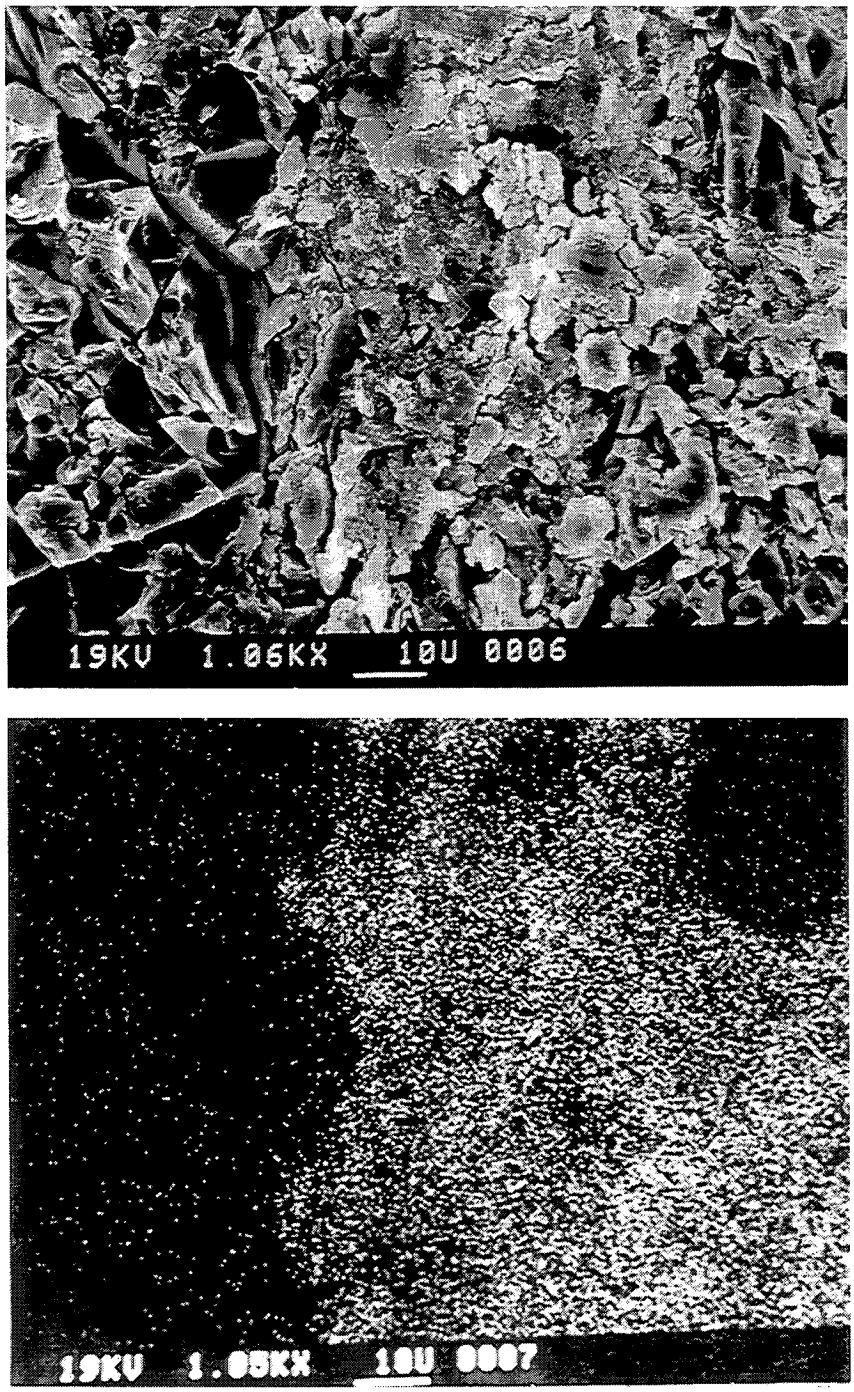

Figure 27. SEM images of S89-7 in contact with quartzite. Top view is a SEI image of the paste/mortar (right) in contact with quartzite (left). Bottom view is a Ca x-ray map. The quartz (no Ca) is on the left and the paste/mortar (Ca-rich) is on the right. A small limestone aggregate is seen at the upper right-hand corner of the paste/mortar.

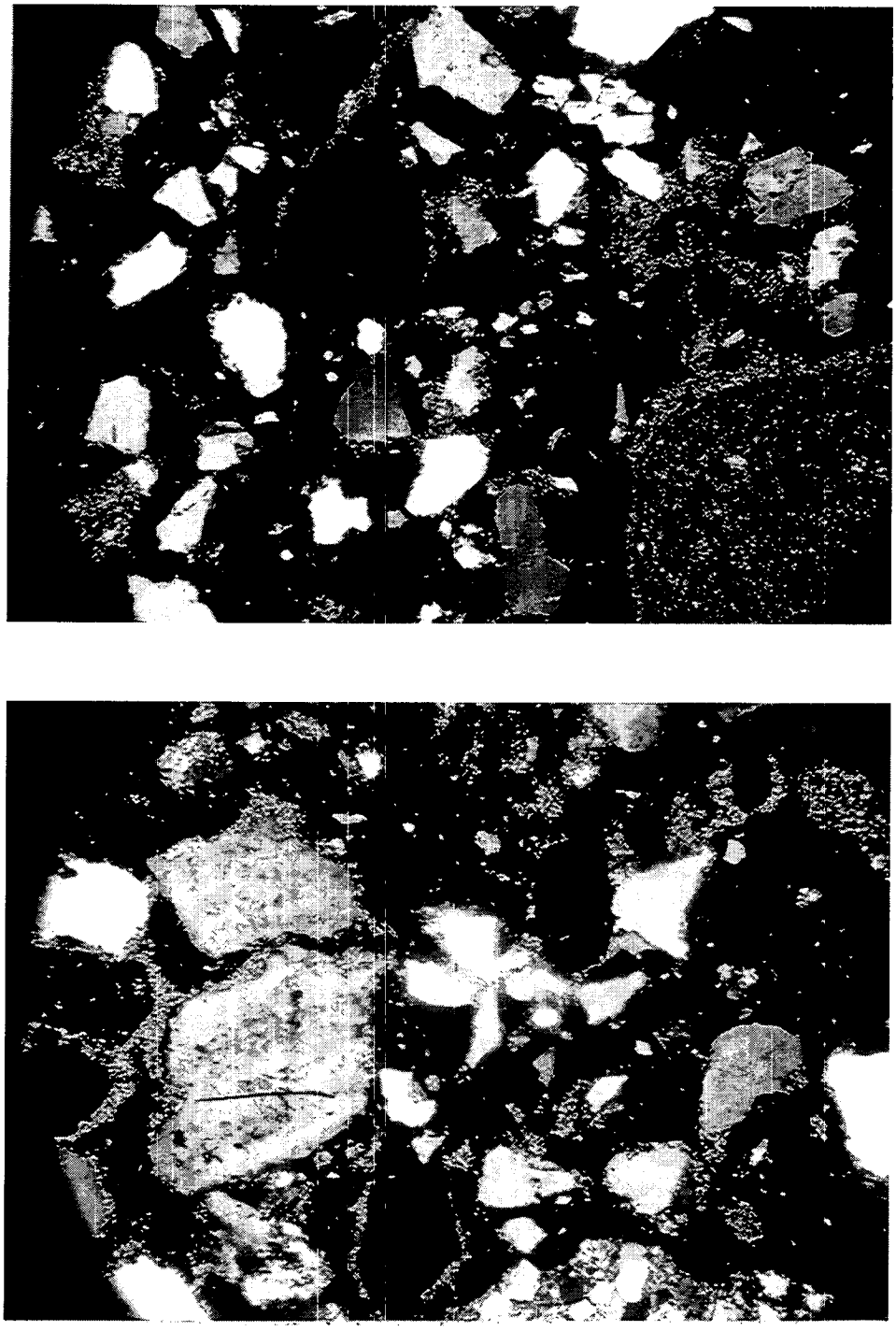

Figure 28. Thin sections of S89-11 cast against a limestone slab (top) and a quartzite slab (bottom).

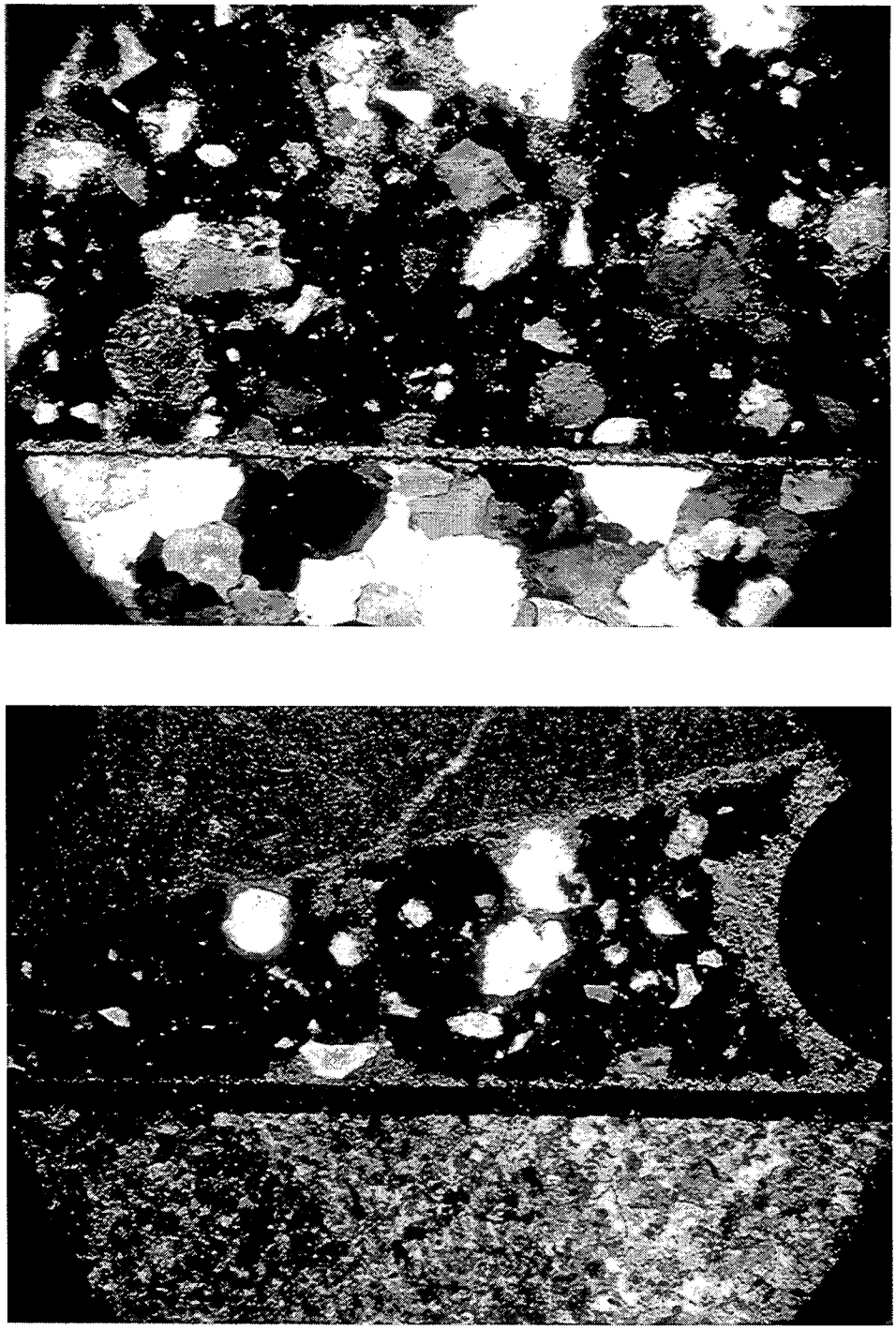

Figure 29. Thin sections of S89-12 engineered interface samples cast against a limestone slab (top) and a quartzite slab (bottom).

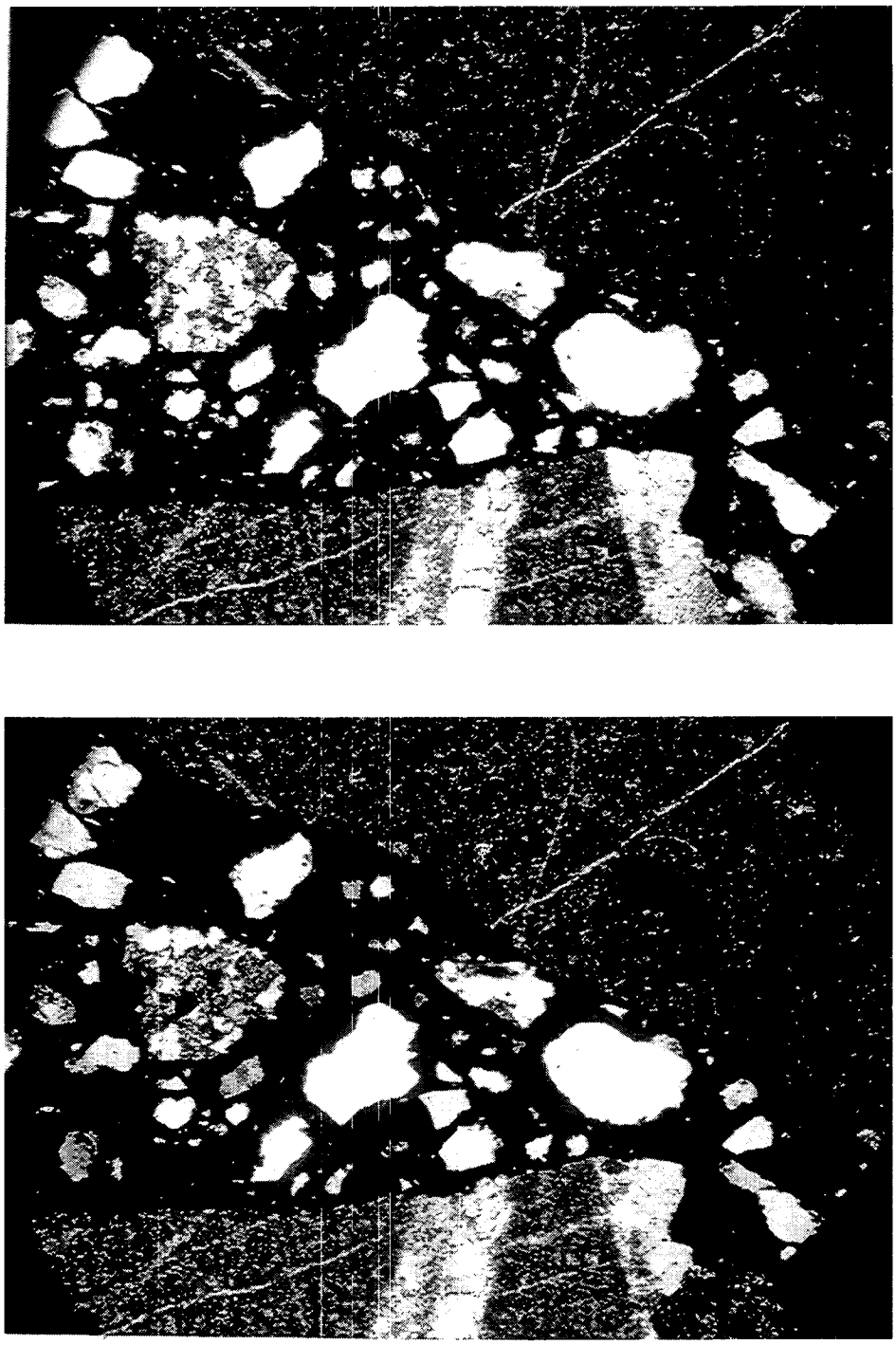

Figure 30. Thin sections of SHRP 13 engineered interface samples cast against a slab. Top view is in ordinary light. Bottom view is in polarized light. Birefringence associated with interfaces in previous figures is no longer evident.

superplasticizer. If our previously presented computer model is correct, by reducing agglomeration one should get better packing at interfaces which, at least in this instance, seems to be the case.

More often than not, engineered interfaces tended to exhibit cracks at the interface. In order to explore the possibility that these were artifacts of drying, thin slices of S89-3 engineered interface samples were allowed to dry in air. Figure 31 represents the development of such cracking at the interface over a day of drying. View (a) represents the wet sample, view (b) 30 minutes of drying, view (c) 60 minutes of drying and view (d) about 24 hours of drying. It is easy to track the development of a white band in the paste directly at the interface. At 24 hours, a distinct crack has appeared at the interface. Apparently samples are very sensitive to drying shrinkage. Realizing that purely optical or SEM methods could not resolve interfacial issues, we initiated a different set of experiments on mortars and pastes. The results of these experiments are given in the following section.

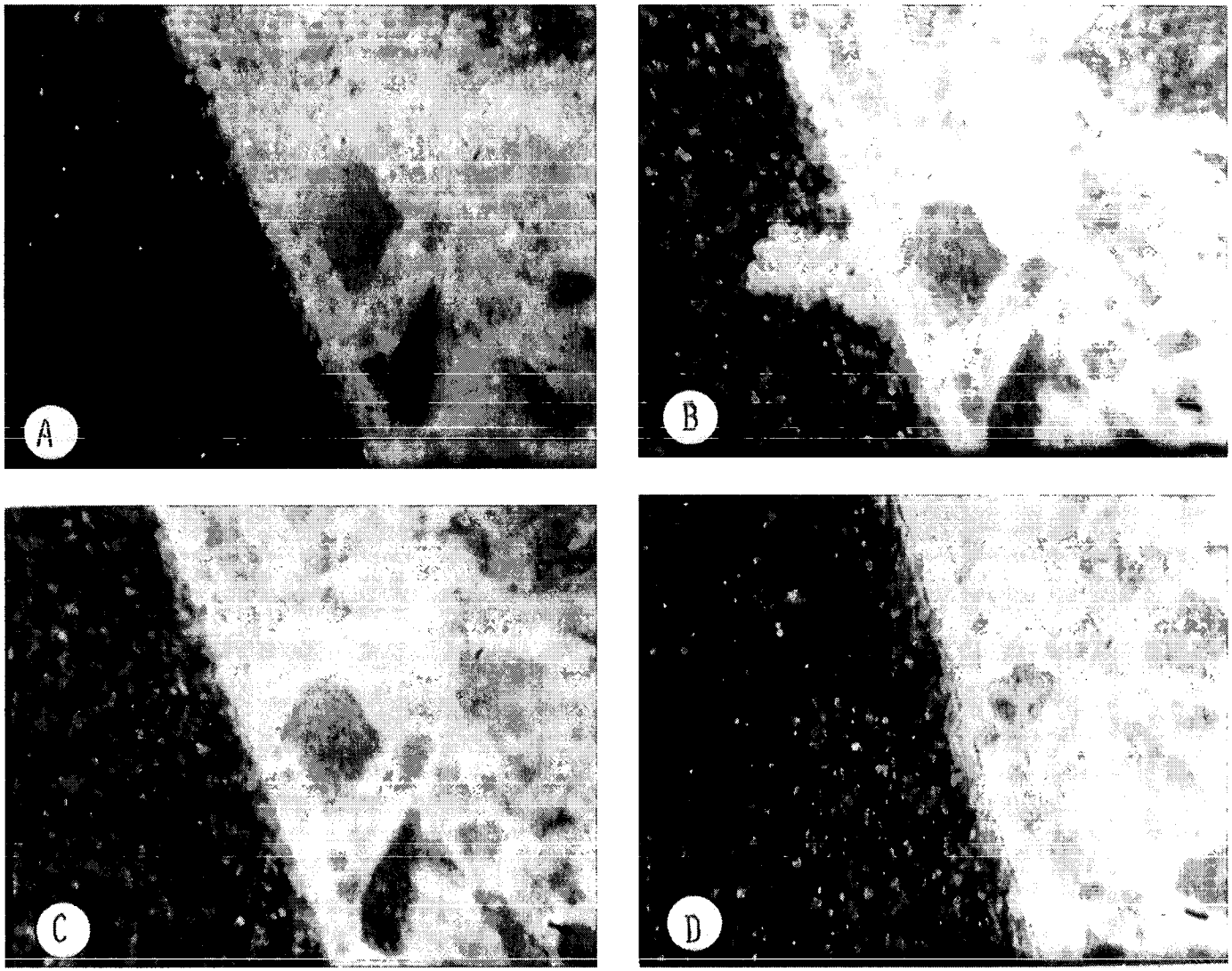

Figure 31. Effect of drying on S89-3 engineered interface samples. The limestone is on the left, the paste on the right. A = wet sample; B = 30 minutes of air drying; C = 60 minutes of air drying; D = approximately 24 hours of air drying.

IV. MICROSTRUCTURE OF PASTE/SAND INTERFACES IN MORTARS

Up to this point, it has been observed that concrete samples were difficult to study with the SEM, but satisfactory in thin sections. Thin section data suggested interfacial porosity could be eliminated through the use of silica fume and a superplasticizer. Engineered samples tended to have cracks along interface surfaces, perhaps due to drying or cutting stresses. In all cases, the data were highly subjective, cracks occurred along some interfaces and not along others. In order to deal with this uncertainty, a new set of experiments were designed and implemented. By careful design, we were able to apply additional tests and thus supplement optical or SEM examination.

It was proposed that, given a specific paste formulation (OPC or blended portland cement), a 50 volume % paste, 50 volume % sand sample containing the same paste, should exhibit 1/2 the porosity and 1/2 the permeability of the paste sample. This hypothesis was based on the assumption that interfaces were sharp and contributed no additional porosity or permeability. In reality, we knew this was not the case and expected some positive deviation from the predicted 1/2 value, but we did not know how much or how great the interfacial effect would be. These measurements were to be verified using both optical and SEM examination of the proposed mortar/paste samples.

The mortars were formulated using densities of the starting materials. See Tables 2 and 3 for densities and formulations, respectively. Samples of both paste and equivalent mortar were mixed according to ASTM C305 mixing procedures. After mixing, samples were placed in large cylindrical molds prepared from three-inch ID PVC water pipe. The samples were puddled 25 times and vibrated on a vibrating table for one minute. The molds were sealed at the top and bottom with greased glass plates held in place with rubber bands.

After curing for one day at room temperature the ends of the cylinders were uncovered and the cylinders immersed in saturated $Ca(OH)_2$ solution. At a given time, one cm diameter cylinders were cored from the larger samples. After trimming their ends, the cores were about $1\frac{1}{2}$ inches long. These were then cut in half with a diamond saw both along the axis of the cylinder and through its middle to produce four half-cylinder samples. Additional 1" core samples (permeability) were also cut at the same time. All samples were freeze dried and used in subsequent Hg-porosimetry, SEM and permeability measurements. In this instance, polished freeze-dried samples were examined in the SEM and under reflected light.

In order to verify the volume % of sand and paste in the mortars, SEM photographs taken at ~20× were subjected to image analysis. For SHRP 1-1, 14-day-old mortar, the average sand area was determined to be 43±2 volume %, while the average sand area for SHRP 1-2, 15-day-old mortar, was 50.2±6 volume %. Therefore, the 50:50 mixture design

Table 2. Density and source of starting materials.

	density (g/cc)	supplier
Type I cement	3.3	Bath, PA (Keystone Cement)
Class F fly ash (B92)	2.35	Montoursville, PA (Pa. Power and Light)
Class C fly ash (G07)	2.67	Rockport, IN (IN & MI Electric Co.)
Silica fume (G15)	2.175	Pittsburgh, PA (Elkem)
ASTM C190 sand (C778, 20-30 grade)	2.65	Ottawa, IL (Ottawa Silica Co.)

Table 3. Formulations of paste and mortars.

		weight %					flow table	calculated volume %				calculated initial porosity
		cement	fly ash silica fume	sand	water	w/c*	%	cement	fly ash silica fume	sand	water	(w/w + solids)
SHRP 1	P	74.1	--	--	25.9	0.35	88	46.4	--	--	53.6	53.6
	M	32.5	--	56.2	11.4	0.35	76	23.2	--	50.0	26.8	26.8
SHRP 2	P	60.6	15.2	--	24.2	0.32	98	37.4	13.1	--	49.4	49.4
	M	25.5	6.4	57.0	11.1	0.35	--	17.9	6.3	50.0	25.8	25.8
SHRP 3	P	57.1	14.3	--	28.6	0.40	126	33.8	10.4	--	55.8	55.8
	M	24.2	6.1	57.6	12.1	0.40	105	16.9	5.2	50.0	27.9	27.9
SHRP 1-1	P	73.0	--	--	27.0	0.37	--	45.0	--	--	55.0	55.0
	M	31.7	--	56.6	11.7	0.37	--	22.5	--	50.0	27.5	27.5
SHRP 1-2	P	58.4	14.6	--	27.0	0.37	--	34.8	12.2	--	53.0	53.0
	M	24.9	6.2	57.4	11.5	0.37	--	17.4	6.1	50.0	26.5	26.5
SHRP 1-3	P	58.4	14.6	--	27.0	0.37	--	39.6	6.7	--	53.7	53.7
	M	25.1	6.3	57.1	11.6	0.46	--	17.6	5.4	50.0	26.9	26.9
SHRP 1-4	P	65.7	7.3	--	27.0	0.37	--	39.6	6.7	--	53.7	53.7
	M	28.2	3.1	57.1	11.6	0.37	--	19.8	3.3	50.0	26.9	26.9

*Includes fly ash or silica fume where applicable.

was felt to be reasonably close to actual values. SHRP 3, 1-2, 1-3 and 1-4 were assumed to be 50:50.

In addition, a calculation was made of the interfacial porosity one might expect as a result of a 50 μm wide interface in a 57 paste:43 sand volume % OPC mortar sample (SHRP 1-1). The observed porosity data for the paste and mortar (Fig. 46 given later) was used to solve for the unknown interfacial porosity.

ASTM C190 Ottawa sand was graded to approximately 1 mm in diameter (0.5 mm radius). The paste interfacial zone around each grain is 0.05 mm thick. Using these numbers, the volume of the paste which is allocated to the interfacial zone can be calculated in the following manner:

$$\frac{\frac{4}{3}\pi\,[(0.55)^3 - 0.5^3]}{\frac{4}{3}\pi\,(0.5)^3} = 0.331\,\frac{\text{mm}^3\text{ interfacial zone}}{\text{mm}^3\text{ sand}} \quad . \tag{1}$$

Recall that the calculated volume % sand in SHRP 1-1 was 43% (by image analysis). Assuming a 100 mm^3 totalvolume of a mortar sample, one obtains:

$$43\ \text{mm}^3\text{ sand} \times 0.331\,\frac{\text{mm}^3\text{ of interfacial zone}}{\text{mm}^3\text{ of sand}} \tag{2}$$

$$= 14.2\ \text{mm}^3\text{ of paste can be attributed to interfacial zone in a 100 cc}$$
$$57\text{ paste:}43\text{ sand volume \% mortar.}$$

Using values for 3-day cured specimens (25.5 paste, 14.7 mortar)

$$\frac{(57.0 - 14.2)\ 25.5\% + 14.2\ (x\%)}{100} = 14.7\% \tag{3}$$

one arrives at a value of 26.7% for the interfacial porosity at 3 days. Equivalent values at 7, 14, 28, 56 and 90 days are: 24.6, 26.9, 24.2, 12.9 and 17.8, respectively. These values are reasonable in light of our previous experience (slightly higher than Figure 46 paste values) and values reported in the literature.

SEM

Results of previous SEM examination suggested that concrete mortar and paste samples were sensitive to drying shrinkage. Cracking was more pronounced in samples

that were freeze dried versus those that were solvent exchanged with ethyl alcohol. Photographs which follow are typical mortar-paste results for SHRP 1/1-1, 2/1-2 and 3/1-3 paste-mortar samples. When cracking was present it was random in the pastes, but tended to occur along quartz sand-paste contacts in the mortars.

Figures 32-34 can be used to compare the appearance of freeze-dried SHRP 1-1 paste and equivalent 57:43 volume % mortar samples as a function of time (14, 28 and 56 days of curing). Figures 32 and 34 were made from polished samples whereas Figure 33 is for an "as-cut" sample. The polished samples are far easier to examine, boundaries are sharp and sand grains are relatively flat. Anhydrous starting materials, seen as bright spots in the paste, are easily identifiable. In the polished sample, boundaries are diffuse and the surface of the sand grain has been noticeably roughened by the sawing procedure.

Porosity and cracking seem to be more random in the paste samples, but associated with the interfacial zone in the mortar samples. Figure 35 is a close-up of two interfaces in a SHRP 1-1 sample (quartz sand plus paste). Both are cracked at the interface. In the top photo it appears as if some of the sand has broken away and that fracture occurred in the upper layer of the sand grain itself. In the lower photo it appears as if the crack occurs directly at the interface. Interfacial porosity in the upper photo (~50 μm) does not appear different from the bulk paste further out. Except for the actual crack, the grey levels present, which reflect electron densities of the sample,* are relatively constant. However, in the lower photo, there are distinct grey patches associated with the first 50 μm of paste. In this instance it is assumed that porosity existed at the interface which is now being filled with hydration products.

Figures 36 and 37 represent equivalent paste mortar samples of SHRP 1-2 and SHRP 2 at 15 and 56 days, respectively. The samples were freeze dried, polished with diamond paste, and coated with gold prior to examination. Once again porosity observed in the paste is nearly random, but in one instance perhaps related to some linearity caused by puddling or vibration during casting of the paste (Figure 36, top). In the mortar, porosity is associated more with interfacial areas. During mixing, existing bubbles may be attracted to and attach to the sand surface.

Close-ups of interfaces in the 15-day-old SHRP 1-2 sample are given in Figure 38. Once again, the BSE photographs suggest that the interfacial zone has higher porosity than the surrounding paste.

---

* The brightness of BSE images are related directly to the atomic number of the atom which is backscattering the impinging electron. Therefore, relatively low atomic number elements such as carbon or a pore would appear black, silica sand would appear dark grey, silicate hydrates a lighter grey, $Ca(OH)_2$ relatively bright and anhydrous calcium silicates and aluminates, nearly white.

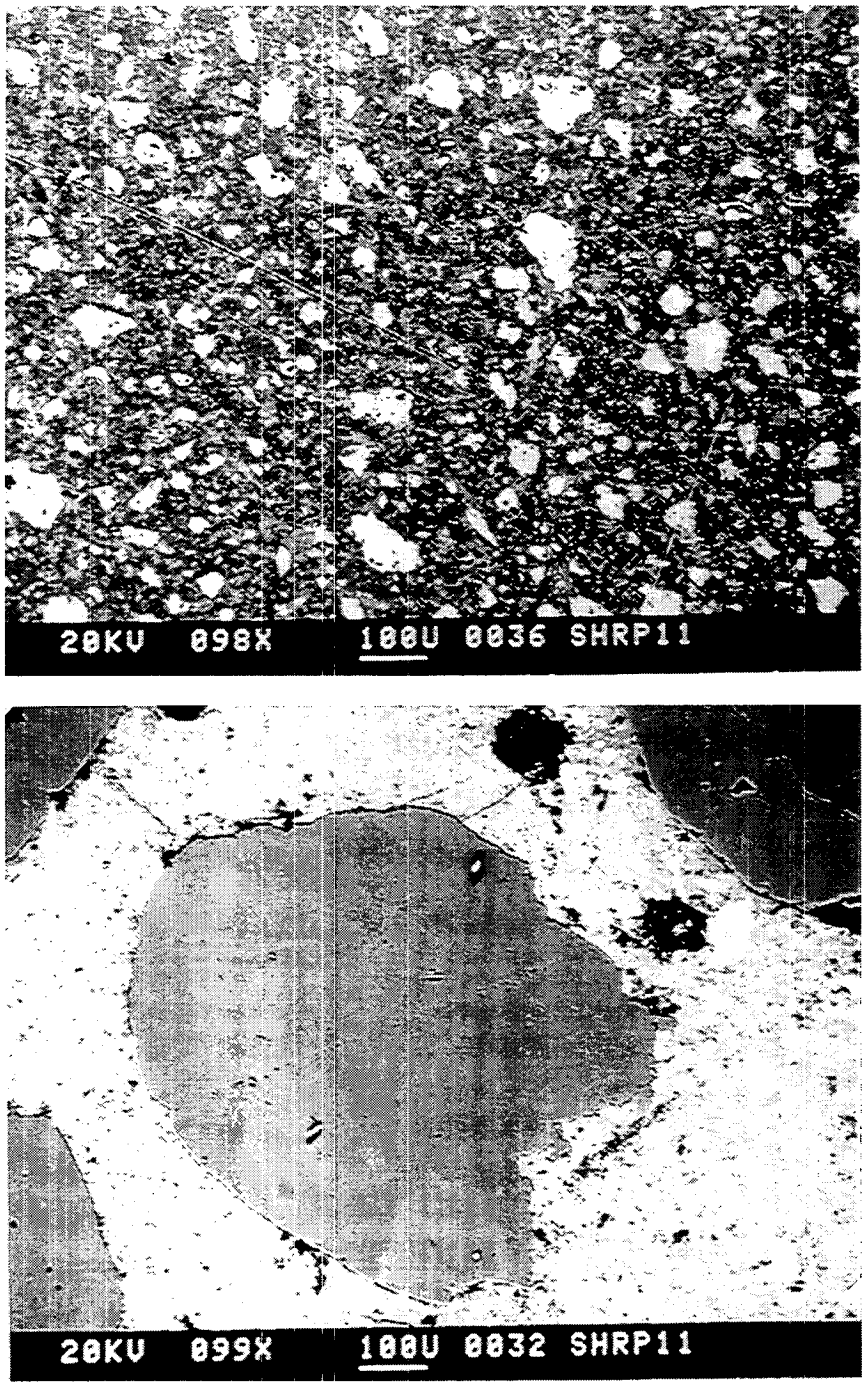

Figure 32. SEM BSE photographs of 14-day-old freeze-dried SHRP 1-1 paste (top) and mortar (bottom). Porosity seen as black spots is random in the paste (upper photo), but associated with interfaces in the mortar (lower photo). Surfaces have been polished with 1 μm diamond paste.

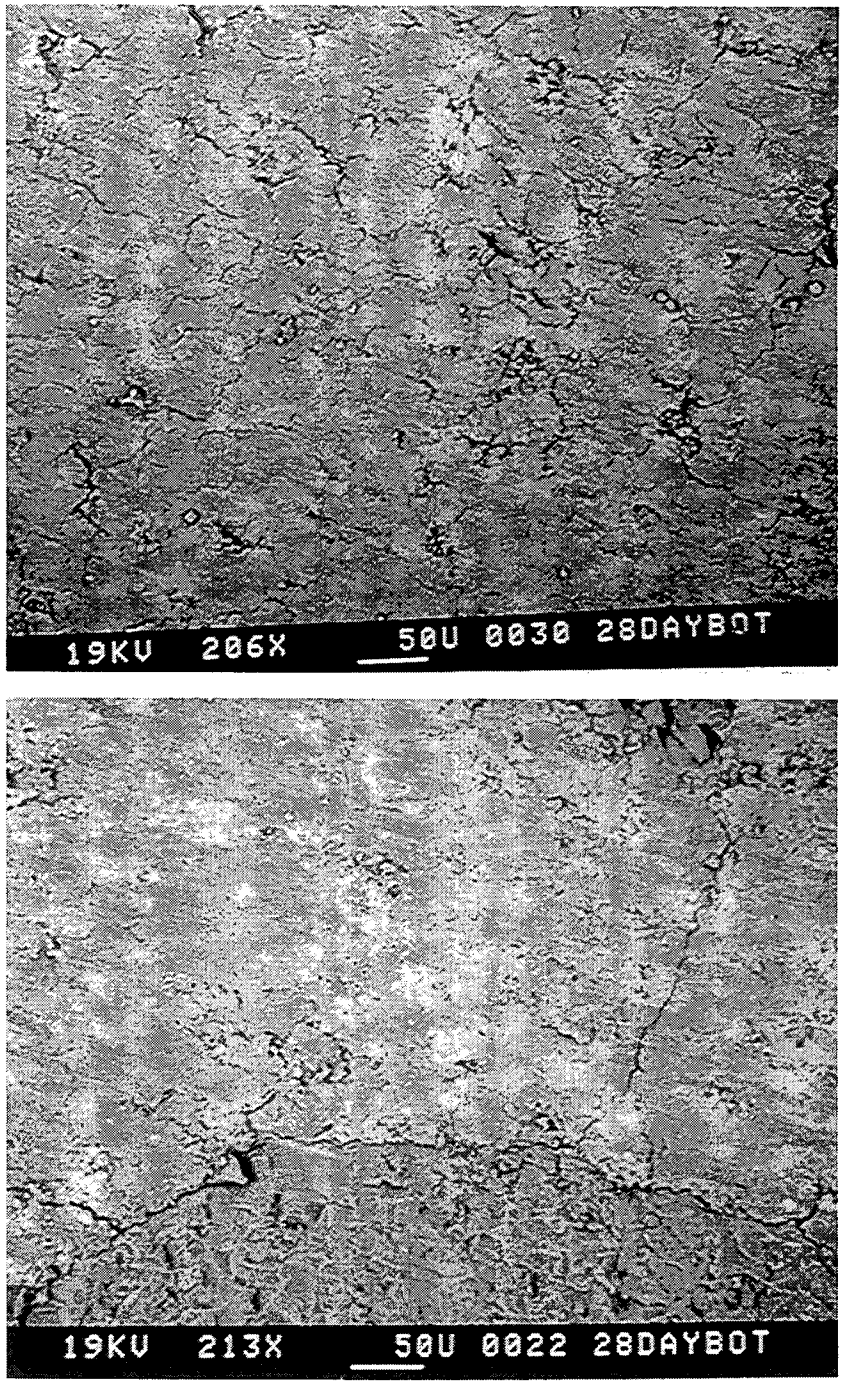

Figure 33. SEM BSE photographs of 28-day-old freeze-dried SHRP 1-1 paste (top) and mortar (bottom). The paste (upper photo) is dominated by randomly oriented drying shrinkage cracks. In the mortar (lower photo), cracks are associated with interfaces. Surface is as cut.

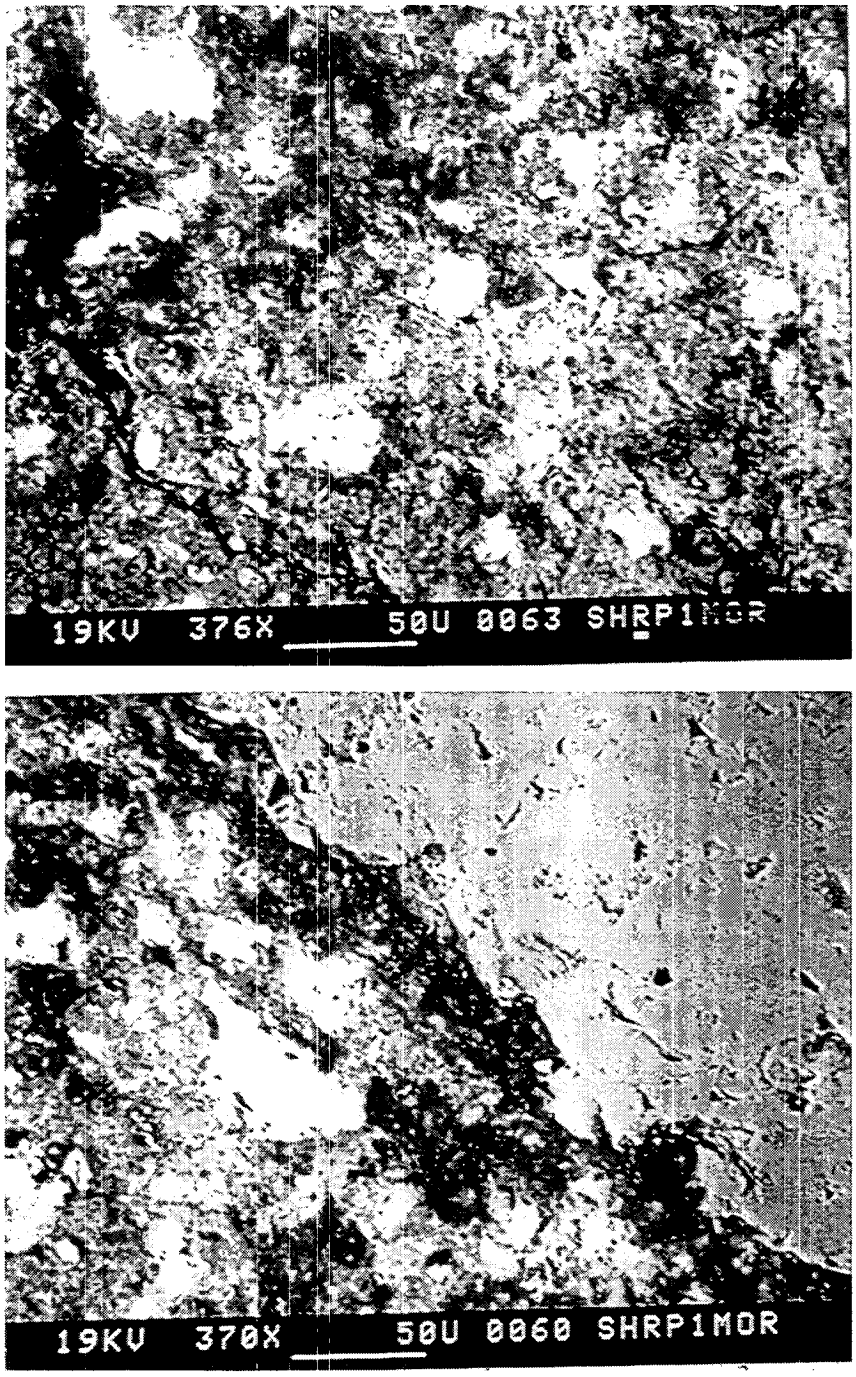

Figure 34. SEM BSE photographs of SHRP 1 paste (top) and mortar (bottom) at 56 days. Freeze dried and polished. Slightly higher magnifications than preceding photos. Paste and interfacial region are relatively free of cracks. Porosity is associated with interfacial region.

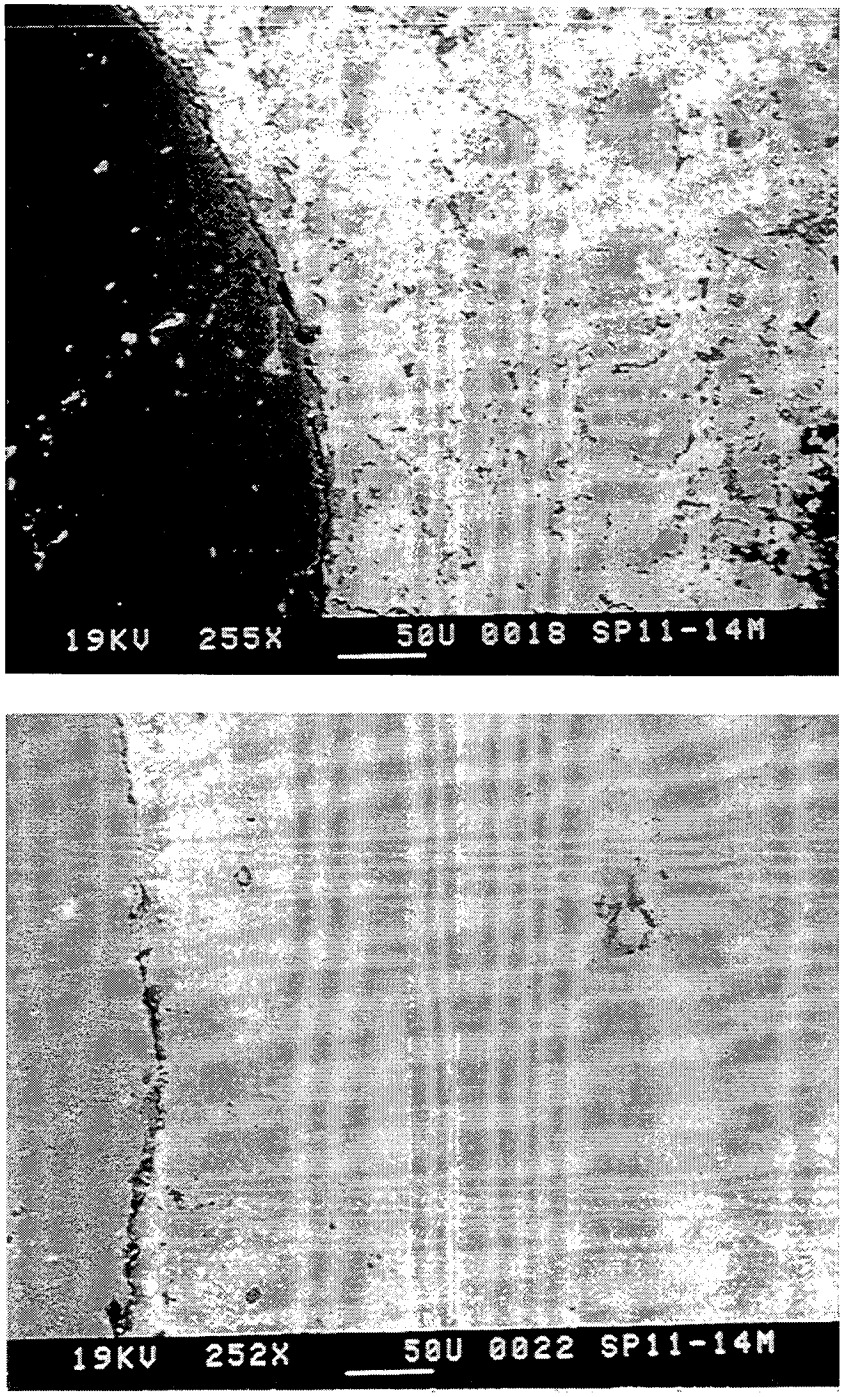

Figure 35. Close-ups of 14-day cured SHRP 1-1 mortar interfaces. Sand grain is on the left; paste on the right. Some of the cracks are due to drying shrinkage or plucking during polishing. The presence of cracks at the interface suggest that this is the weakest bond in the mortar.

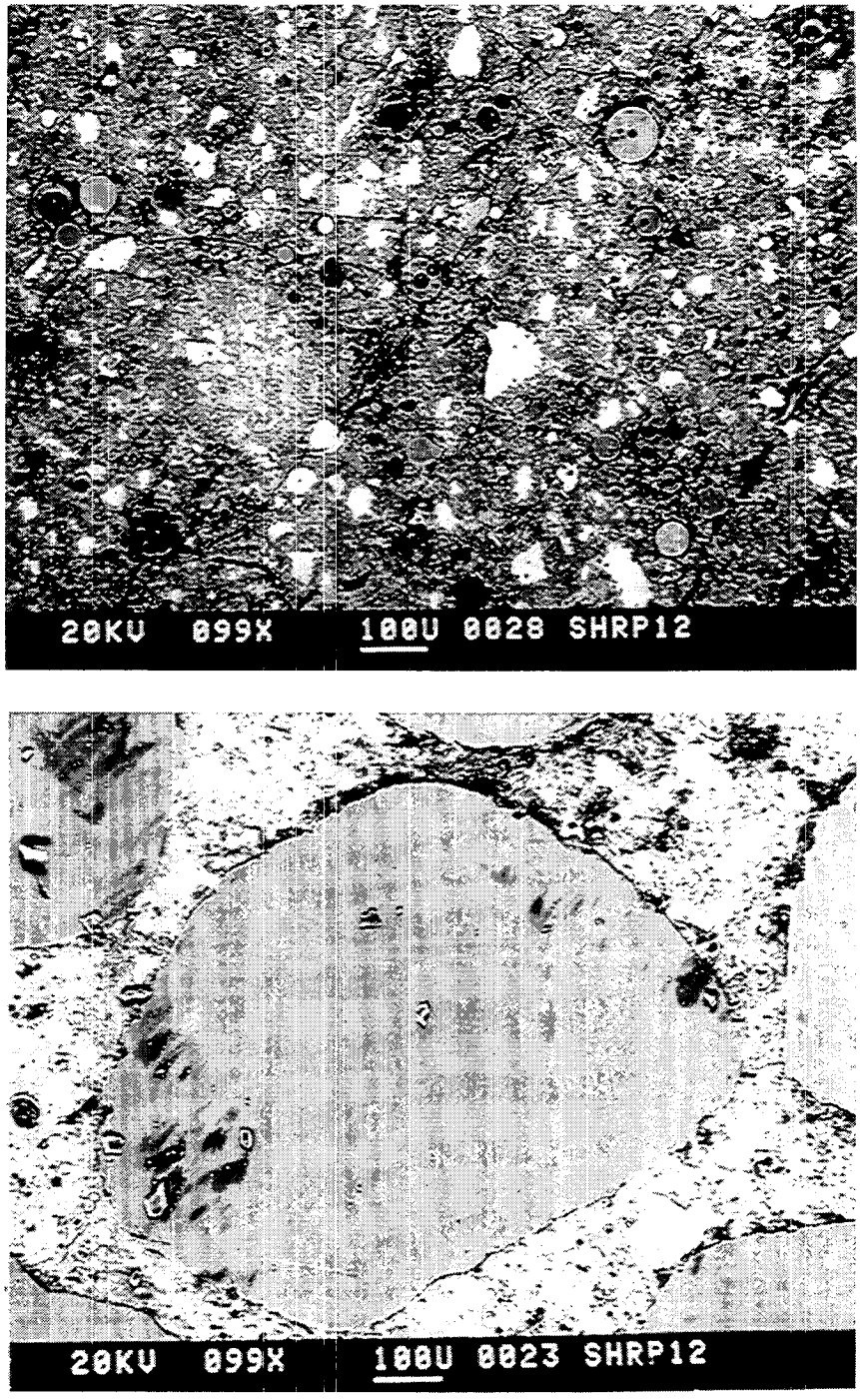

Figure 36. SEM BSE photographs of SHRP 1-2 15-day-old paste (top) and mortar (bottom) samples. Cracking is somewhat oriented in the paste and associated with sand-paste interfaces in the mortar. The small round particles (solid and hollow) are fly ash particles. The bright particles are anhydrous clinker phases, and the intermediate gray areas represent hydration products.

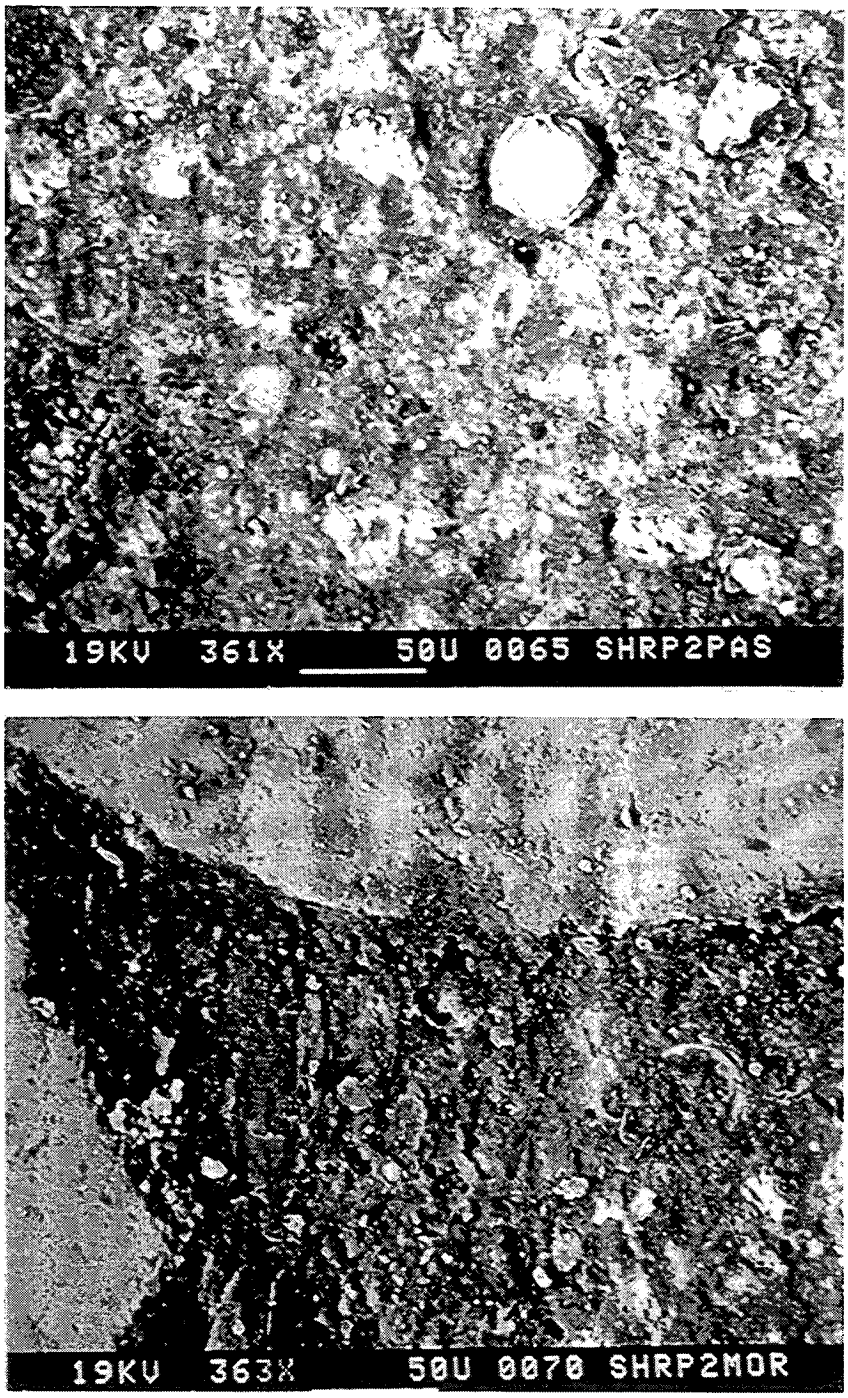

Figure 37. SEM BSE photographs of SHRP 2 paste (top) and mortar (bottom) cured for 56 days. Interfaces (lower photo) tend to show cracks while the paste is relatively free of cracks. The large round grain in the upper photo is a Class F fly ash sphere.

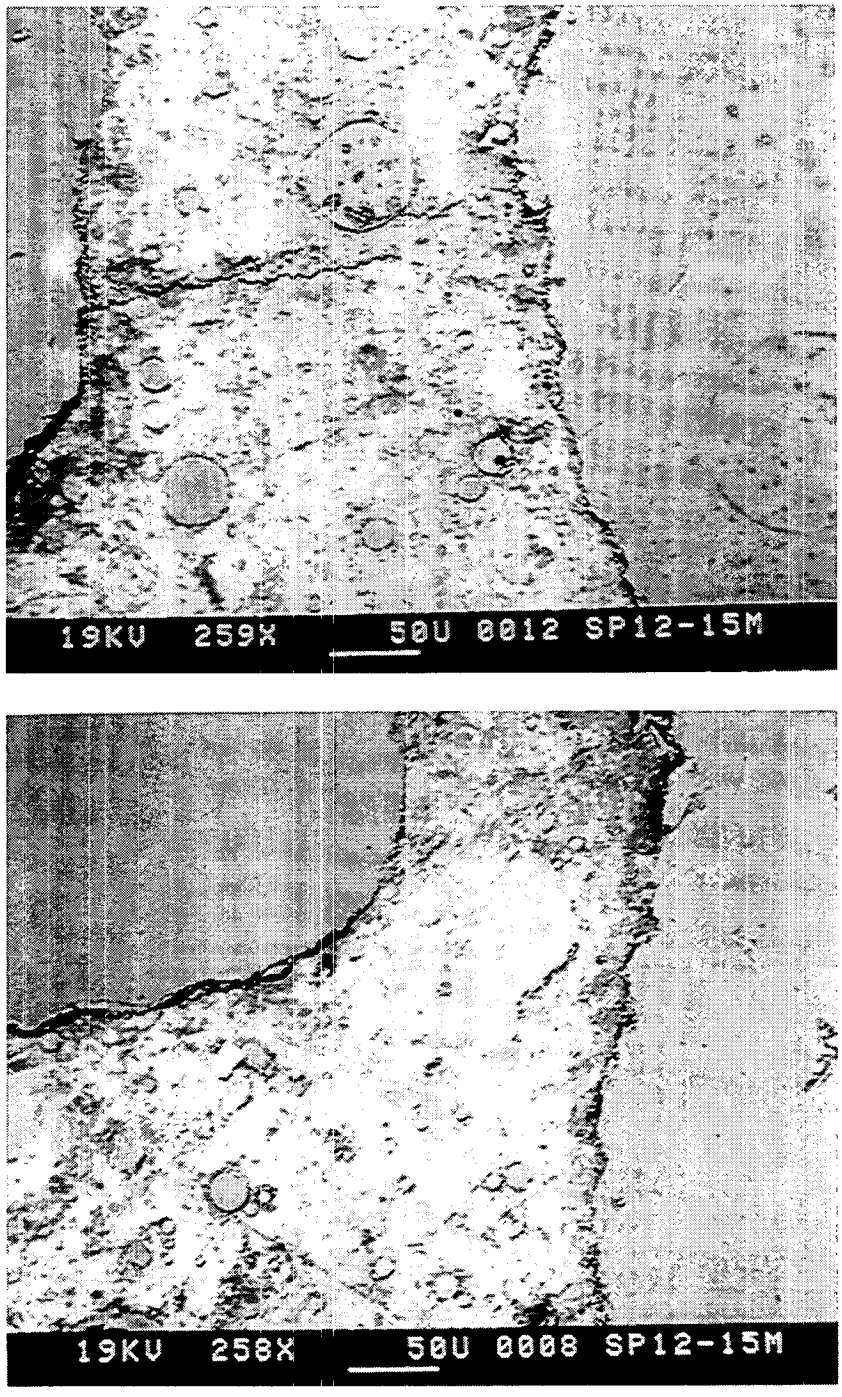

Figure 38. Close-ups of 15-day-old quartz sand-paste interfaces. Cracking appears to be associated with interfacial regions. The round grains in the paste are Class F fly ash spheres.

The final set of four figures in this section (Figures 39–42) are meant to compare paste and mortar samples of SHRP 3 at 28 and 56 days. The SEM examination of polished sections of paste and mortar (in this case, by secondary electron images) suggests that once again additional porosity is associated with the interfacial zone. The polished sections were obtained by first cutting a cored cylinder in half with a diamond saw and then polishing it successively with a 600 grit silicon carbide paper, and 6 and 1 μm diamond pastes.

Figures 39 and 40 are useful to compare the microstructures of SHRP 3 paste and mortar at 28 days of hydration. The paste (Figure 39) appears to contain many more unhydrated clinker grains (larger particles seen in Views B and C) than the equivalent mortar (Figure 40). The mortars seem to contain noncontinuous and localized areas of porosity, predominantly along sand-paste interfaces. In both instances, differences in hardness of the particles and hydrated paste has caused a fair amount of relief to form during polishing. This could in part explain some of the interfacial voids—their lower strength due to higher porosity, could cause them to erode at a faster rate than the bulk paste.

SEM images of 56-day samples of paste and mortar are pictured in Figure 41 and 42, respectively. Once again, the pastes (Figure 41) contain a large number of anhydrous particles; but, in this case, they are surrounded by obvious hydration rims (bright particles with gray rims). Cracking (both photos) seems to be random. In addition, the paste appears to be both denser and more homogeneous than its mortar counterpart. The mortars (Figure 42) tend to exhibit cracks at the sand-paste interfaces, but little additional associated interfacial porosity when compared to bulk paste samples further from the interface (see Figure 42).

We assume that the association of porosity with interfaces is a real phenomena as was demonstrated by our earlier reported thin section work (Figures 28 and 29), and as such, the interfacial zone is weaker and thus more susceptible to observed tendency of the interface to crack and suffer losses due to erosion during polishing. The lack of cracking and relief in Figure 43 (as cut, not polished, solvent exchanged) seems to confirm this observation.

POLISHED SECTIONS—REFLECTED LIGHT

An attempt was made to impregnate our paste and mortar samples with a fluorescent dye. However, due to unforeseen circumstances, the commercial vendor we had contracted with (not GMIC) was unable to fully accomplish this task. However, for sake of discussion, one of the two successfully impregnated mortar samples is given as an example (see Figure 44).

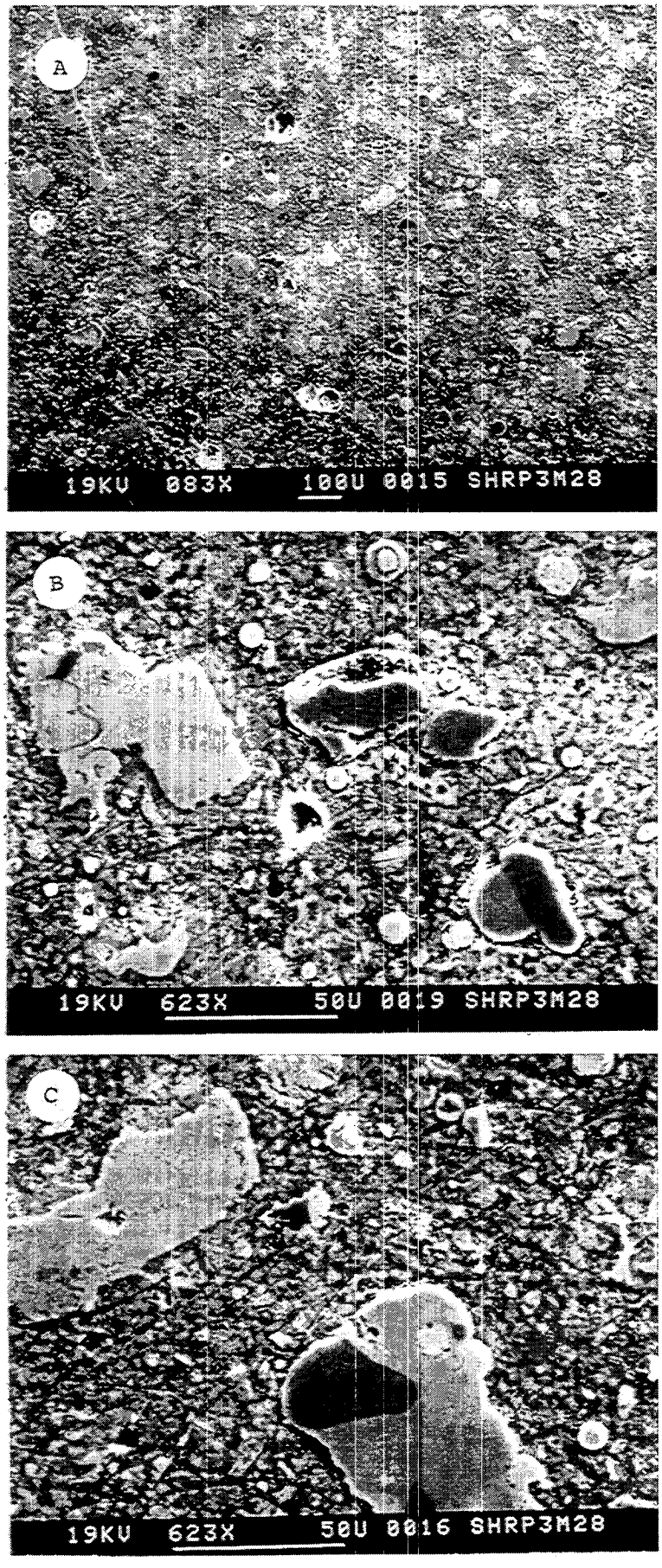

Figure 39. SEM micrographs of 28-day SHRP3 paste. The paste pictured in View A is similar in appearance to that of the paste seen in Figure 33A. Fly ash spheres and unhydrated cement grains (angular, roughly rectangular material) are evident. Views B and C are enlarged views of the paste. When comparing these with the mortar (Figure 33, Views B-D), it appears that the paste contains a far greater percentage of unhydrated clinker grains (angular, roughly rectangular material). This may be an artifact of polishing, since the harder material resists polishing. The sand in Figure 33 resists polishing, and the matrix is less polished, while in this figure the clinker grains take a high polish whereas the softer material (hydrated paste matrix) is not as smooth.

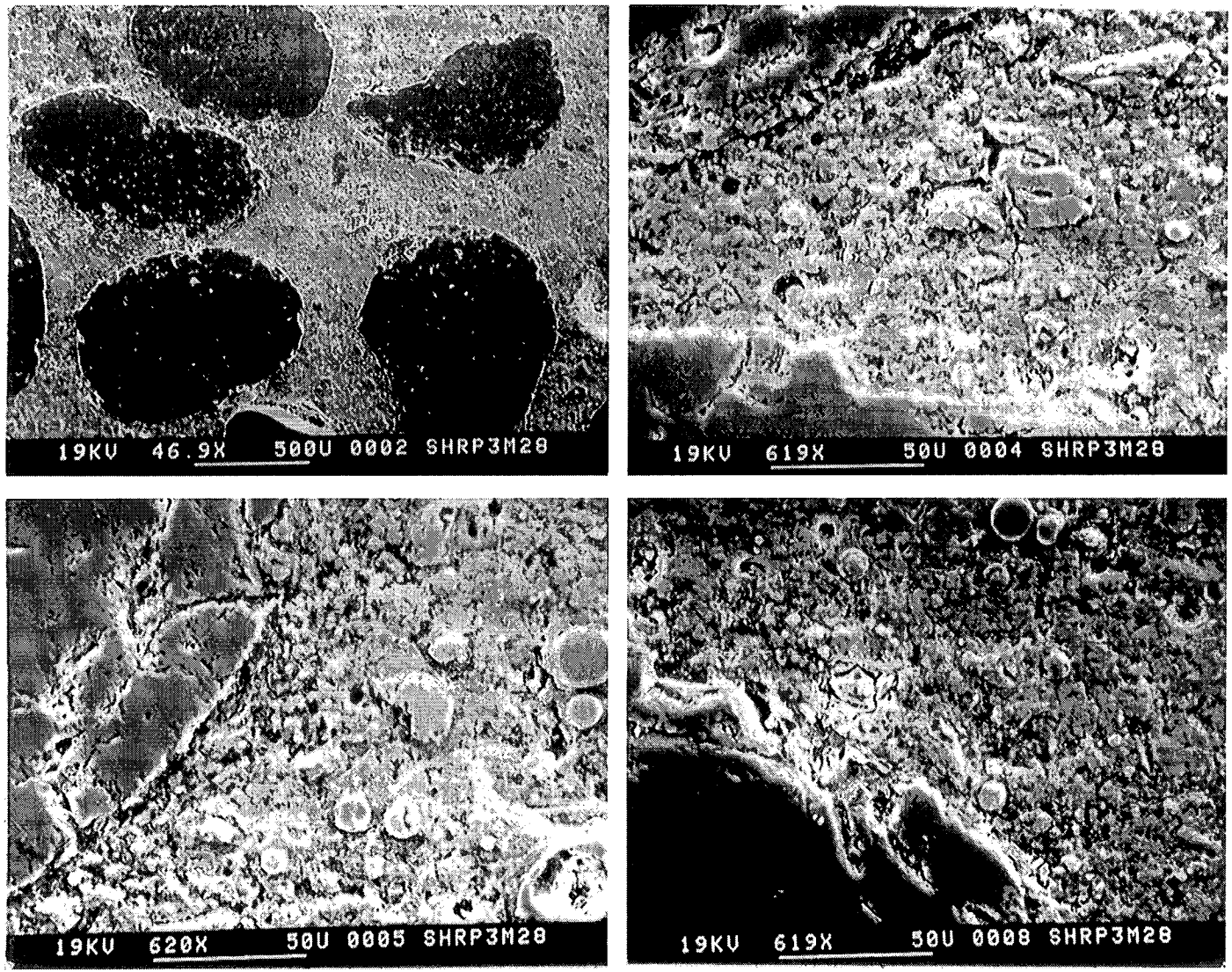

Figure 40. SEM micrographs of 28-day SHRP3 mortar. View A is an overview at 47× suggesting that interface porosity varies from place to place along the sand-paste interface. View B is an enlargement of the central portion of the two left-most sand grains in View A. The Upper interface is quite porous, while the lower one is relatively free of such porosity. View C is a continuation of the interfacial zone of the upper sand grain, still showing a crevice and more porous interfacial zone. View D is a continuation of the lower grain and it, too, shows some porosity but to a lesser extent than View C. In all cases (Views B-D) the rounded particles are fly ash grains.

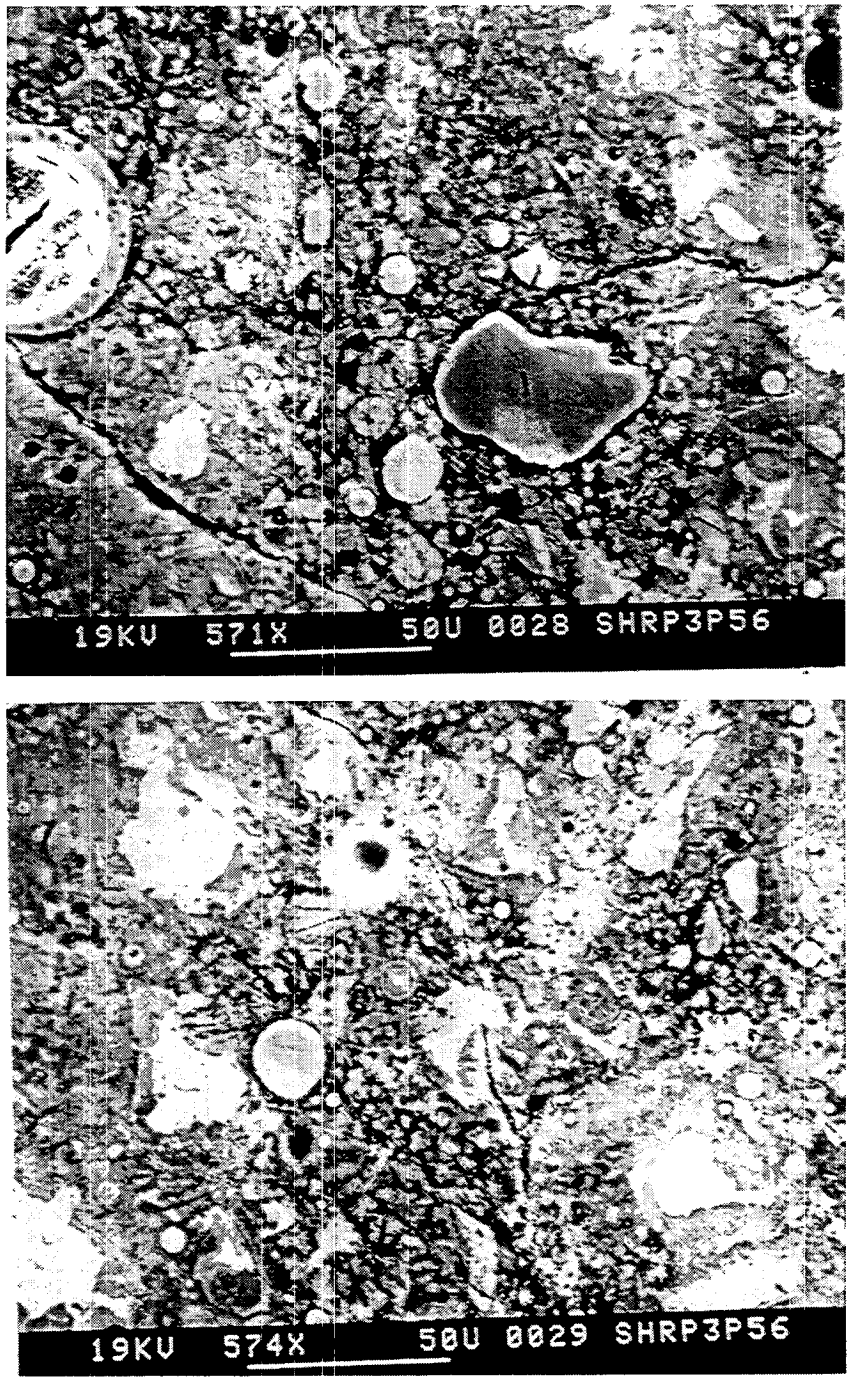

Figure 41. SEM micrographs of 56-day SHRP 3 paste. Views A and B are of paste at 571-574×. The paste appears similar to that pictured for the mortar-samples (Figures 35A and B). Hydration rims are evident around clinker grains (View B, lower right-hand corner) as well as fly ash spheres. Other than occasional random cracks, the paste looks fairly homogeneous throughout.

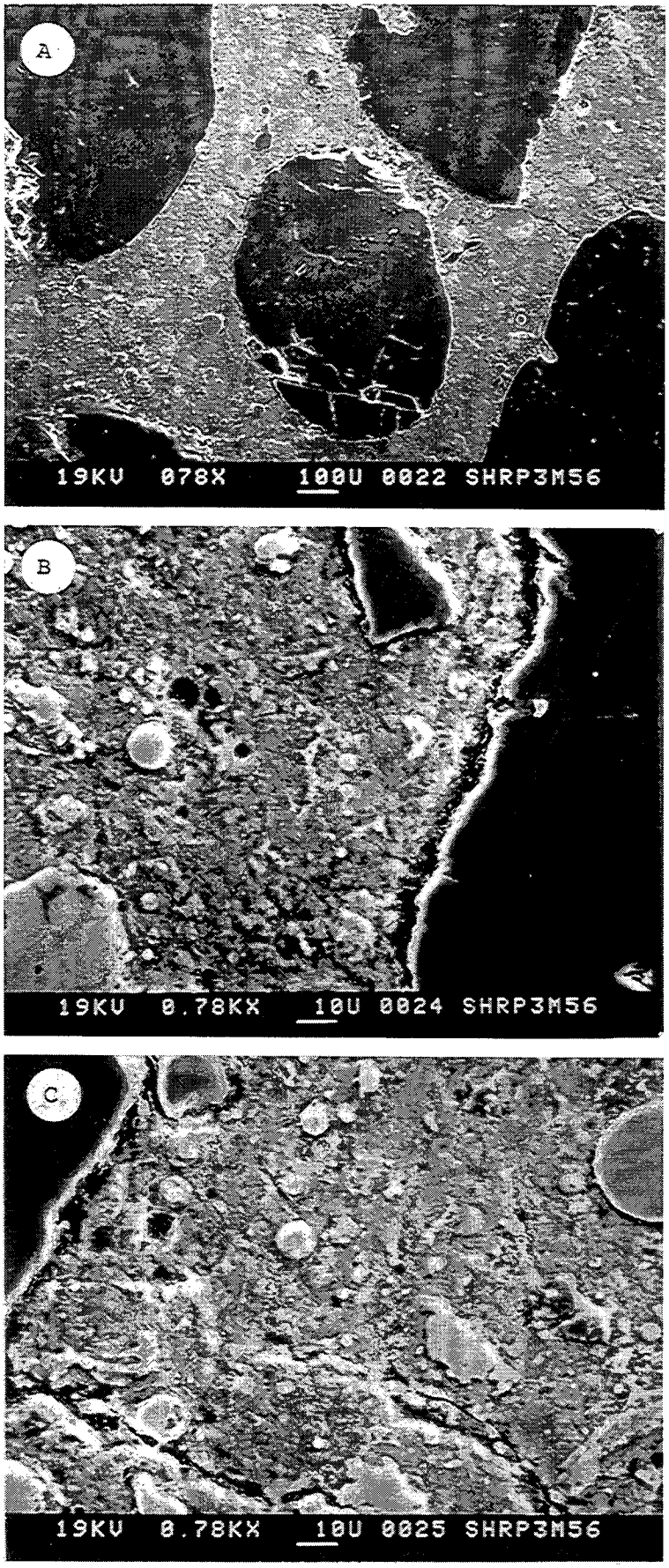

Figure 42. SEM micrographs of 56-day SHRP3 mortar. View A is an overview at 78× showing what appear as cracks along many of the paste-sand interfaces, and emanating into the paste. The paste contains unhydrated cement grains and an occasional fly ash sphere, appearing similar to the 28-day sample given in Figure 34A. Enlarged views of interfaces and paste are given in Views B and C. View B is a view of the upper left-hand side of the central grain. View C is an enlargement of the lower right-hand side of the corner grain in the upper left-hand side of the photograph. Each has a crack associated with the interface, but little in the way of associated paste porosity in the interfacial zone (first 50 μm of paste). The paste looks rather homogeneous.

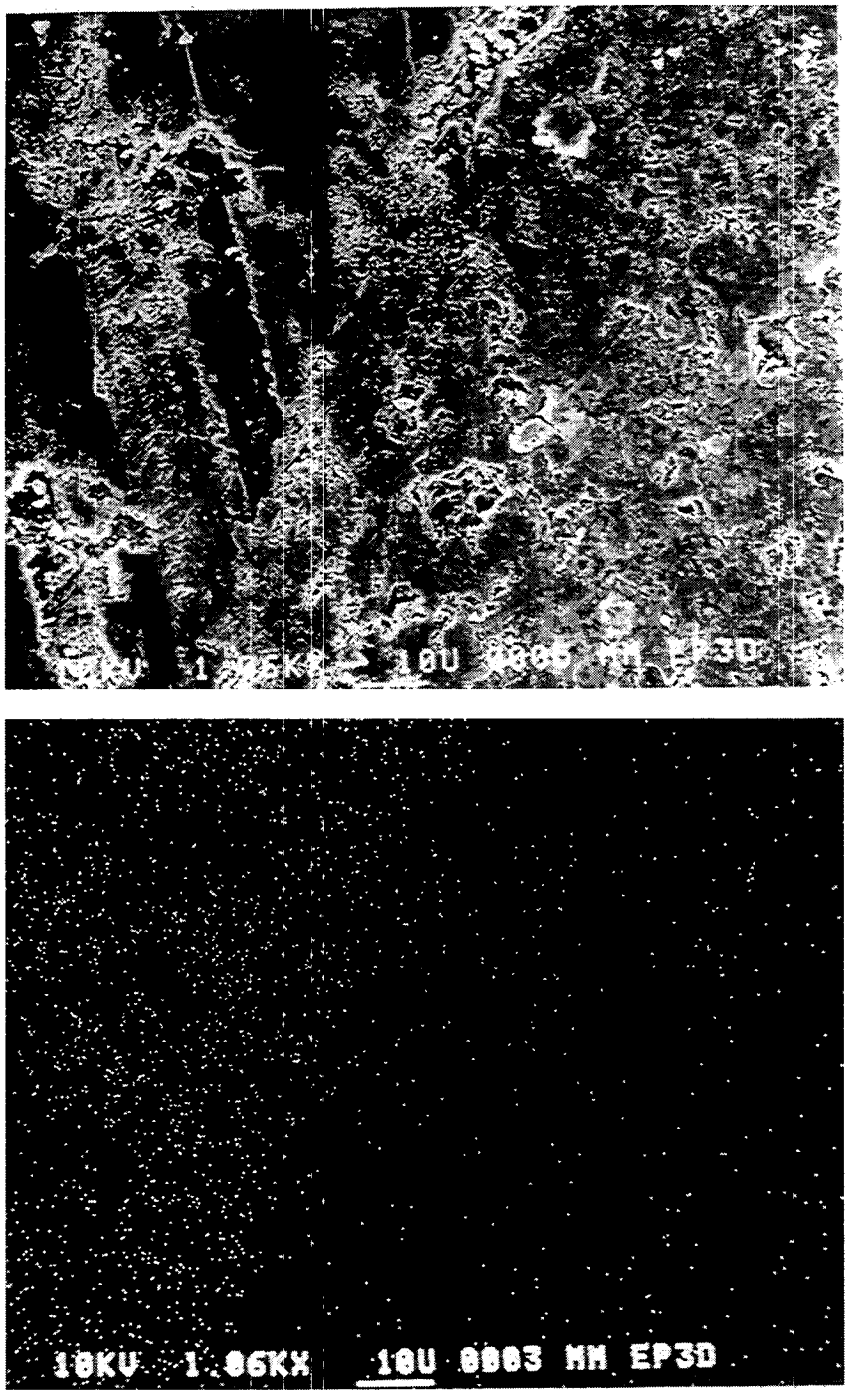

Figure 43. SEM SEI photograph of an as-cut, unpolished 3-day-old mortar sample (top photo). The sample was solvent exchanged in ethyl alcohol. The Ca x-ray map (bottom) shows the location of the interface (the quartz sand is on the right). The paste is on the left and shows stirations due to the saw blade. The interface is relatively tight.

Figure 44. Photomicrograph (78×) of a freeze-dried SHRP 1-1 mortar sample cured for 7 days in $Ca(OH)_2$ solution. Interfaces appear slightly brighter than the bulk paste, presumably due to enhanced interfacial porosity.

A reflected-light sample differs from a thin section in that the dye is forced into the surface to be examined by reflected light metallographic microscopy. If care is not exercised, most or all of the impregnated dye can be "polished" away during sample preparation. This is apparently what happened to the majority of our samples.

The example given in Figure 44 is of a 7-day-old freeze-dried SHRP 1-1 mortar sample. The quartz sand grains appear dark, the hydrated paste yellow to green, and the anhydrous clinker phase as black inclusions in the paste. The samples were examined using a combination of U.V. light and a yellow filter. The degree of brightness of the fluorescence is directly related to the porosity. The sand grains are surrounded by slightly "brighter" rims, suggesting enhanced porosity at the interfaces. The rims are on the order of 50 μm wide.

HG POROSIMETRY

Mercury porosimetry data were collected for SHRP 3 and the repeat mixtures SHRP 1-1, 1-2, 1-3 and 1-4. Porosity measurements were made using a Quantachrome scanning Hg-porosimeter. Upper intrusion pressures were approximately 55,000 psi. dV/dP plots of the Hg-intrusion volume versus pressure curves were distinctly bimodal, suggesting that both fine 10-30 nm(100-300Å) and coarse 200 nm (~2000Å) pores developed during the hydration reaction. However, differences between the paste and mortar samples were significant.

Plots of total porosity versus time for SHRP 3, 1-1, 1-2, 1-3 and 1-4 paste and mortars are given in Figures 45-49, respectively. Differences in formulations and initial porosities can be found in Table 3 at the beginning of this section. SHRP 1-1 was an ordinary portland cement paste, SHRP 1-2 and SHRP 3, and 1-3 contained Class F and C fly ash, respectively, and SHRP 1-4 contained silica fume. As was mentioned earlier, it was hypothesized that the 50:50 volume % mortars would have $\frac{1}{2}$ the porosity of the equivalent paste value (assuming the quartz sand to be nonporous). Also plotted in the figures is a dashed curve which represents $\frac{1}{2}$ of the paste value.* If our hypotheses were correct, the mortar porosity would be superimposed by this line. More often than not, the mortar had higher than expected porosities; only SHRP 1-3 was seen to superimpose.

All total porosities tended to decrease with time as space originally occupied by the water became filled by developing hydration products. The OPC [SHRP 1-1 (Figure 46)] and the Class C fly ash containing mixtures [SHRP 3 (Figure 45) and 1-3 (Figure 48)], and the

* Earlier in this section we had reported on image analysis of SHRP 1-1 and 1-2 samples. SHRP 1-1 was found to be 57% paste while SHRP 1-2 was 50%. Other samples were not measured but are assumed to be 50% paste.

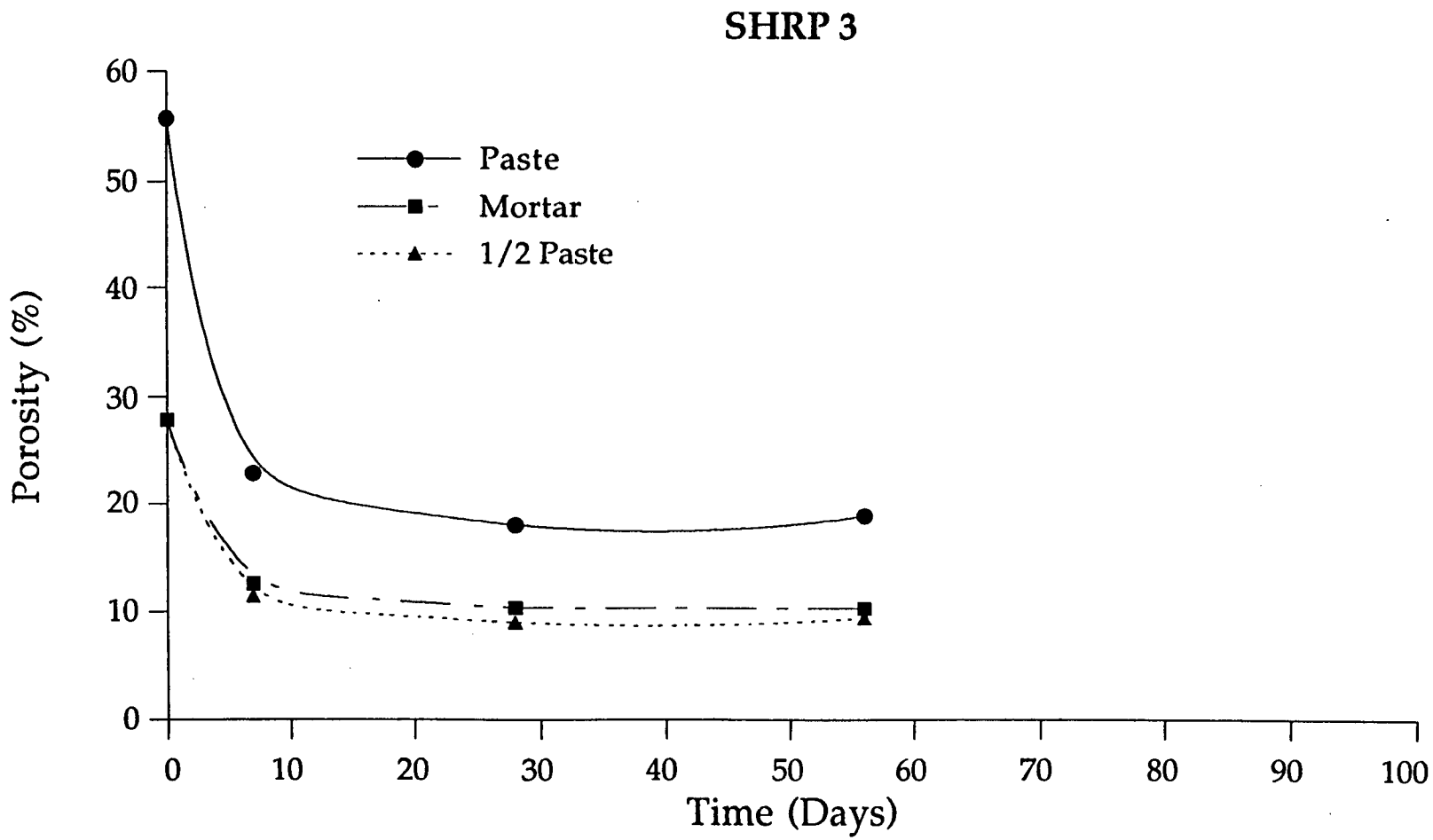

Figure 45. SHRP 3 Hg-porosimetry data. The dashed line represents 0.50 of the paste values.

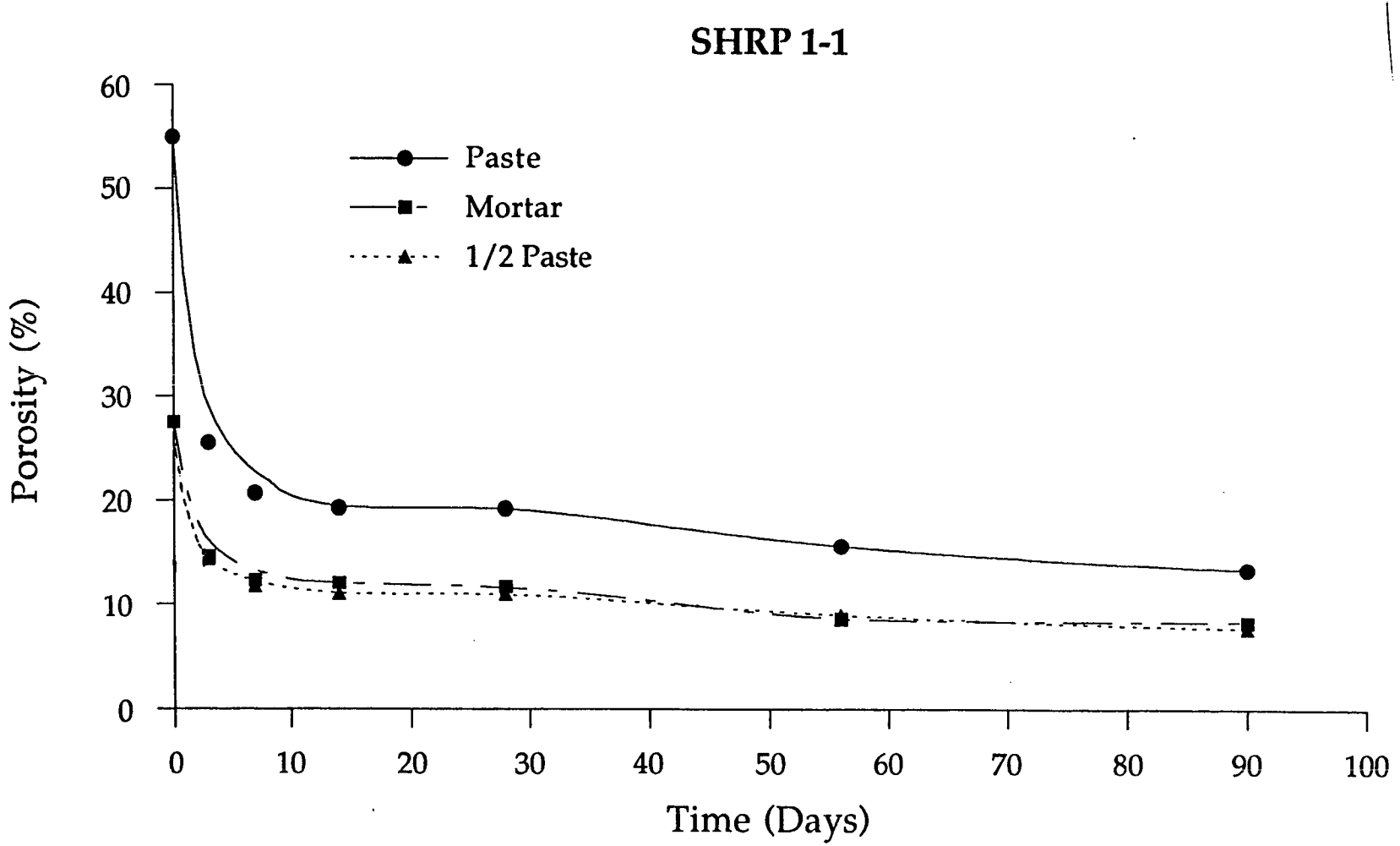

Figure 46. SHRP 1-1 Hg-porosimetry data. The dashed line represents 0.57 of the paste values.

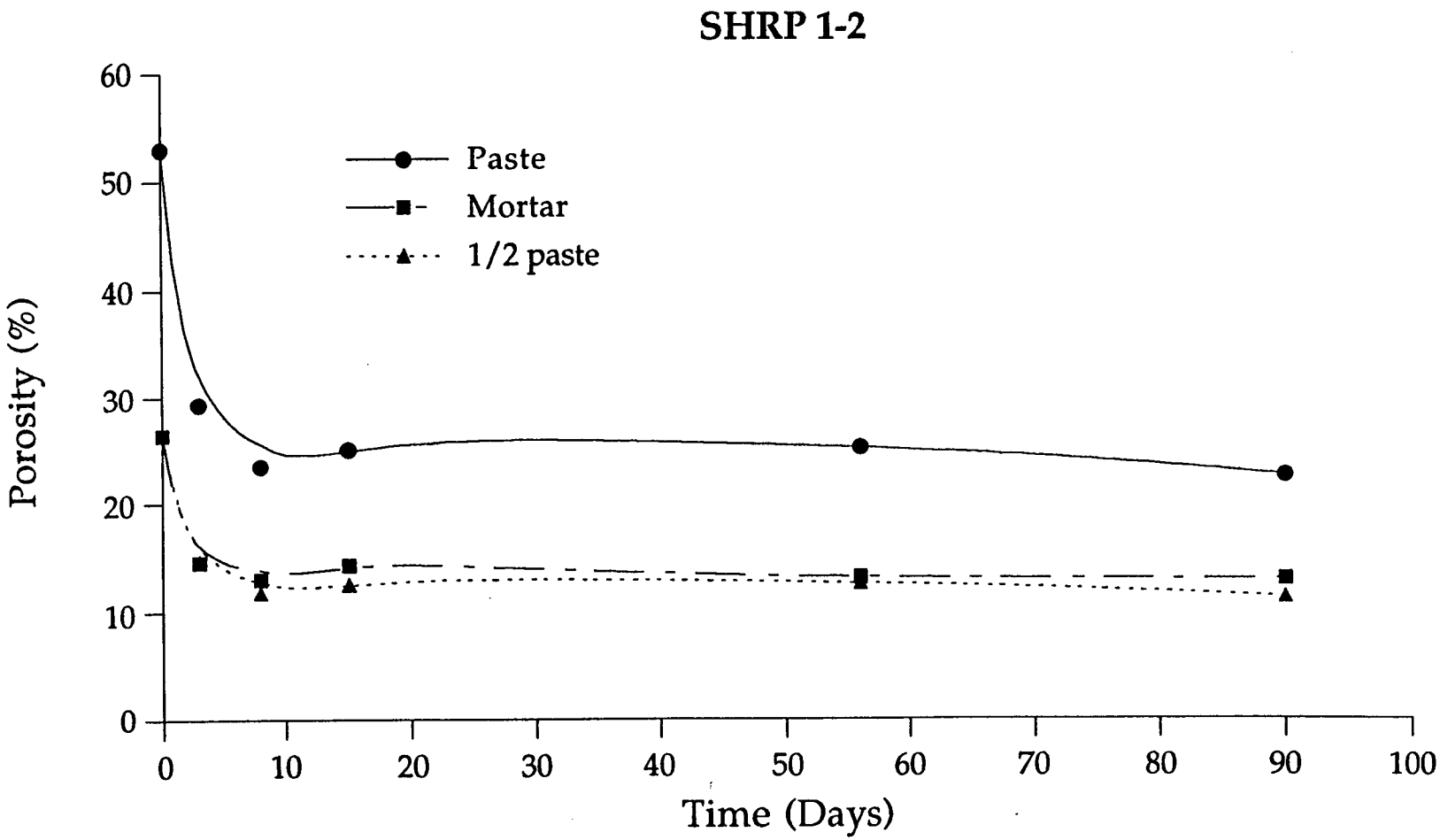

Figure 47. SHRP 1-2 Hg-porosimetry data. The dashed line represents 0.50 of the paste values.

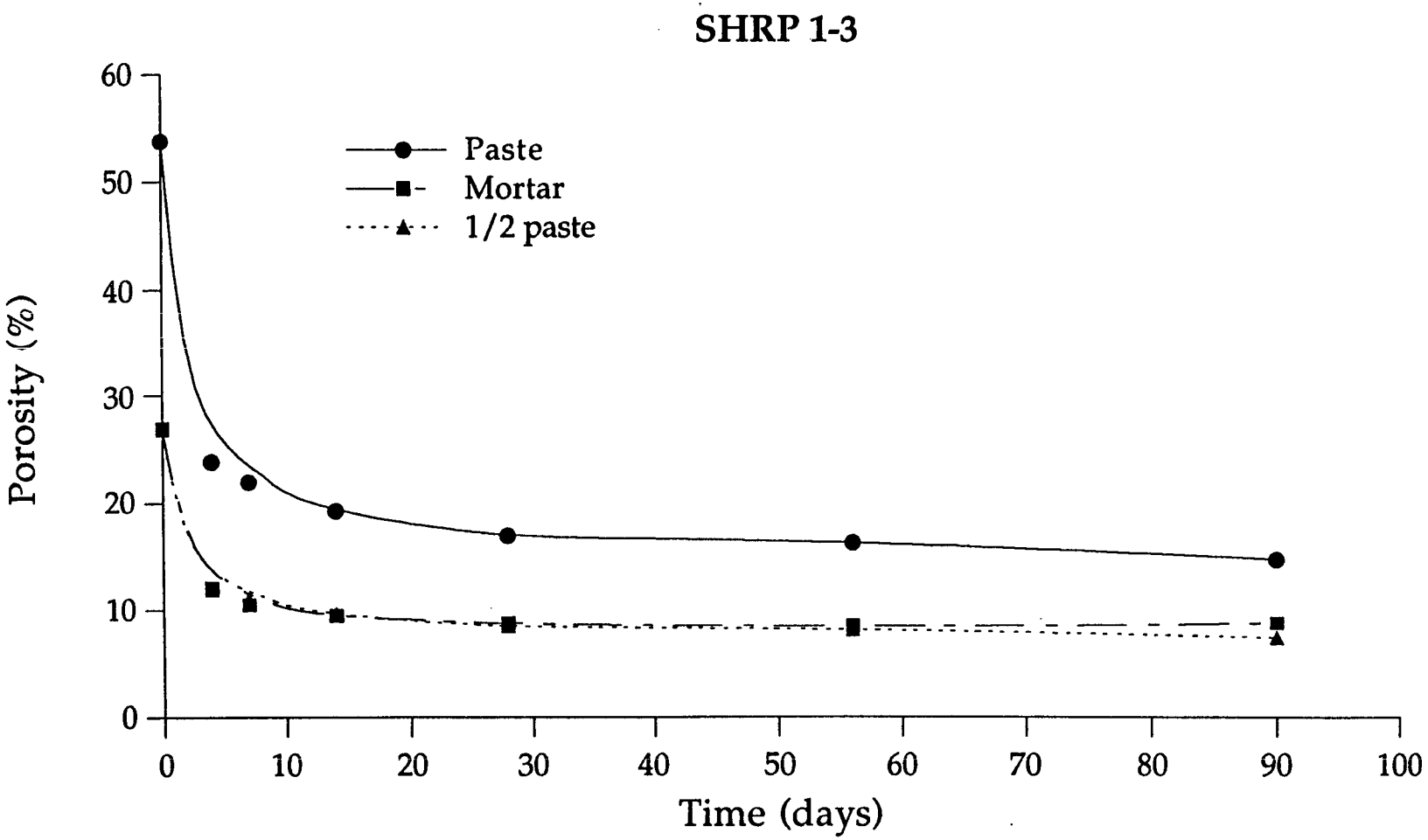

Figure 48. SHRP 1-3 Hg-porosimetry data. The dashed line represents 0.50 of the paste value.

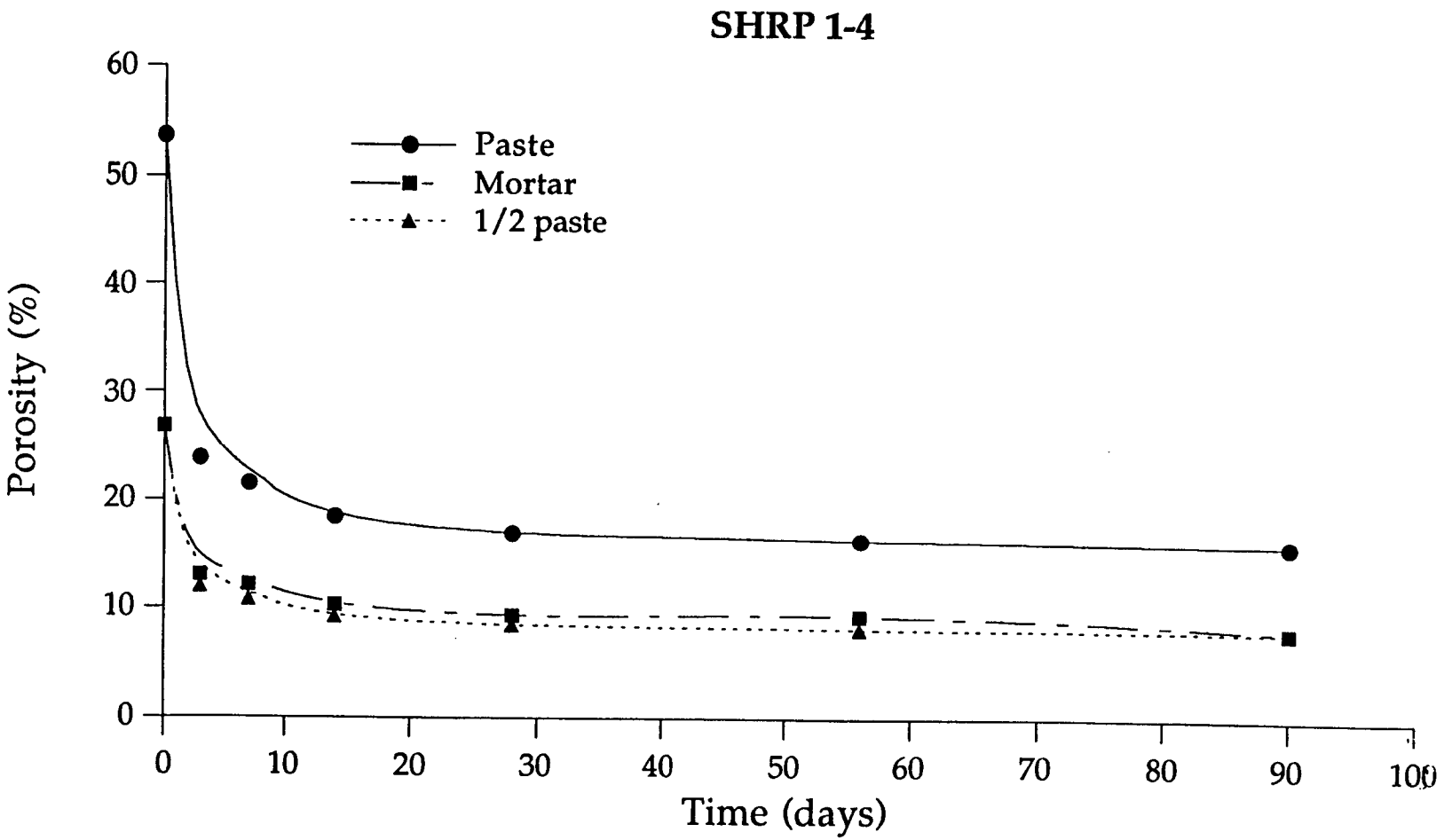

Figure 49. SHRP 1-4 Hg-porosimetry data. The dashed line represents 0.50 of the paste value.

silica fume-containing mixture [SHRP 1-4 (Figure 49)] exhibited the largest drops in total porosity. The Class F containing fly ash mixture [SHRP 1-2 (Figure 47)] dropped considerably less. For example, at 56 days, the paste values for SHRP 3, 1-1, and 1-3 are 19.8, 15.7 and 16.3. The paste value for SHRP 1-2 is 25.3. The corresponding mortar values are 10.4, 8.6, 8.5 and 15.7. Apparently the Class C fly ash hydrates very nearly as rapidly as the OPC itself. However, the Class F fly ash is much less reactive, acting more like a non-reactive aggregate. Thus the cement in SHRP 1-2 must hydrate to a greater extent in order for the hydrates to fill the space originally occupied by the water.

In all cases except SHRP 1-3 (Figure 48) the mortar porosities are slightly higher than the predicted fraction of the paste values. As a group, the Class F fly ash containing mixture exhibited the largest deviation, while the OPC, Class C fly ash- and silica-fume containing mixtures, the smallest deviation.

Finally, at least in the OPC paste (Figure 46) and the silica fume-containing paste (Figure 42), the differences between predicted and observed mortar porosities tends to narrow with time. This suggests that interfacial porosities may close with time, and that older, longer-cured materials, may be less sensitive to interfacial effects (lower strength, vulnerability to chemical attack).

In addition to the porosity plots, we have also tabulated the average size of the bimodal $\frac{dV}{dP}$ porosity distributions and their intensities (arbitrary units) as a function of time. These values are given in Tables 4–8 which follow.

As can be seen from these tables, the pastes contained predominantly 7-35 nm (70-350 Å) pores; the largest pores occurring in the relatively unreactive SHRP 1-2 Class F fly ash mixture. On the average, these smaller pores tended to decrease both in relative intensity and absolute size, i.e. they became smaller and less prevalent with time. The relative amounts of the larger 200 nm (2000 Å) pores tended to decrease with time, but their sizes remained constant. The mortars behaved quite differently. They contained predominantly 200 nm (2000 Å) pores with significantly smaller amounts of the 8.5-45 nm (85-450 Å) pores so common in the paste (even less than $\frac{1}{2}$ as might be expected). In addition, there were few clearcut trends in the mortars. Sizes of the pores and their relative intensities tended to fluctuate with increasing time. The biggest difference between the mortars and the pastes was the unquestionable predominance of the 200 nm (2000 Å) pores in the mortars. This suggests that extra porosity is present (large 200 nm) which can be attributable only to the presence of sand-paste interfaces.

Table 4. SHRP 3 pore size distribution.

Time	Paste, Å (rel. intensity)	Mortar, Å (rel. intensity)
7	2000 (1), 180 (14)	2000 (12.5), 250 (5.5)
28	2000 (5), 110 (2)	2000 (<1), 85 (5.5)
56	2000 (1.5), 70 (3.5) 2000 (2.5), 65 (3.5)	2000 (15.5), 125 (1.5) 2000 (14), 120 (1.5)

Table 5. SHRP 1-1 pore size distribution.

Time	Paste, Å (rel. intensity)	Mortar, Å (rel. intensity)
3	2000 (6.5), 140 (16.5) 2000 (6.5), 140 (17)	2000 (14), 180 (6) 2000 (13), 180 (7)
7	2000 (4), 12.5 (14) 2000 (3), 115 (14.5)	2000 (12), 130 (4.5) 2000 (11.5), 140 (4.5)
14	2000 (4), 75 (7.5) 2000 (10), 80 (8)	2000 (11.5), 110 (2.5) 2000 (20), 11.5 (2.5)
28	2000 (3.5), 70 (7) 2000 (2), 70 (7)	2000 (13), 110 (1.5) No duplicate
56	2000 (1), 175 (12.5) No duplicate	2000 (12.5), 190 (3.5) No duplicate
90	2000 (1.5), 190 (15) No duplicate	2000 (10), 220 (5) No duplicate

Table 6. SHRP 1-2 pore size distribution.

Time	Paste, Å (rel. intensity)	Mortar, Å (rel. intensity)
3	2000 (3.5), 350 (17.5) 2000 (8.5), 350 (22.5)	2000 (3), 450 (8) 2000 (4.5), 350 (6.5)
8	2000 (1), 115 (7.5) 2000 (3), 130 (10)	2000 (4), 125 (4) 2000 (3), 130 (4.5)
15	2000 (<1), 180 (25)	2000 (6), 190 (10)
56	2000 (1.5), 130 (15.5)	2000 (7), 160 (5.5)
90	2000 (2.5), 950 (6.5)	2000 (13.5), 150 (3)

Table 7. SHRP 1-3 pore size distribution.

Time	Paste, Å (rel. intensity)	Mortar, Å (rel. intensity)
4	1000 (shoulder), 260 (23.5)	2000 (8), 250 (8)
7	2000 (6), 220 (23)	2000 (9), 240 (5)
14	2000 (3), 200 (16.5)	2000 (17), 220 (3.5)
28	2000 (3.5), 180 (11.5) 50 (4)	2000 (11.5), 180 (3)
56	2000 (3.5), 120 (7)	2000 (10.5), 140 (2)
90	2000 (2.5), 120 (5.5) and 85 (4.5)	2000 (12.5), 130 (1.5)

Table 8. SHRP 1-4 pore size distribution.

Time	Paste, Å (rel. intensity)	Mortar, Å (rel. intensity)
3	2000 (6), 175 (26.5)	2000 (18.5), 200 (7.5)
7	2000 (6.5), 170 (19.5)	2000 (16), 180 (7)
14	2000 (10), 140 (11.5)	2000 (15.5), 170 (4.5)
28	2000 (9), 130 (5), 90 (4)	2000 (15), 130 (3)
56	2000 (6), 110 (3.5)	2000 (16.5), 105 (1)
90	2000 (11.5), 130 (4)	2000 (10), 90 (1)

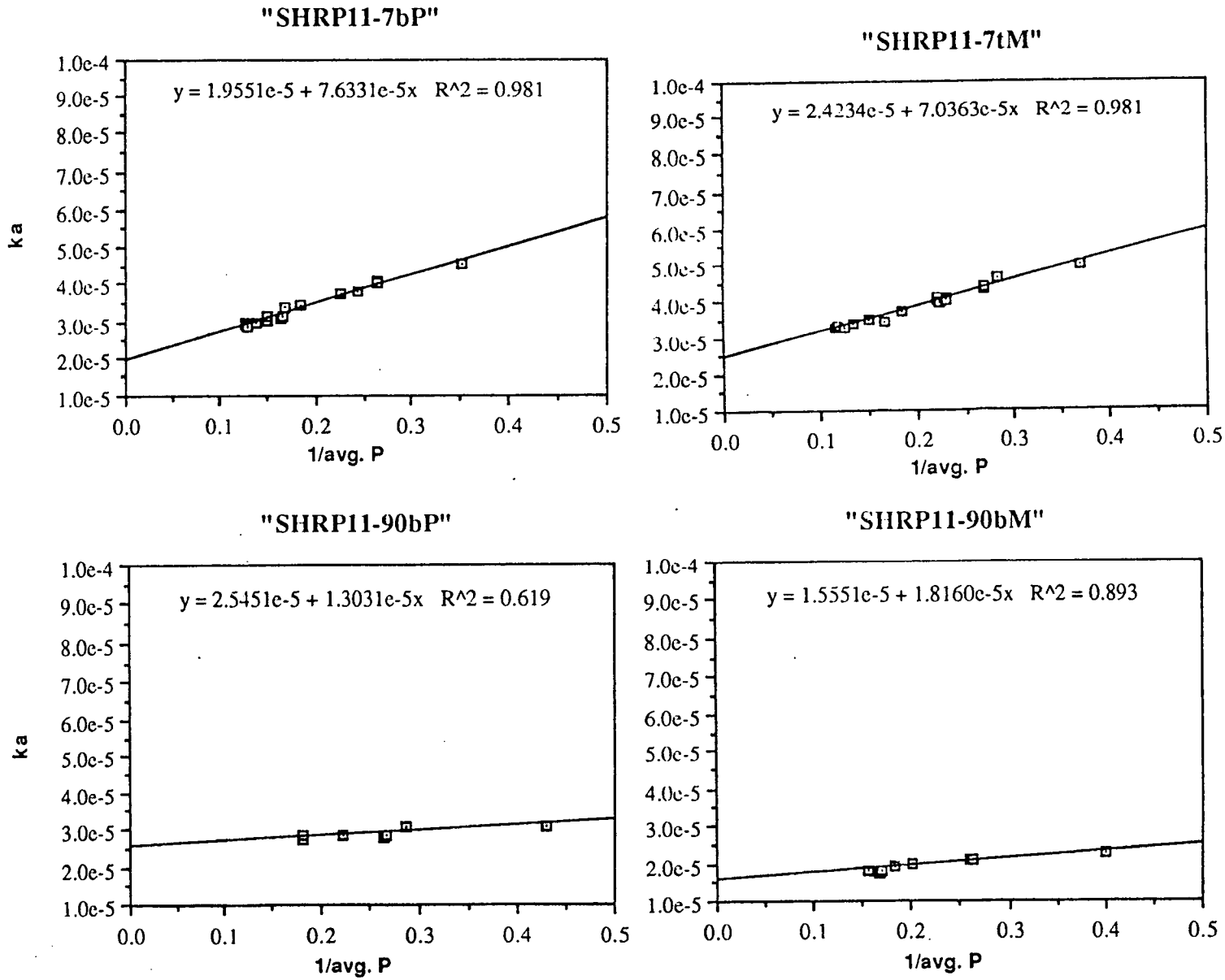

Figure 50. Typical plot of nitrogen permeability (k) versus atm^{-1} for SHRP 1-1 paste (left) and mortar (right) samples. The upper plots are for 7-day-old samples. The lower plots are for 90-day-old samples.

AIR PERMEABILITY

Air permeability data were collected for freeze-dried samples of SHRP 1-1 paste and mortar. Our intent was to explore the relationship of the observed higher interfacial porosity of our mortars to their permeability.

The sample was ~1 inch in diameter and 1 inch long. It was contained in a pressurized rubber sleeve (~350 psi) while dry nitrogen gas was passed through the sample at various pressures (usually 50–150 psi). By plotting apparent permeability (k) in darcys versus the reciprocal of the average pressure (atm^{-1}) and extrapolating to 0 atm^{-1}, one can get an equivalent water permeability value. This procedure is based on Klinkenberg's paper "The Permeability of Porous media to Liquid Gases."* Examples of typical plots are given in Figure 50. Pastes are on the left and mortars are on the right. Seven-day samples are at the top and 90-day samples are at the bottom. The extrapolated values of k are given in Table 9. For ease of discussion, the k values have also been plotted in Figure 51. Although the values may be higher than water permeability values obtained on wet samples, they actually better reflect conditions in dried samples which were used for all of the companion studies (SEM, microscopy, Hg-porosimetry).

In most instances, the permeabilities of the mortars are greater than the expected percentage of the paste value. As discussed earlier, this particular mortar had 43% sand and 57% paste. The 57% paste values are given in the last column of Table 1 and as a dashed line on Figure 51. The one exception (the 28-day paste sample kept leaking) is the 56-day mortar sample which is less permeable than expected.

The most significant permeability observation, which seems to parallel similar findings in the total Hg-porosimetry data (Figure 46), is that the interface seems to contribute a far greater proportion of permeability pathways and/or porosity to the younger samples (3-, 7-day) compared with the older 56- and 90-day samples. It appears that at 56 and 90 days the early positive deviations in porosity attributed to interfacial porosity, which are contributing to permeability (see next section) become less influential and the mortar samples do in fact approach predicted percentage values of the paste. With time, interfacial porosity becomes more nearly like the bulk paste (homogeneous) as the diffusion-controlled system drives towards equilibrium.

* L.J. Klinkenberg, "The Permeability of Porous Media to Liquids and Gases," Drilling and Production Practice, 200-213 (1941).

Table 9. Observed and calculated air permeability data (darcys) of SHRP 1-1 paste and mortar samples.

Time	Paste	Mortar	(0.57 × paste value)
3	2.9×10^{-5}	3.2×10^{-5}	1.65×10^{-5}
7	2.0×10^{-5}	2.4×10^{-5}	1.14×10^{-5}
14	3.5×10^{-5}	2.8×10^{-5}	2.00×10^{-5}
28	leaking sample	3.8×10^{-5}	--
56	5.1×10^{-5}	2.1×10^{-5}	2.90×10^{-5}
90	2.5×10^{-5}	1.55×10^{-5}	1.42×10^{-5}

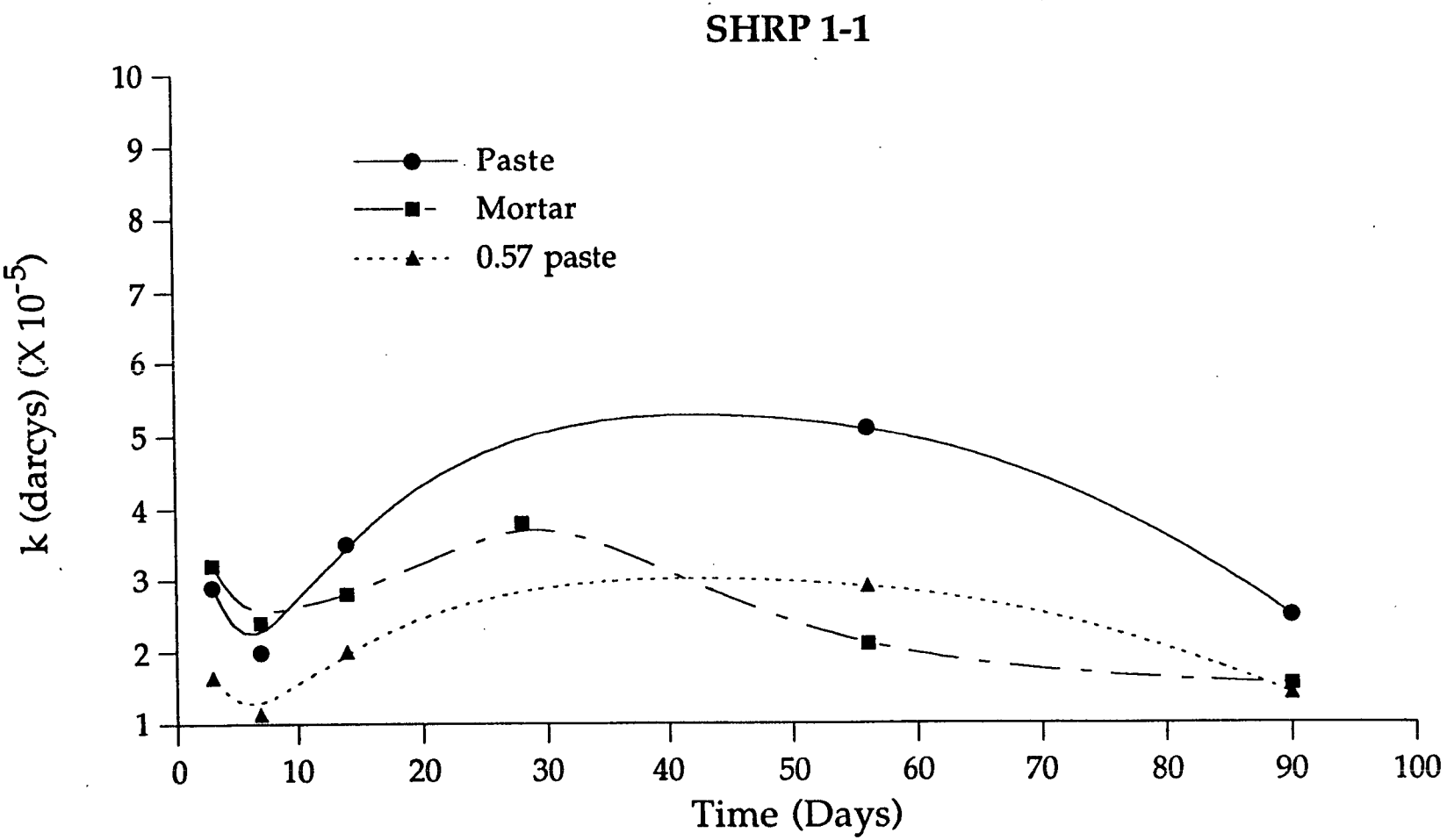

Figure 51. SHRP 1-1 air permeability data. The dashed line represents 0.57 of the paste value.

SUMMARY AND CONCLUSIONS

Interfacial porosity, as a function of distance from the interface, is dictated by the original packing of particles at the interface during mixing of the aggregate and the paste components. The porosity gradient decreases from a maximum directly at the interface, to that of the bulk paste over some interval directly related to the diameter of the particles. In cement this is ~50 μm, whereas our model predicts it to be 2-3 particle diameters. If one assumes a nominal 20 μm cement particle this puts the predicted value in the right ballpark.

As the original porosity fills with hydration products, the porosity of the sample decreases. In a mortar or concrete, the concentration of the hydration products are presumably lower in the interfacial region, because more space must be filled. Additionally, due to the nature of the hydration reaction which produces excess lime, the interfacial region may also provide both space and nucleation sites for $Ca(OH)_2$ crystals to grow.

As a result, this zone may be more sensitive to effects of carbonation and drying. For example, our studies have shown that sand-paste interfaces are often cracked and eroded due to polishing. Air drying of an engineered interface sample resulted in the formation of a crack at the interface. Additionally, Hg-porosimetry and air permeability results confirm higher than expected values in early age mortar samples when compared to pure paste samples.

Air permeability may be directly related to the presence and relative amounts of the larger 200 nm (2000 Å) pores in the paste and mortar samples. Fluctuations in permeability are more nearly related to the increase or decrease inthe amounts of the 200 nm (2000 Å) pores than the smaller 7-40 nm (70-400 Å) pores. Unfortunately, due to time constraints, only an OPC was tested for air permeability, so the above observation is somewhat tentative.

The silica fume containing sample seemed to provide additional confirmation of the above observations. The OPC and fly ash substituted pastes and mortars tended to behave in the same fashion. This may be related to the fact that particle sizes in these samples are nearly the same. However, in the silica-fume sample, the particles are significantly different. The sub-micrometer fume particles can fill in pore spaces at the interface as well as in the bulk paste. Interface microscopy in thin section and 90-day porosimetry showed silica-fume samples of mortar to be free of interfacial porosity. Our model has shown that the reduction in sticking probability would lead to improvements in particle packing. The use of superplasticizer in SHRP 1-4 and the interparticle packing may in fact be responsible for the observed differences.